A Thesis for the Degree of Ph.D. in Science

Comparative Analysis of the Unfolded Protein Response Caused by Small Molecule Compounds

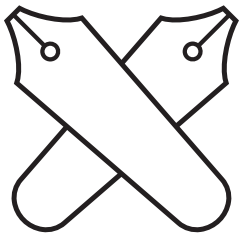

June 2013

Graduate School of Science and Technology
Keio University

Satoko Shinjo

Abbreviations

AARE	cis-acting amino acid response element
Arf	ADP-ribosylation factor
ATF4	activating transcription factor 4
ATF6	activating transcription factor 6
BiFC	bimolecular fluorescence complementation
CHOP	C/EBP homologous protein
EDEM	enhancer mannosidase alpha-like protein
eIF2α	eukaryotic initiation factor 2α
ER	endoplasmic reticulum
ERAD	ER associated degradation
ERdj4	ER-localized DnaJ 4
ERSE	ER stress response element
FRET	fluorescence resonance energy transfer
GADD34	growth arrest- and DNA damage-inducible gene 34
GBF1	Golgi-specific brefeldin A resistance factor 1
GCN2	general control nonrepressed 2
GEF	guanine nucleotide-exchanging factor
GRP78/94	glucose-regulated proteins 78/94

HRI	haem-regulated eIF2α kinase
IRE1	inositol-requiring kinase 1
MHC	major histocompatibility complex
$p58^{IPK}$	protein kinase inhibitor of 58 kDa
PDI	protein disulfide isomerases
PERK	protein kinase regulated by RNA-like ER kinase
PKR	dsRNA-dependent/regulated protein kinase
RT-PCR	reverse transcription PCR
TaV	Thosea asigna virus
UPR	unfolded protein response
UPRE	unfolded protein response element
VSVG	vesicular stomatitis virus G
XBP1	x-box binding protein 1

Chapter 1

Introduction

1-1. Protein folding in the ER

The cell is the basic structural and functional unit of all known living organisms. The cells mainly consist of proteins, lipids, nucleic acids, and sugars. Among then, proteins are the most important molecules to keep the structure and function of the cells. Proteins achieve particular function only when they get proper structures.

In 1960s, Anfinsen et al. reported that resulting native three-dimensional structure is determined by the amino acid sequence (known as Anfinsen's dogma) (Anfinsen et al., 1961). However, since the intracellular is filled with high concentration of proteins, the native structure is hard to obtain. Therefore, family proteins that called as molecular chaperones help their folding.

The folding reaction of transmembrane and secreted proteins takes place at the endoplasmic reticulum (ER). In the ER, proteins undergo folding into their native conformation, glycosylation (Hubbard and Ivatt, 1981; Kornfeld and Kornfeld, 1985), and the formation of intra- and intermolecular disulfide bonds (Fewell et al., 2001) and consequently matured to correct conformation. The major difference between cytosol and the ER as a folding machinery is the quality control system called the unfolded protein response (UPR), which is activated by the perturbation of the folding system in the ER.

1-2. Unfolded protein response

Only correctly conformational maturated proteins can be exported to the Golgi complex from the ER, while incorrectly folded proteins are retained in the ER to complete the folding process or to be targeted for degradation through the machinery referred as ER associated degradation (ERAD) (Ellgaard et al., 1999). Disruption of any of these processes causes ER stress, the accumulation of unfolded proteins in the ER, and activates UPR to recover from the ER stress (Schroder and Kaufman, 2005).

The UPR is initiated by the binding of glucose regulating protein 78 (GRP78) to the unfolded proteins. This binding releases GRP78 from three sensors at the ER membrane that are subsequently activated: the activating transcription factor 6 (ATF6), inositol requiring enzyme 1 (IRE1) and RNA-activated protein kinase R (PKR)-like ER kinase (PERK). Release of GRP78 from ATF6 allows its transport to the Golgi, where it is processed by site1 and site2 proteases (Lee et al., 2002). This processing releases ATF6 from the membrane after which it translocates to the nucleus, where it activates transcription of UPR target genes through binding to the consensus sequence referred ER stress response element (ERSE), which is located in the 5' UTR of several UPR target genes including GRP78/94 (Yoshida et al., 1998). IRE1 is activated by autophosphorylation upon GRP78 release. The phosphorylation activates the endonuclease activity of IRE1, which leads to the non-conventional cytoplasmic splicing of X-Box binding protein 1 (XBP1) mRNA (Yoshida, 2007). The splicing

excises a 26 nt intron, shifting the reading frame and resulting in the active transcription factor XBP1, that also activates transcription of UPR target genes through binding to ERSE and unfolded protein response element (UPRE), which is located in the 5' UTR of several UPR target genes including enhancer mannosidase alpha-like proteins (EDEMs). The activation of PERK is also initiated by autophosphorylation, which results in translational attenuation through phosphorylation of eukaryotic initiation factor2α (eIF2α) (Scheuner et al., 2001). This prevents the further build-up of protein load in the ER. Paradoxically, this leads to selective translation of activating transcription factor 4 (ATF4) (Wek and Cavener, 2007). ATF4 can bind to cis-acting amino acid response element (AARE) and activates transcription of pro-survival genes, but also induction of the pro-apoptotic gene C/EBP homologous protein (CHOP) is highly dependent on ATF4. Therefore, to summarize the downstream events of the three sensors, four responses are executed through these transcriptional activation of UPR target genes, as follows; (1) translational attenuation to limit further protein load at the ER *via* phosphorylation of eIF2α , (2) enhancement of the capacity of the protein folding system through the up-regulation of ER chaperones, co-chaperones or folding enzymes such as GRP78 and 94, ER-localized DnaJ 4 (ERdj4), protein disulfide isomerase (PDI); (3) ERAD, which involves in EDEMs; and, (4) the induction of cellular apoptosis where CHOP is thought to play an important role, if adaptive responses (1–3) are insufficient to relieve ER stress (reviewed in (Ron and Walter,

2007; Zhao and Ackerman, 2006)).

Whereas the research field of UPR has been developed in recent 30 years, there are some unsolved questions as described in the literature (Walter and Ron, 2011). One of the questions is “What is the basis for toxicity of unfolded or misfolded proteins in the ER?” UPR was reported to be involved in various diseases, including neurodegenerative disease, diabetes and cancer. However, the roles of UPR on each disease are reported to be different; UPR contributes to cell death in neurodegenerative disease and diabetes, but in cancer it contributes to cell survival even under the severe condition such as low oxygen and nutrition. Therefore, in other words, “Why the roles of UPR on each disease are different?”, it is one of the questions in the field of UPR. The author guessed that the difference in the mechanisms how the proteins in the ER was accumulated would affect the downstream event such as the upregulation of particular UPR target genes. Therefore, to approach this presumption, the author used the small molecule compounds.

1-3. UPR inducing compounds

As described in section 1-2, the accumulation of unfolded protein is referred to as ER stress and thought to activate UPR. This concept of UPR was established in 1970-1980s, because various compounds, which were possible to induce the accumulation of incorrectly folded proteins, were reported to induce UPR. Tunicamycin,

a disruptor of N-linked glycosylation *via* UDP-GlcNAc: dolichol-P GlcNAc-1-P transferase inhibition (Heifetz et al., 1979), was reported to induce UPR (Takatsuki et al., 1975), which might be caused by the accumulation of unglycosylated proteins in the ER. 2-deoxyglucose, an analog of glucose and could inhibit glycolysis, also induced UPR (Pouyssegur et al., 1977), which is caused by the inhibition of glycosylation of the proteins (Kurtoglu et al., 2007). DTT, a reducing reagent (Cleland, 1964), induced UPR (Halleck et al., 1997), which might be caused by the impairment of disulfide bond formation of the proteins in the ER. Moreover, also in 1990s-2000s, much more compounds that have different mode of action than the previous ones were reported to induce UPR. Thapsigargin, an ER Ca^{2+}-ATPase inhibitor (Thastrup et al., 1990), induced UPR (Price et al., 1992) *via* impairment of Ca^{2+} dependent ER chaperone activity (Di Jeso et al., 2003) and is likely to accumulate unfolded proteins in the ER. Brefeldin A, an inhibitor of Golgi-specific brefeldin A resistance factor 1 (GBF1) (Citterio et al., 2008), induced UPR (Liu and Ou, 1992). GBF1 is a guanine nucleotide-exchanging factor (GEF) of ADP-ribosylation factor (Arf) GTPase, which is responsible for the vesicle transport from the ER to the Golgi apparatus (Zhao et al., 2006). Therefore, in the case of brefeldin A, the accumulation of the proteins that were destined to deliver to the Golgi apparatus is thought to be induced. Moreover, eeyarestatin I, an ERAD inhibitor (Fiebiger et al., 2004), was also reported to induce UPR (Wang et al., 2009).

Using these compounds, the author sought to address the question, whether the difference in the mechanisms how the proteins in the ER were accumulated would affect the downstream event such as the upregulation of particular UPR target genes. Several reports, which showed that the intensity of UPR target genes, the periods to induce them or the effect of the GRP78 inhibitor, versipelostatin, toward the expression of GRP78 were different among the compounds (Harding et al., 2000; Nakagawa et al., 2000; Park et al., 2004), raised the possibility that the difference in the cause of UPR would affect the downstream event in the UPR. Therefore, in Chapter 2, the author compared the expression patterns of nine UPR target genes induced by seven UPR inducing compounds that have different modes of action. As a result of hierarchical clustering using Pearson's correlation coefficient as a similarity, the expression patterns induced by seven compounds were classified into two clusters, cluster A and B. The genes were also classified into two clusters; cluster I, which were relatively highly upregulated by the treatment of cluster A compounds and cluster II, which were relatively highly upregulated by the treatment of cluster B compounds. These results suggested that the mode of action of the compounds could determine which of UPR target genes were relatively highly upregulated. Further analysis indicated that the difference of the expression patterns of UPR target genes might be dependent on which of the ER stress sensors were activated by the compounds.

1-4. Methods for monitoring the UPR

Another unsolved question in the UPR research is "Are the ER stress sensors activated in the same extent and with similar kinetics in response to the various physiological or pharmacological conditions?" A previous study by DuRose et al. revealed that the activation kinetics of the three sensors was distinct among the three pharmacological reagents, DTT, tunicamycin, and thapsigargin (DuRose et al., 2006). The study described in Chapter 2 of this thesis also suggested that the sensitivity of ER stress sensors might be different among the several UPR-inducing compounds. Moreover, recently, the mechanisms for activation of three ER stress sensors were implied to be more nuanced than a single uniform mechanism and be dependent on the physiological condition (Rutkowski and Hegde, 2010). Therefore, the intensity or time series variation of the activation of each ER stress sensor would differ among the various physiological and pharmacological conditions. However, there is a technical limitation to address this issue. As described in section 1-2, proteolytic processing of ATF6 and phosphorylation of PERK and IRE1α can serve as markers of their activation status. However, detection of cleaved ATF6, phospho-PERK, and phospho-IRE1α is quite difficult as these are expressed at very low levels and there is currently a lack of good commercial antibodies to detect them (Samali et al., 2010). The activation of PERK and IRE1α could be also evaluated by detection of phosphorylation of eIF2α and splicing of XBP1 mRNA, respectively, however, these methods were indirect.

Therefore, several detection systems were established for detection of the activation of ER stress sensors, particularly, IRE1α.

Iwawaki et al. reported a transgenic mouse model for monitoring XBP1 mRNA splicing with the fluorescence of yellow fluorescent protein, venus (Iwawaki et al., 2004). In this report, venus was fused to downstream of a partial sequence of human XBP1, including the 26 nt of splicing site, which is spliced by IRE1α upon its activation. Furthermore, the detection systems for IRE1 dimerization were recently developed. Pincus et al. reported the detection system for yeast IRE1 dimerization with FRET analysis and suggested that GRP78 binding to IRE1 contributes to the efficient de-oligomerization of active IRE1 complexes (Pincus et al., 2010). Li et al. reported the detection system for human IRE1α dimerization (Li et al., 2010). In this report, by treatment of tunicamycin, IRE1α-GFP localized into discrete foci, which correlated well with the splicing of XBP1 mRNA and phosphorylation of IRE1α-GFP, whereas the IRE1α-GFP was diffusely distributed in the ER membrane without tunicamycin treatment.

Although the detection systems for the activation of IRE1 has been developed, the detection system for other two ER stress sensors, ATF6 and PERK, were now not available. Therefore, the author sought to establish the detection system for the activation of three ER stress sensors in a single cell with imaging analysis using three fluorescent proteins which exhibit different three colors: blue, yellow, and red.

Therefore, in this thesis, the author aimed to establish a detection system for IRE1α dimerization using Bimolecular Fluorescence Complementation (BiFC), which detects protein-protein interaction through the complementation of non-fluorescent fragments of fluorescent protein, as described in Chapter 3. Since BiFC assay is based on the formation of a fluorescent complex when two proteins fused to non-fluorescent fragments of a fluorescent protein interact with each other, BiFCassay enables visualization of protein interactions in living cells with subcellular resolution using the single excitation/emission characteristics of the parent protein. The author constructed the plasmid encoding N-terminal domain of IRE1α fused to either N- or C-terminal domain of blue fluorescent protein, cerulean and established stably expressing cells of both fusion proteins. Whereas the fluorescence of cerulean was hardly detected under normal condition, it was observed upon the treatment of DTT. Therefore, it is suggested that this BiFC system also useful to detect IRE1α dimerization.

Chapter 2

Comparative Analysis of the Expression Patterns of UPR Target Genes Caused by UPR-inducing Compounds

2-1. Introduction

As described in Chapter 1, ER is the organelle for folding and conformational maturation of transmembrane and secreted proteins. ER stress, which is the accumulation of unfolded proteins in the ER, leads to a process known as the UPR. UPR is triggered by the activation of the three ER stress sensors (ATF6, IRE1α and PERK) and executed by the transcriptional induction of UPR target genes (reviewed in (Ron and Walter, 2007; Zhao and Ackerman, 2006)).

In most studies, UPR has been typically induced by treating *in vitro* cell models with compounds described in section 1-3, such as tunicamycin, thapsigargin, DTT, brefeldin A, 2-deoxyglucose and eeyarestatin I. Since these compounds have different modes of action, the mechanisms for protein accumulation in the ER induced by each compound are thought to be different; however, it is unclear whether these compounds up-regulate each UPR target gene with similar kinetics or not. Therefore, in order to address this question, the author investigated by comparing the time-course expression profile of UPR-target genes subsequent to treatment with UPR-inducing compounds.

At first, the author selected six compounds commonly used as UPR inducers: 2-deoxyglucose, brefeldin A, DTT, eeyarestatin I, thapsigargin, and tunicamycin. Furthermore, exploratory chemical screening indicated that monensin induced the expression of GRP78 and other eight UPR-target genes, so this was added as a prospective UPR inducer (see section 2-2-3). The author measured the expression of

nine UPR target genes (ATF4, CHOP, EDEM1, ERdj4, growth arrest- and DNA damage-inducible gene (GADD) 34, GRP78, GRP94, protein kinase inhibitor of 58 kDa ($p58^{IPK}$), and PDI). GADD34 and $p58^{IPK}$ were reported to act as feedback regulators of UPR(Novoa et al., 2001; Yan et al., 2002). The expression profiles of these genes appeared to have characteristic patterns among the compounds. Hierarchical clustering analysis based on the kinetics of the expression of UPR target genes revealed at least two types of UPR target gene expression profiles, which are dependent on the mode of action of the UPR-inducing compound.

2-2. Results

2-2-1. Effects of six UPR-inducing compounds on cell viability and GRP78 protein expression

The first investigation was to determine suitable concentrations of six compounds (2-deoxyglucose, brefeldin A, DTT, eeyarestatin I, thapsigargin, and tunicamycin) for the induction of UPR. Since GRP78 is a well-known UPR marker protein, its protein expression was examined in HeLa cells after 24-hour treatment with each of the six compounds (Fig. 1-1). As shown in Fig. 1-1A, 2-deoxyglucose induced the expression of GRP78 in a dose-dependent manner, with an approximately 1.5-fold increase at 0.2 mM and a maximum increase at 2 mM, neither dose affecting cell viability. Similarly, brefeldin A, thapsigargin, and tunicamycin also increased the expression of GRP78 in a dose-dependent manner, with maximum increases at 50 ng/ml, 30 nM, and 10 μg/ml, and with moderate increases (approximately 1.5-fold) at 15 ng/ml, 1 nM, and 1 μg/ml, respectively. These doses also did not affect cell viability (Figs. 1-1B, E, and F). DTT and eeyarestatin I were able to induce GRP78 expression at 3 mM and 3 μM, respectively (Figs. 1-1C and D). Additionally, each compounds except brefeldin A, induced the expression of GRP94 similar to GRP78. Upon the treatment of brefeldin A, the expression of GRP94 was increased in a dose-dependent manner, which was maximized at 50 ng/ml and then declined. The concentrations sufficient to induce maximum and moderate levels of UPR were defined with the expression of GRP78 in

protein level as summarized in Table 1-1.

A. 2-deoxyglucose

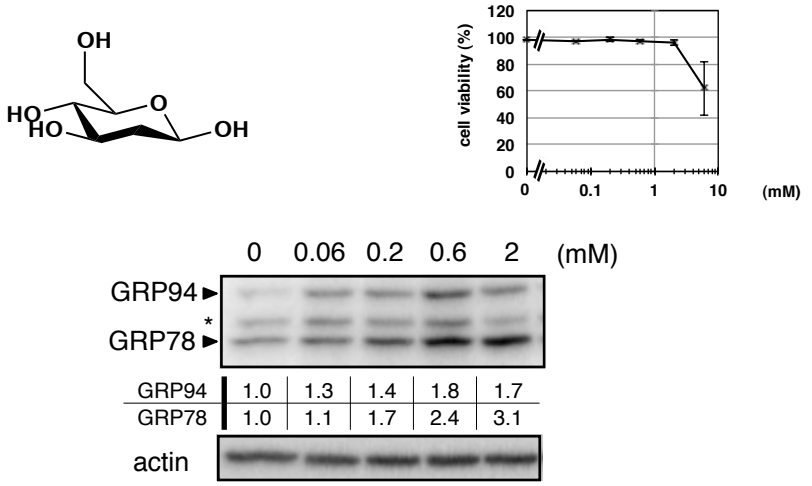

B. brefeldin A

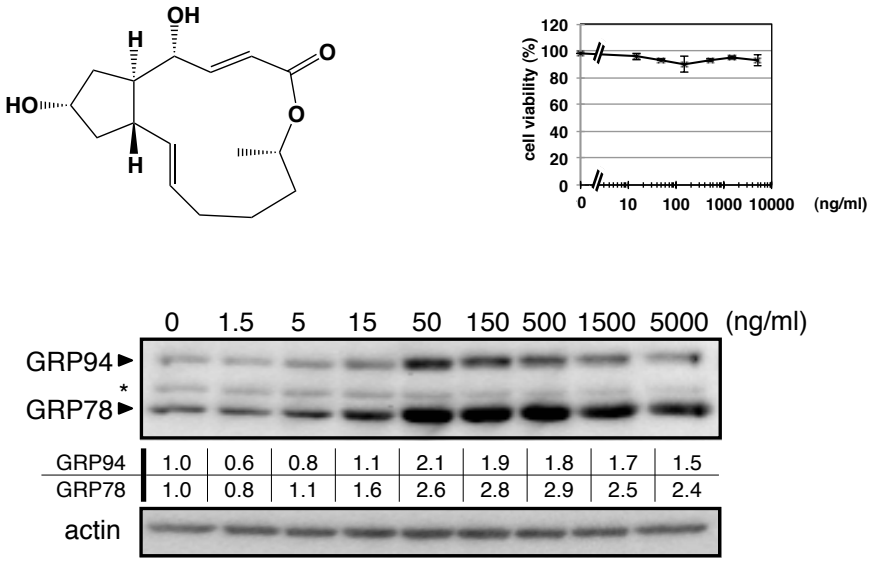

Fig 1-1. UPR-inducing compounds induce GRP78 expression without affecting cell viability.

Biological activity of six UPR-inducing compounds: 2-deoxyglucose (A) and brefeldin A (B). (Upper left panel) Chemical structure (Upper right panel) HeLa cells were treated with the indicated concentration of each compound for 24 hours. Cell viability was assessed using trypan blue dye exclusion assays. Values are the means of three independent determinations. Bars, SD. (Lower panel) HeLa cells were treated with the indicated concentration of each compound for 24 hours. GRP78 and GRP94 was detected by immunoblotting with the anti-KDEL antibody. *; nonspecific band. The intensities of the bands of GRP78 and GRP94 were divided by that of β-actin and indicated below the bands

C. DTT

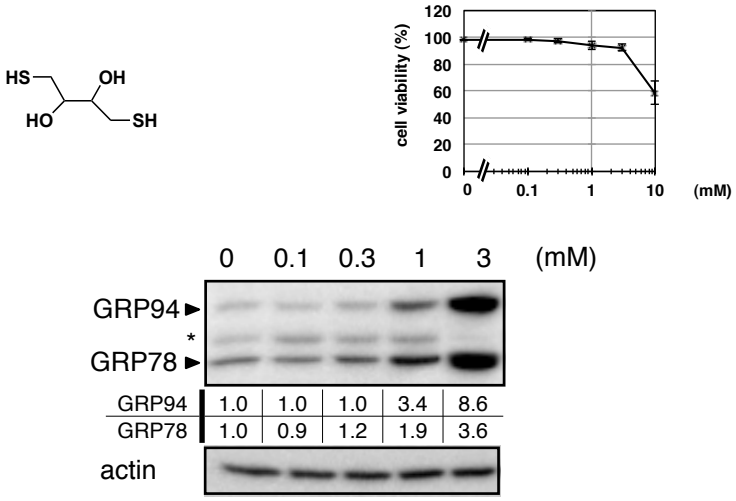

D. eeyarestatin I

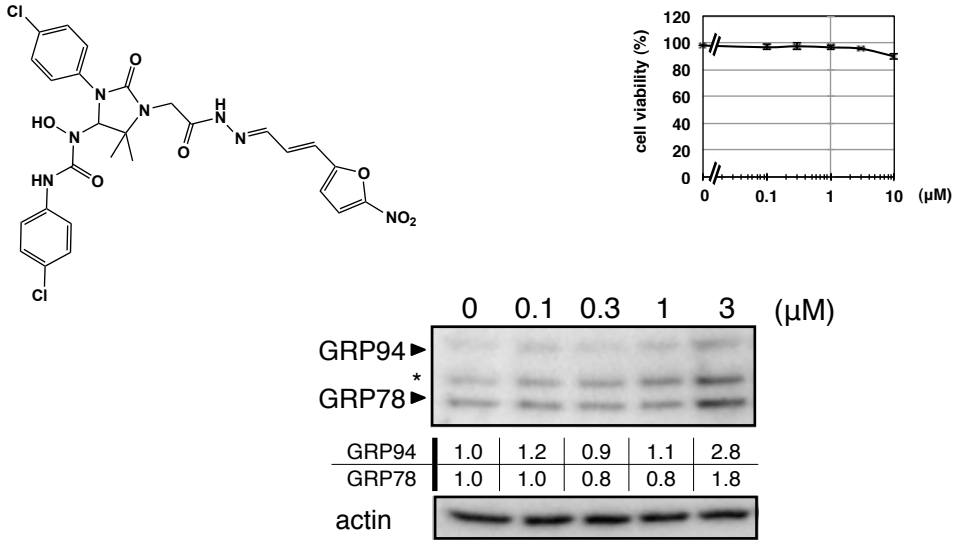

Fig 1-1. UPR-inducing compounds induce GRP78 expression without affecting cell viability. (continued)

Biological activity of six UPR-inducing compounds: DTT (C) and eeyarestatin I (D).

E. thapsigargin

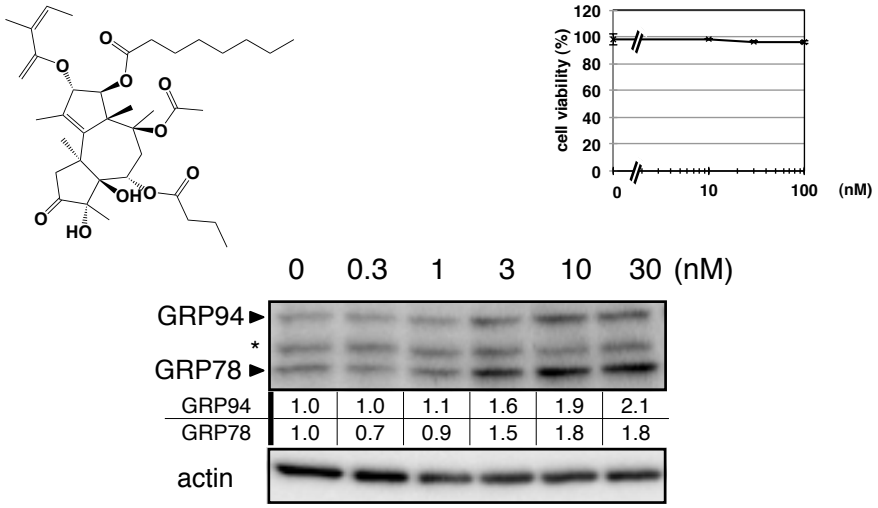

F. tunicamycin

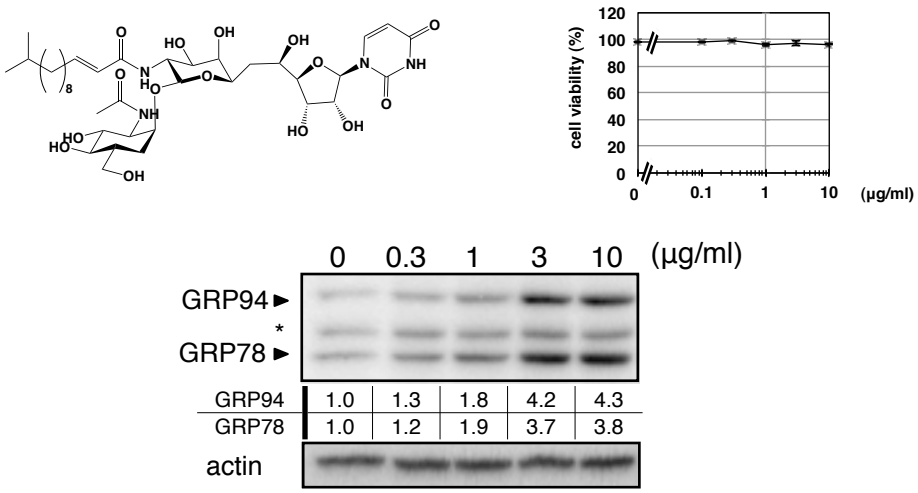

Fig 1-1. UPR-inducing compounds induce GRP78 expression without affecting cell viability. (continued)

Biological activity of six UPR-inducing compounds: thapsigargin (E) and tunicamycin (F).

Table 1-1: Concentrations of the UPR inducing compounds

Compounds	Concentrations	
	Induces Maximum GRP78 Levels	Induces Moderate GRP78 Levels
thapsigargin	30 nM	1 nM
tunicamycin	10 μg/ml	1 μg/ml
2-deoxyglucose	2 mM	0.2 mM
DTT	3 mM	-
brefeldin A	50 ng/ml, 5000 ng/ml	15 ng/ml
eeyarestatin I	3 μM	-

2-2-2. Measurement of the time-course expression of nine UPR-target genes mRNA levels

To compare among the expression patterns of UPR-target genes induced by the six UPR-inducing compounds, the author measured the mRNA levels of GPR78. HeLa cells were treated with one of the six compounds at the concentration indicated in Table 1-1 and the amount of GRP78 mRNA was measured by real-time reverse transcription PCR (RT-PCR). As shown in Fig. 1-2, all of the six compounds increased the amount of GRP78 mRNA. For instance, 30 nM thapsigargin increased it after 4-hour treatment, which reached a plateau at a ~10-fold increase after 12-hour treatment. 2 mM 2-deoxyglucose and 10 μg/ml tunicamycin also increased the amount of GRP78 mRNA, which peaked after approximately 12-16 hours of treatment, resulting in 20- and 15-fold increases, respectively, and then declined by the end of the 24-hour treatment (Fig. 1-2). When the cells were treated with 50 ng/ml brefeldin A, the amount of GRP78 mRNA increased in a time-dependent manner for 24 hours, showing an approximately 8-fold rise in expression (Fig. 1-2). Taken together, the time-course expression data of GRP78 mRNA appears to have characteristic patterns among the six compounds.

Moreover, there were similar expression patterns of GRP78 mRNA when HeLa cells were treated with 15 ng/ml, 50 ng/ml, or 5000 ng/ml of brefeldin A. Furthermore, when the cells were treated with 0.2 mM and 2 mM of 2-deoxyglucose, or 1 nM and 30 nM of thapsigargin, the expression patterns of GRP78 mRNA were also similar. In

addition, 1 μg/ml tunicamycin showed a slightly delayed expression pattern of GRP78 mRNA compared to 10 μg/ml tunicamycin. Overall, the differences in the concentration of each compound did not have a notable effect on the expression patterns of GRP78 mRNA.

The author further measured the changes in the amount of mRNA of additional eight UPR target genes, ATF4, CHOP, EDEM1, ERdj4, GADD34, GRP94, PDI, and $p58^{IPK}$, induced by the six compounds. As shown in Fig. 1-3, all compounds increased the amount of eight UPR target genes mRNA at the concentrations indicated in Table 1-1.

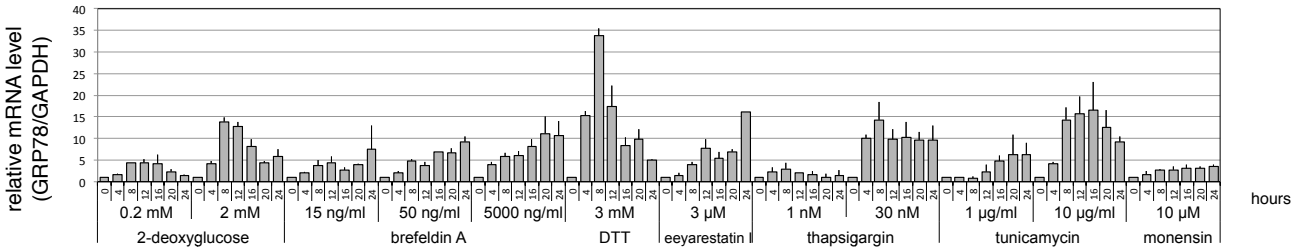

Fig 1-2. UPR-inducing compounds increase the amount of GRP78 mRNA in HeLa cells.

HeLa cells were treated with UPR-inducing compounds at the indicated concentrations for 4–24 hours. Relative mRNA levels of GRP78 were quantified using real-time RT-PCR. All values were normalized using GAPDH as an internal control. Values are the means of three independent determinations. Bars, SD.

A. ATF4

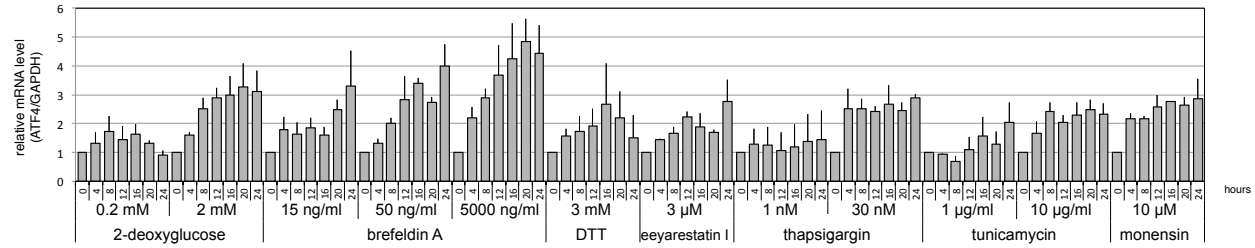

B. CHOP

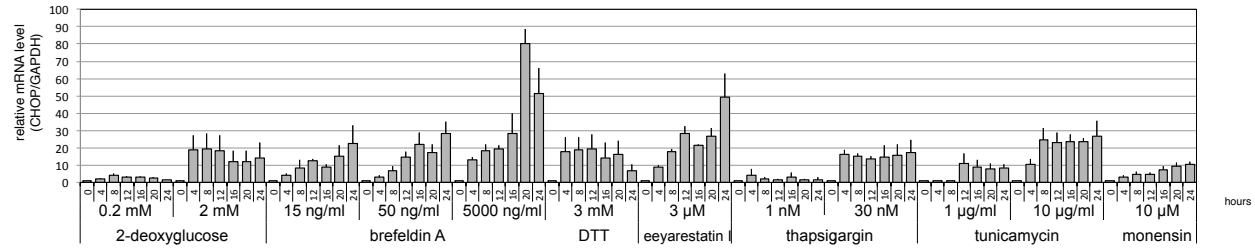

C. EDEM1

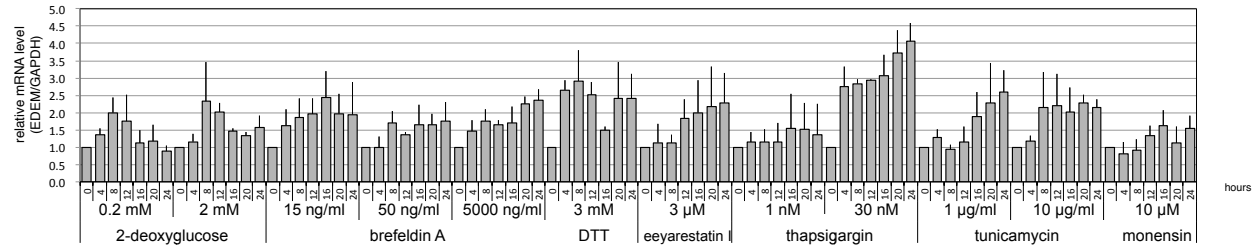

Fig 1-3. Effects of UPR-inducing compounds on expression of UPR-target genes.

HeLa cells were treated with UPR-inducing compounds at the indicated concentrations for 4–24 hours. Relative mRNA levels of UPR-target genes, (A)ATF4, (B) CHOP and (C) EDEM1 were quantified with real-time RT-PCR. All values were normalized using GAPDH as an internal control. Values are the means of three independent determinations. Bars, SD.

D. ERdj4

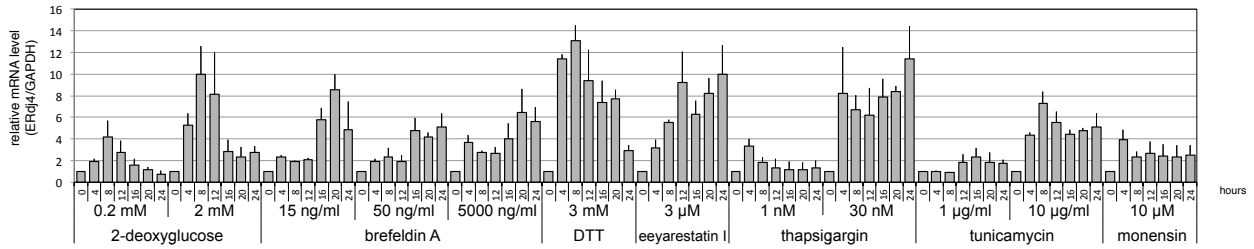

E. GADD34

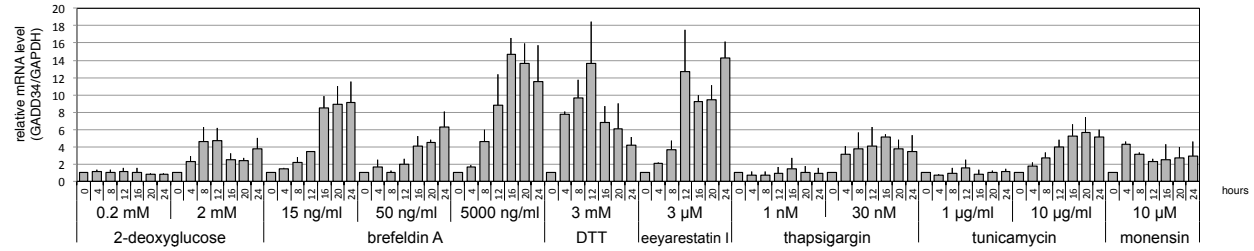

F. GRP94

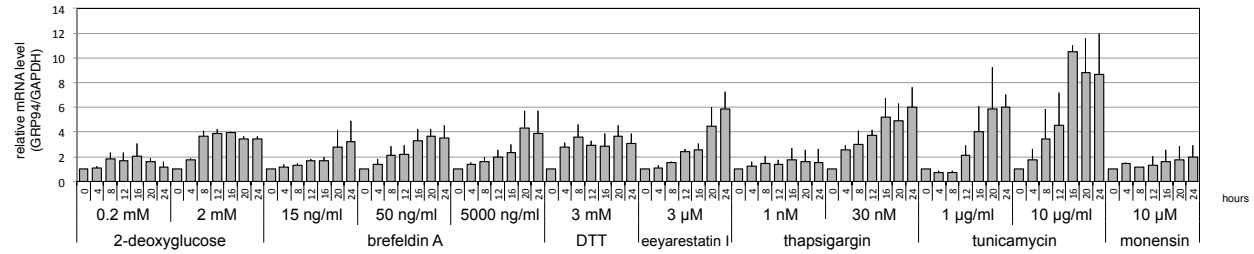

Fig 1-3. Effects of UPR-inducing compounds on expression of UPR-target genes. (continued)

HeLa cells were treated with UPR-inducing compounds at the indicated concentrations for 4–24 hours. Relative mRNA levels of UPR-target genes, (D)ERdj4, (E) GADD34 and (F) GRP94 were quantified with real-time RT-PCR. All values were normalized using GAPDH as an internal control. Values are the means of three independent determinations. Bars, SD.

G. p58^{IPK}

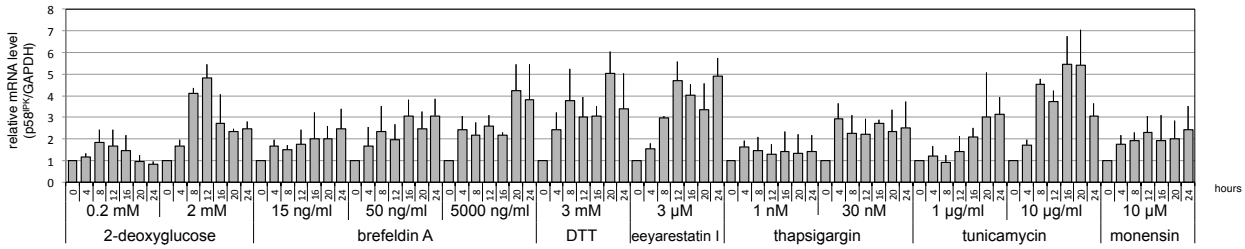

H. PDI

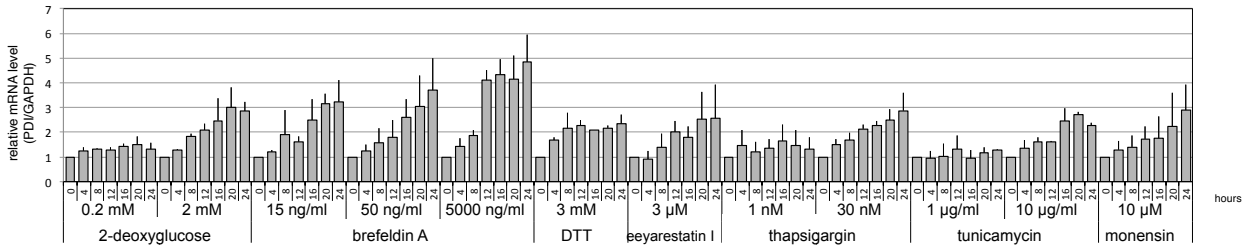

Fig 1-3. Effects of UPR-inducing compounds on expression of UPR-target genes. (continued)

HeLa cells were treated with UPR-inducing compounds at the indicated concentrations for 4–24 hours. Relative mRNA levels of UPR-target genes, (G)p58^{IPK} and (H) PDI were quantified with real-time RT-PCR. All values were normalized using GAPDH as an internal control. Values are the means of three independent determinations. Bars, SD.

2-2-3. Monensin up-regulated UPR target genes

An in-house chemical library, which included commercially available compounds as well as compounds isolated from microbial origin by our laboratory, was screened for additional potential UPR-inducing compounds. It was found that monensin, a compound isolated from *Streptomyces cinnamonensis* and known as a Na^+ ionophore (Haney and Hoehn, 1967), increased the amount of GRP78 at 10 μM (Fig. 1-4C) without affecting cell viability (Fig. 1-4B). Monensin also increased the amount of GRP78 mRNA slightly for 4-24 hour treatment (Fig. 1-2), as well as the other eight UPR target genes of interest (Figs. 1-3, A-H). Furthermore, monensin induced phosphorylation of eIF2α, a well-known substrate of PERK (Harding et al., 1999) (Fig. 1-5A). Since four kinases (PERK, dsRNA-dependent/regulated protein kinase (PKR), haem-regulated eIF2α kinase (HRI), and general control nonrepressed 2 (GCN2)) are known to phosphorylate eIF2α, the author examined whether monensin-induced phosphorylation of eIF2α occurs through PERK activation. As shown in Fig. 1-5A, monensin-induced phosphorylation of eIF2α was impaired in siPERK-transfected HeLa cells where knockdown of PERK was confirmed by immunoblotting (Fig. 1-5B), suggesting that monensin activated PERK. Taken together with these results, it appears that monensin induced UPR. Thus, monensin was added to the further experiments in the study. Since another polyether K^+/H^+ ionophore, nigericin (Feinstein and Felsenfeld, 1971), also upregulated the expression of GRP78 (Fig. 1-6), activity of Na^+ ionophore

might cause the expression of GRP78 (see discussion).

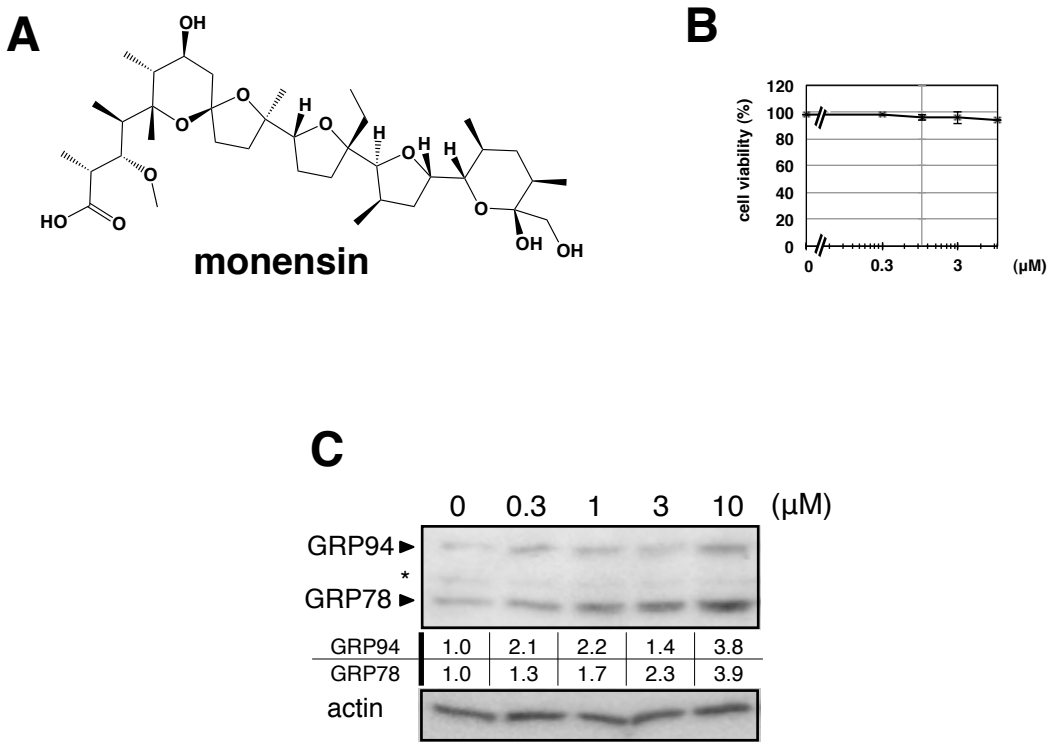

Fig 1-4. Monensin induces UPR

(A) Chemical structure of monensin. (B and C) Biological activity of monensin. (B) HeLa cells were treated with the indicated concentration of each compound for 24 hours. Cell viability was assessed using trypan blue dye exclusion assays. Values are the means of three independent determinations. Bars, SD. (C) HeLa cells were treated with the indicated concentration of monensin for 24 hours. GRP78 and GRP94 was detected by immunoblotting with anti-KDEL antibodies. *; nonspecific band. The bands intensities of GRP78 and GRP94 were divided by that of β-actin and indicated below the bands.

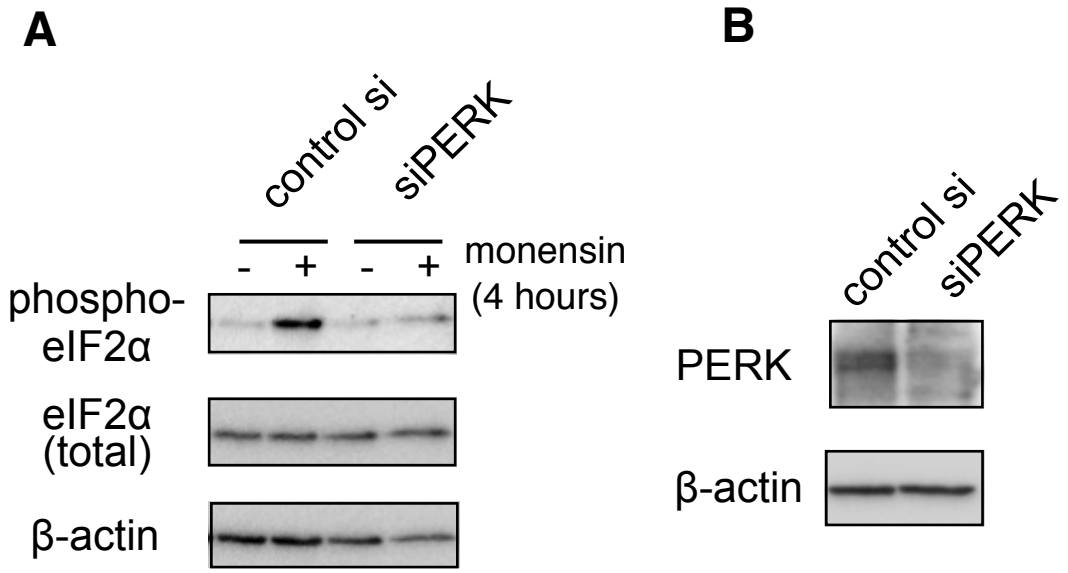

Fig 1-5. Monensin induces PERK activation

(A) Control or PERK siRNA-transfected HeLa cells were treated with 10 μM monensin for 4 hours. Total and phospho-eIF2α were detected by immunoblotting. (B) The successful knockdown of PERK by siRNA was confirmed by immunoblotting with anti-PERK antibody. β-Actin was immunoblotted as a loading control.

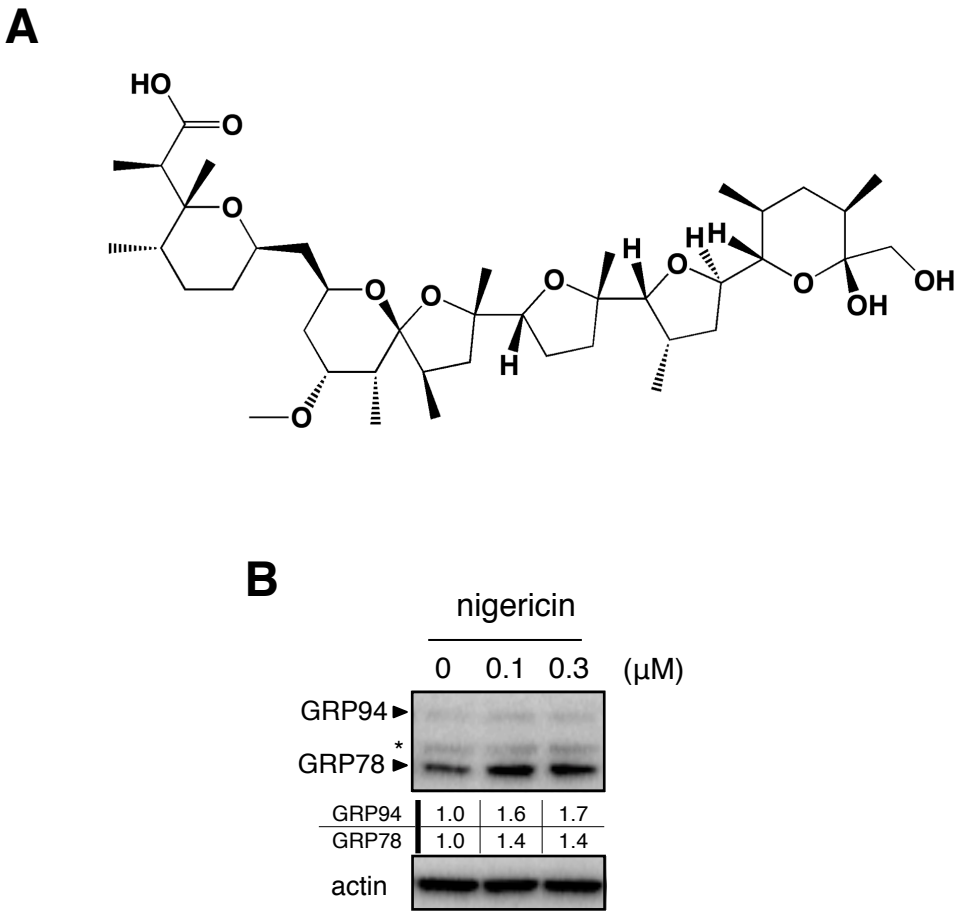

Fig 1-6. Nigericin induces UPR

(A) Chemical structure of monensin. (B) HeLa cells were treated with the indicated concentration of monensin for 24 hours. GRP78 and GRP94 was detected by immunoblotting with anti-KDEL antibodies. *; nonspecific band. The bands intensities of GRP78 and GRP94 were divided by that of β-actin and indicated below the bands.

2-2-4. Clustering of compounds based on the expression profile of nine UPR target genes using Pearson's correlation coefficient

It was observed that the kinetics of UPR target gene expression had characteristic patterns among the 12 experimental conditions tested (seven compounds, some with multiple concentrations). The acquired data were analyzed by hierarchical clustering, with the aim of classifying the expression profiles of the nine UPR target genes, to clarify which of the genes were relatively highly upregulated by the compounds. Real-time RT-PCR data of each UPR target gene obtained from the 12 experimental conditions were normalized to acquire "UPR fingerprints of genes". Furthermore, the normalized data were reordered by condition in order to acquire "UPR fingerprints of compounds" (Fig. 1-7). Each type of fingerprint was analyzed by hierarchical clustering using Pearson's correlation coefficient as a similarity and average-linkage method. As a result of clustering analysis of the compounds, as shown in the left side of Fig. 1-8, the 12 conditions could be divided into two groups: clusters A and B. Cluster A contained thapsigargin, tunicamycin 2-deoxyglucose, and DTT; cluster B contained brefeldin A, monensin, and eeyarestatin I. When thapsigargin, tunicamycin, 2-deoxyglucose, or brefeldin A was used over different concentrations, the expression patterns of nine UPR target genes remained classified in the same cluster (Fig. 1-8). Furthermore, as a result of clustering analysis of the genes, as shown at the top of Fig. 1-8, the 9 genes could be divided into two groups: cluster I and II (Fig. 1-8). Cluster I contained GRP78, ERdj4,

EDEM1, $p58^{IPK}$ and GRP94, and cluster II contained GADD34, CHOP, PDI and ATF4. Based on two-way clustering analysis, a heat map displayed the expression data of each gene and under each condition by reordering the data by rows and columns (Fig. 1-8), which showed that the expression intensity of cluster I genes in the fingerprints of cluster A was higher than in cluster B; conversely, the expression intensity of cluster II genes in the fingerprints of cluster A was lower than in cluster B.

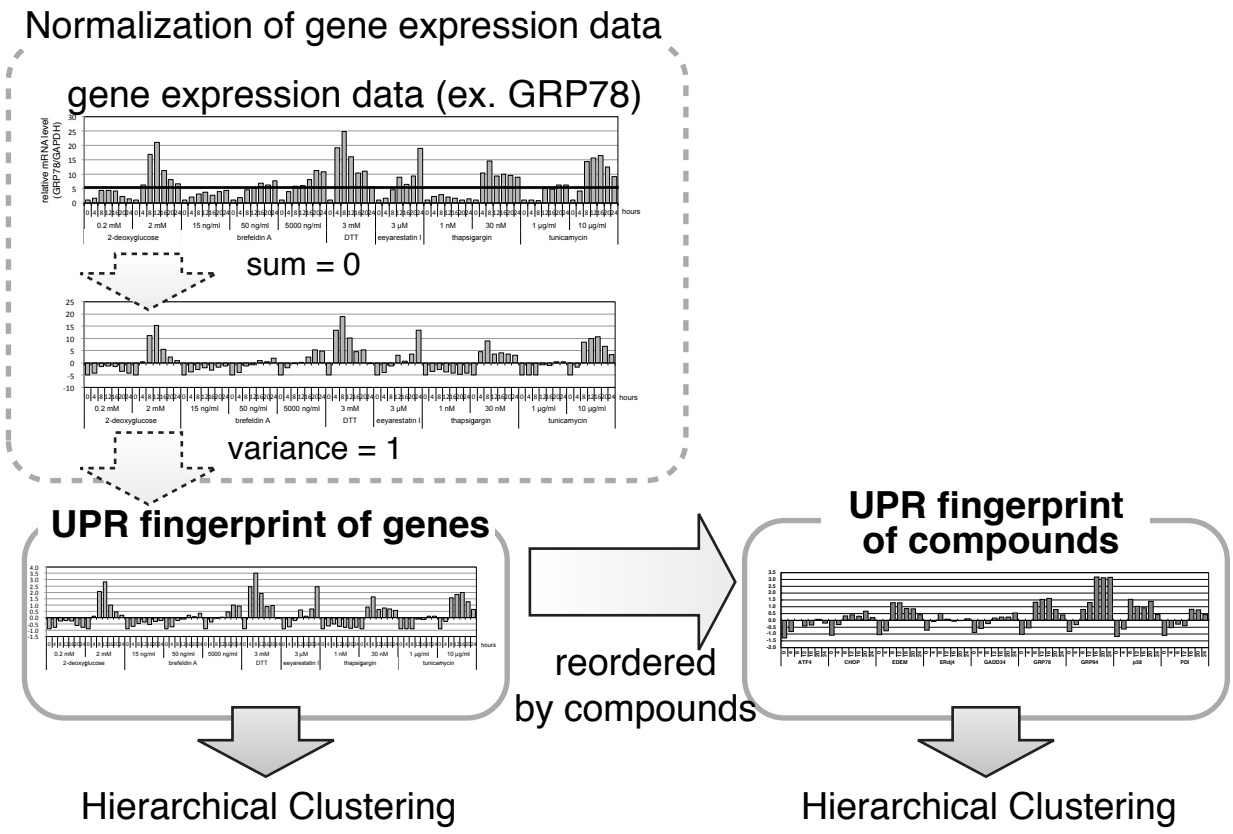

Fig 1-7. Schematic illustration of the method used for data analysis

The relative mRNA levels of each gene were normalized by subtracting the average value from the result at each time point and dividing by the standard deviation. A “UPR fingerprint of genes” was obtained. The author created a separate “UPR fingerprint of compounds” by reordering the data by compound. Similarities between the two UPR fingerprints (Pearson’s correlation coefficient) were calculated and analyzed using hierarchical clustering.

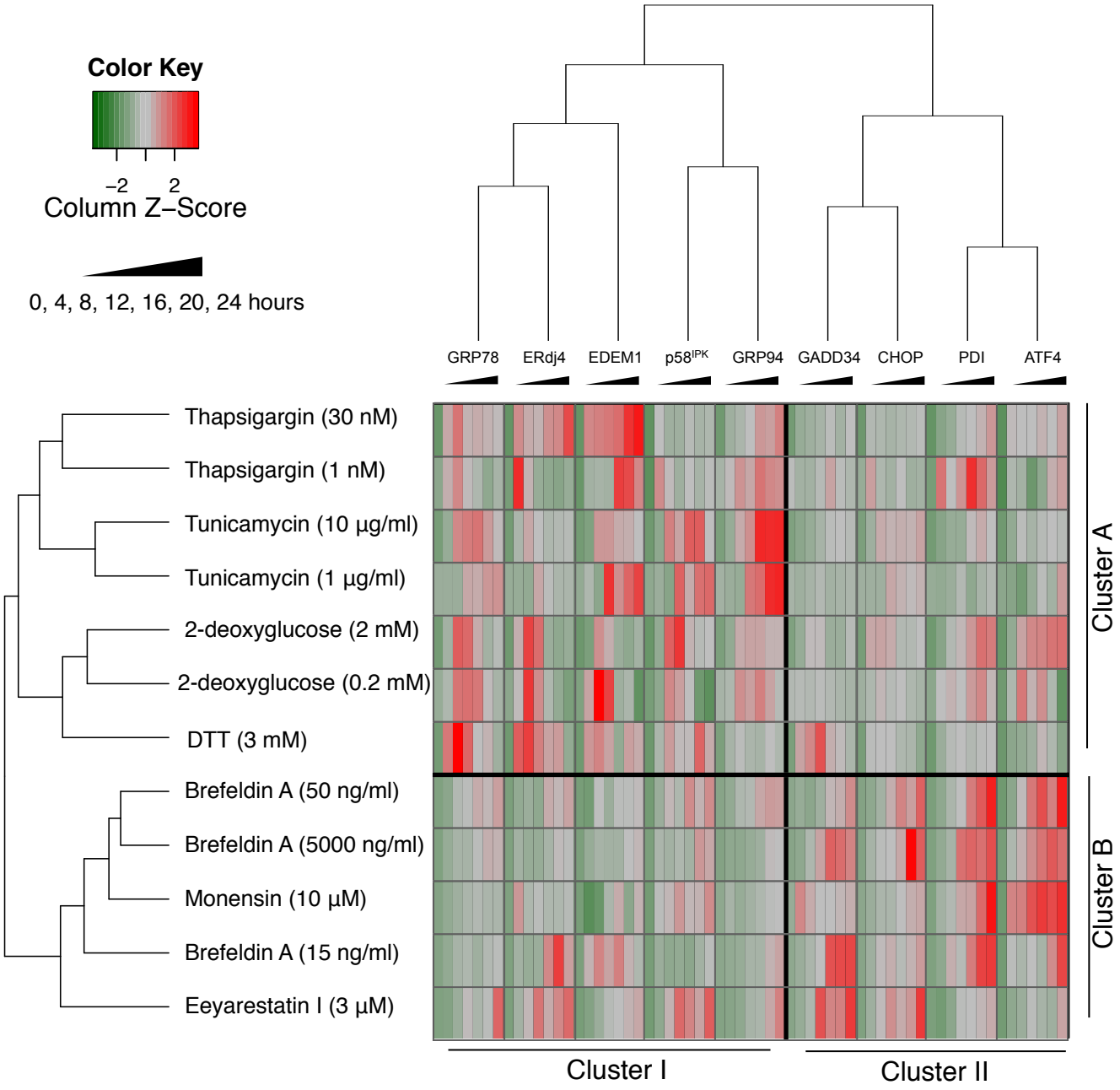

Fig 1-8. Two-dimensional clustering analysis of genes and UPR-inducing compounds on the basis of Pearson's correlation coefficients.

Rows, compounds; columns, genes; red, positive scores; green, negative scores, obtained in the UPR fingerprint. UPR fingerprints were analyzed using hierarchical cluster analysis. A dataset of 12 conditions or 9 genes was clustered based on the average-linkage method using Pearson's correlation coefficients.

2-2-5. Clustering of compounds based on the expression intensity of UPR target genes using Euclidean distance

Since the analysis described in previous paragraph (2-2-4) were focused on the relative expression levels of UPR-target genes and lacked the information of absolute levels of the expression, it was unsuitable to speculate which of the ER stress sensors were activated by which of the compounds. Therefore, in order to examine which of the compounds showed similar absolute levels of expression of UPR target genes, the author also performed cluster analysis using Euclidean distance as similarity. Real-time RT-PCR data of each UPR target gene, obtained from seven compounds with the concentrations that induce maximum levels of GRP78 treated samples, were logarithmic transformation and normalized to acquire "UPR fingerprints of genes". Furthermore, the normalized data were reordered by condition in order to acquire "UPR fingerprints of compounds" (Fig. 1-9). UPR fingerprints of genes and compounds were analyzed by hierarchical clustering using Pearson's correlation coefficient and Euclidean distance, respectively, as a similarity and complete-linkage method.

As a result of clustering analysis of the compounds, as shown in the left side of Fig. 1-10, the seven compounds could be divided into three groups: Clusters A', B', and C'. Cluster A' contained thapsigargin, DTT, tunicamycin, and 2-deoxyglucose; cluster B' contained eeyarestatin I; cluster C' contained monensin and brefeldin A.

Furthermore, as a result of clustering analysis of the genes, as shown at the top of

Fig. 1-10, the 9 genes could be divided into three groups: cluster I', II', and III' (Fig. 1-10). Cluster I' contained PDI and ATF4, cluster II' contained GADD34, $p58^{IPK}$ and CHOP, cluster III' contained GRP94, EDEM1, GRP78, and ERdj4. Based on two-way clustering analysis, a heat map displayed the expression data of each gene and compound by reordering the data by rows and columns (Fig. 1-10), which showed that the expression of cluster III' genes were much less induced by the compounds in cluster C' compared with the compounds in cluster A' and B'.

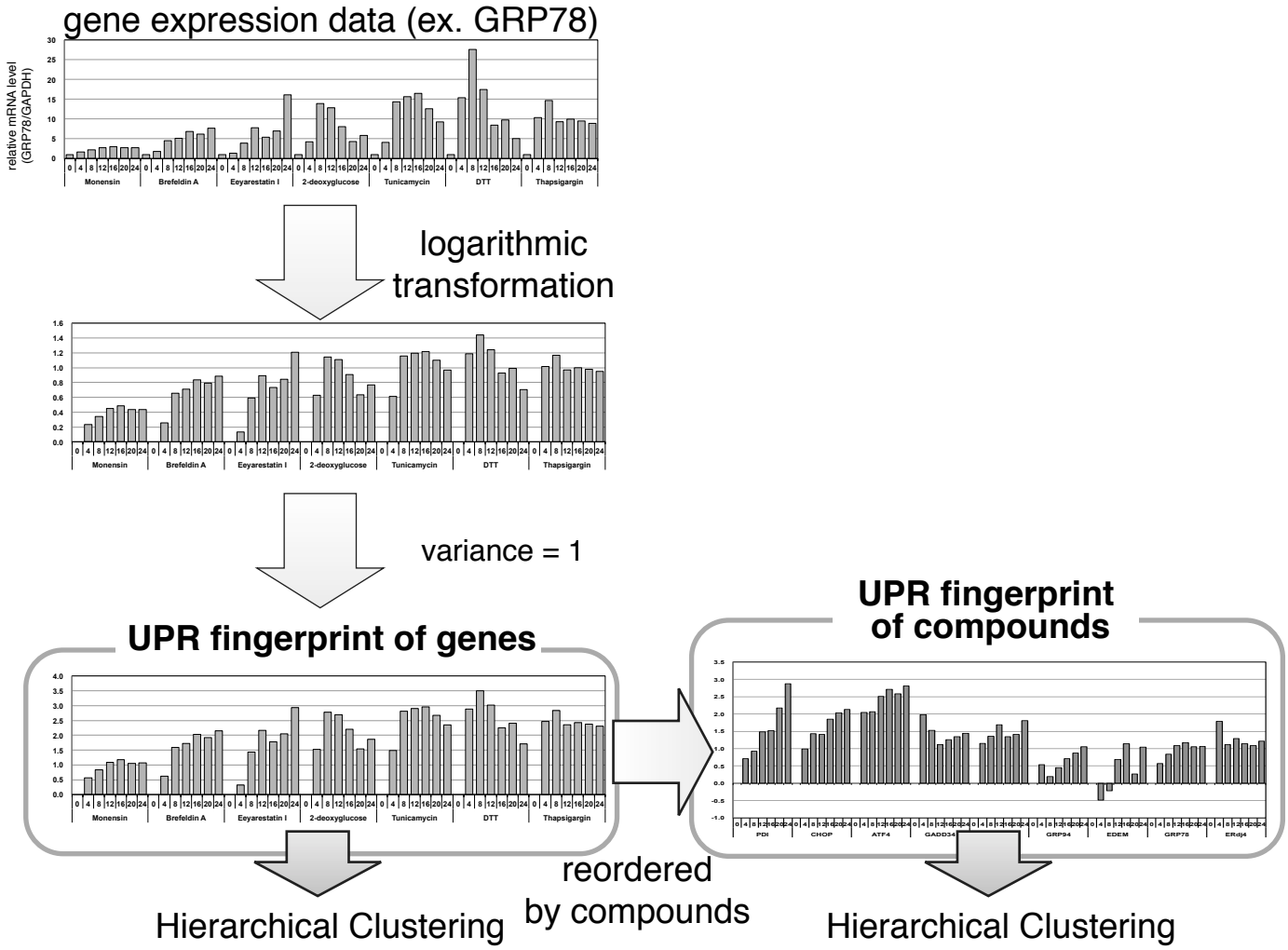

Fig 1-9. Schematic illustration of the method used for data analysis

The relative mRNA levels of each gene were logarithmic transformed and divided by the standard deviation. A “UPR fingerprint of genes” was obtained. The author created a separate “UPR fingerprint of compounds” by reordering the data by compound. Similarities between the two UPR fingerprints (Euclidean distance) were calculated and analyzed using hierarchical clustering.

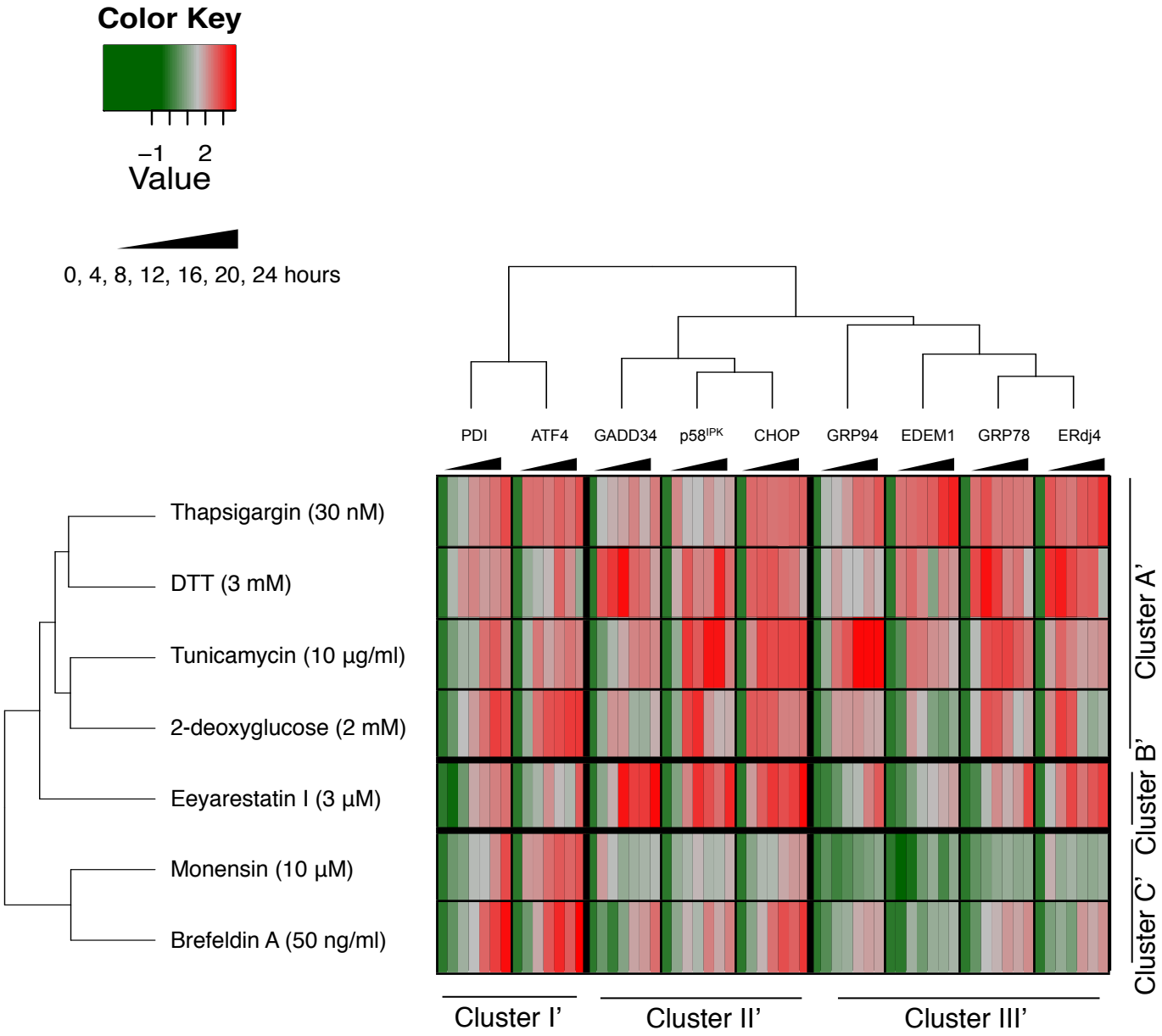

Fig 1-10. Two-dimensional clustering analysis of genes and UPR-inducing compounds on the basis of Euclidean distance.

UPR fingerprints were analyzed using hierarchical cluster analysis. A dataset of 7 compounds or 9 genes was clustered based on the complete-linkage method using Euclidean distance. Rows indicate 7 different small molecular compounds. Columns indicate the 9 UPR target genes, including the 7 different time points. The heat map shows a gradient color scale from green, indicating the score in UPR fingerprint of compounds negative, to red, indicating the the score positive, interpolated over gray for the score zero. The seven compounds and the nine genes were clustered into three and two groups, respectively.

2-2-6. The effects of UPR inducing compounds on the activation of ER stress sensors

Since the genes in Cluster III' were reported to be regulated by ATF6 and IRE1α (Lee et al., 2003; Okada et al., 2002; Wu et al., 2007), it is suggested that the compounds in cluster C' could not activate ATF6 and IRE1α. Therefore, the author examined whether treatment of these compounds activates PERK, ATF6, and IRE1α with detecting the phosphorylation of eIF2α, decrease of inactive form of ATF6, and the splicing of XBP1 mRNA, respectively. As results shown in Fig. 1-11, the compounds in Cluster A', B' and C' induced the phosphorylation of eIF2α indicating that these compounds could activate PERK. As results shown in Fig. 1-12, the compounds in cluster A' and B' decreased the inactive form of ATF6, suggesting these compounds could activate ATF6. On the other hand, the compounds in cluster C' did not decrease the inactive form of ATF6 indicating that these compounds did not or hardly activate ATF6, as suggested. However, as results shown in Fig. 1-13, the compounds in cluster A' induced XBP1 splicing but the compounds in cluster B' and C' hardly induced that; therefore it is suggested that the compounds in cluster A' activated IRE1α but the compounds in cluster B' and C' did not or hardly activated IRE1α. Therefore, in summary, it is suggested that the compounds in cluster A' might activate all of three ER stress sensors, the compounds in cluster B' might activate PERK and ATF6, and the compounds in cluster C' might activate only PERK.

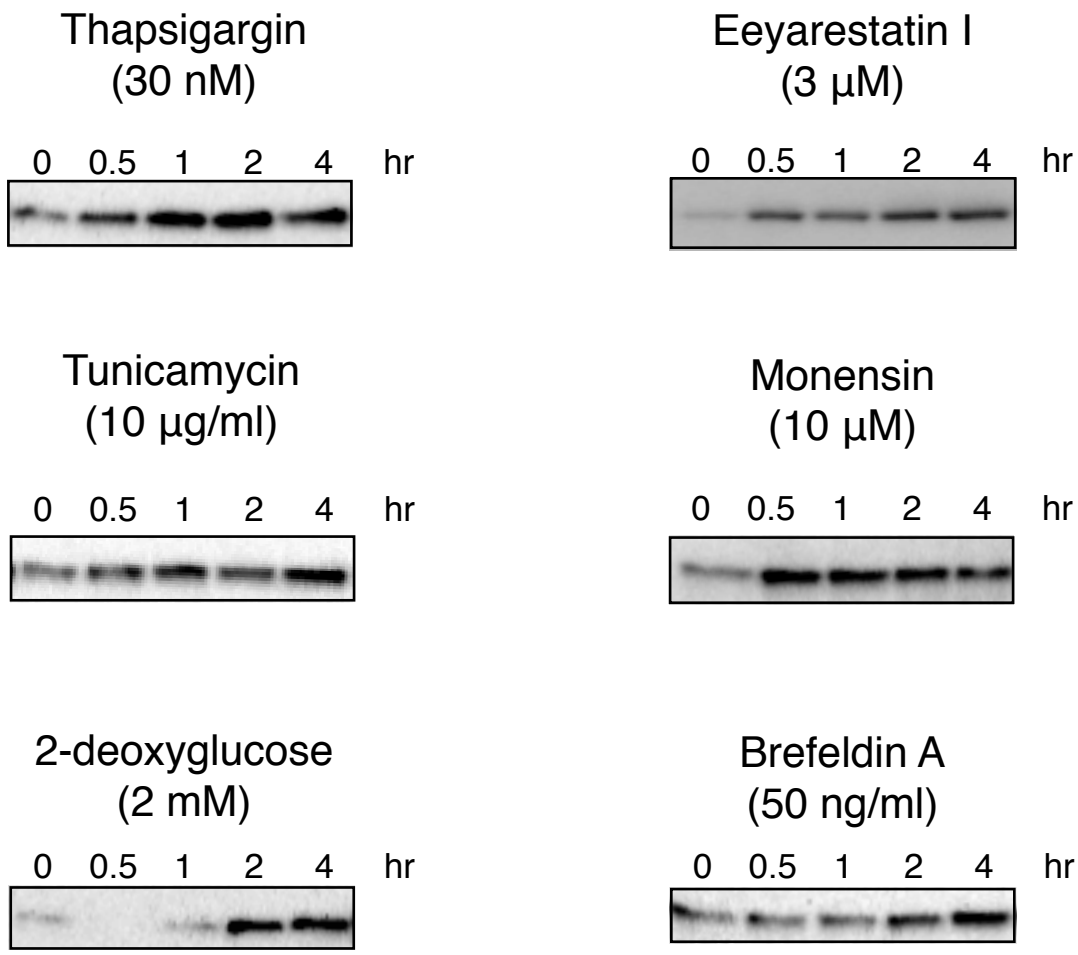

Fig 1-11. Effect of UPR-inducing compounds on the phosphorylation of eIF2α

HeLa cells were treated with 30 nM thapsigargin, 10 μg/ml tunicamycin, 2 mM 2-deoxyglucose, 3 μM eeyarestatin I, 10 μM monensin, or 50 ng/ml brefeldin A for indicated periods. Phospho-eIF2α was detected by immunoblotting.

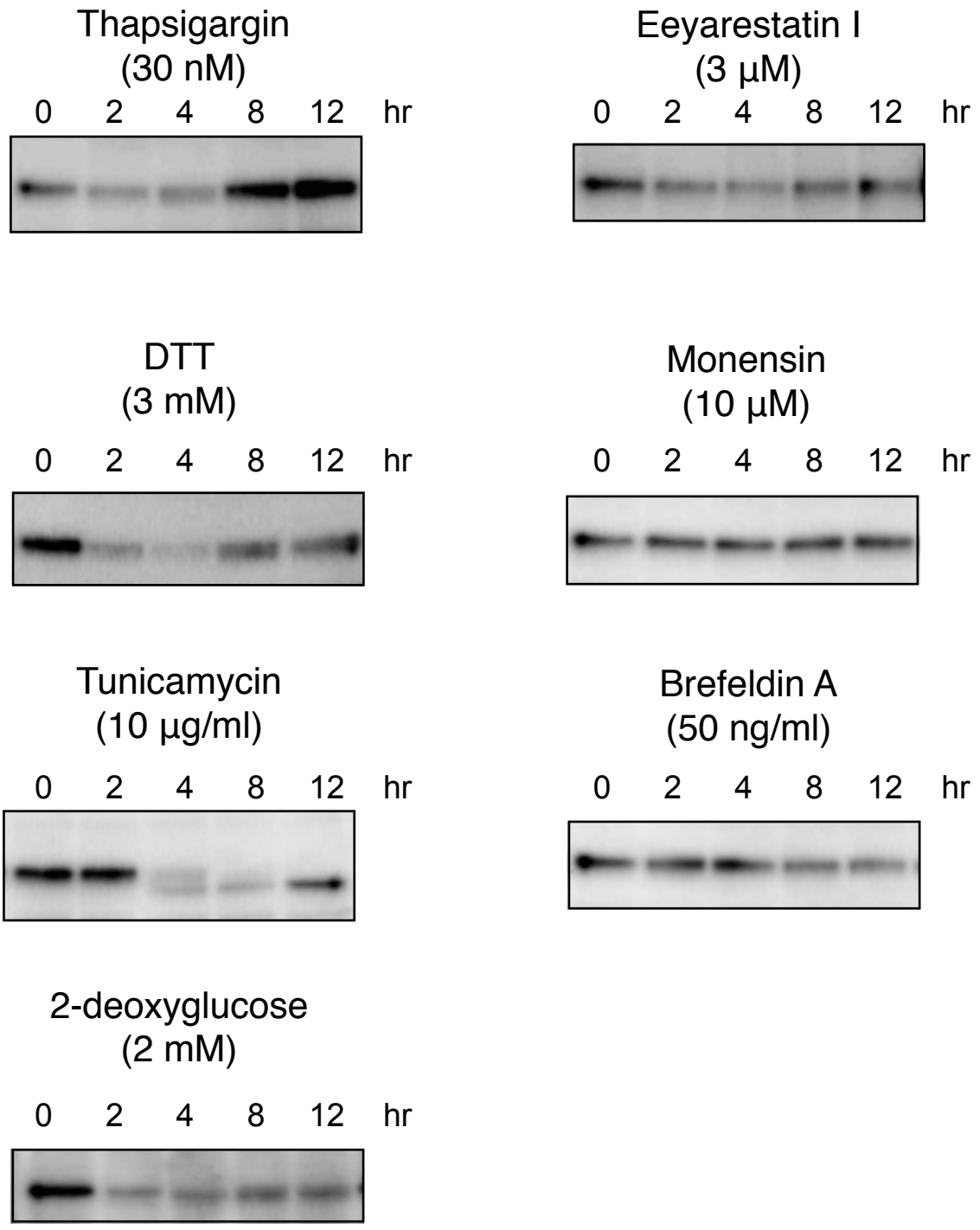

Fig 1-12. Effect of UPR-inducing compounds on the ATF6 activation

HeLa cells were treated with 30 nM thapsigargin, 3 mM DTT, 10 μg/ml tunicamycin, 2 mM 2-deoxyglucose, 3 μM eeyarestatin I, 10 μM monensin, or 50 ng/ml brefeldin A for indicated periods. Inactive form of ATF6 (90 kDa) was detected by immunoblotting.

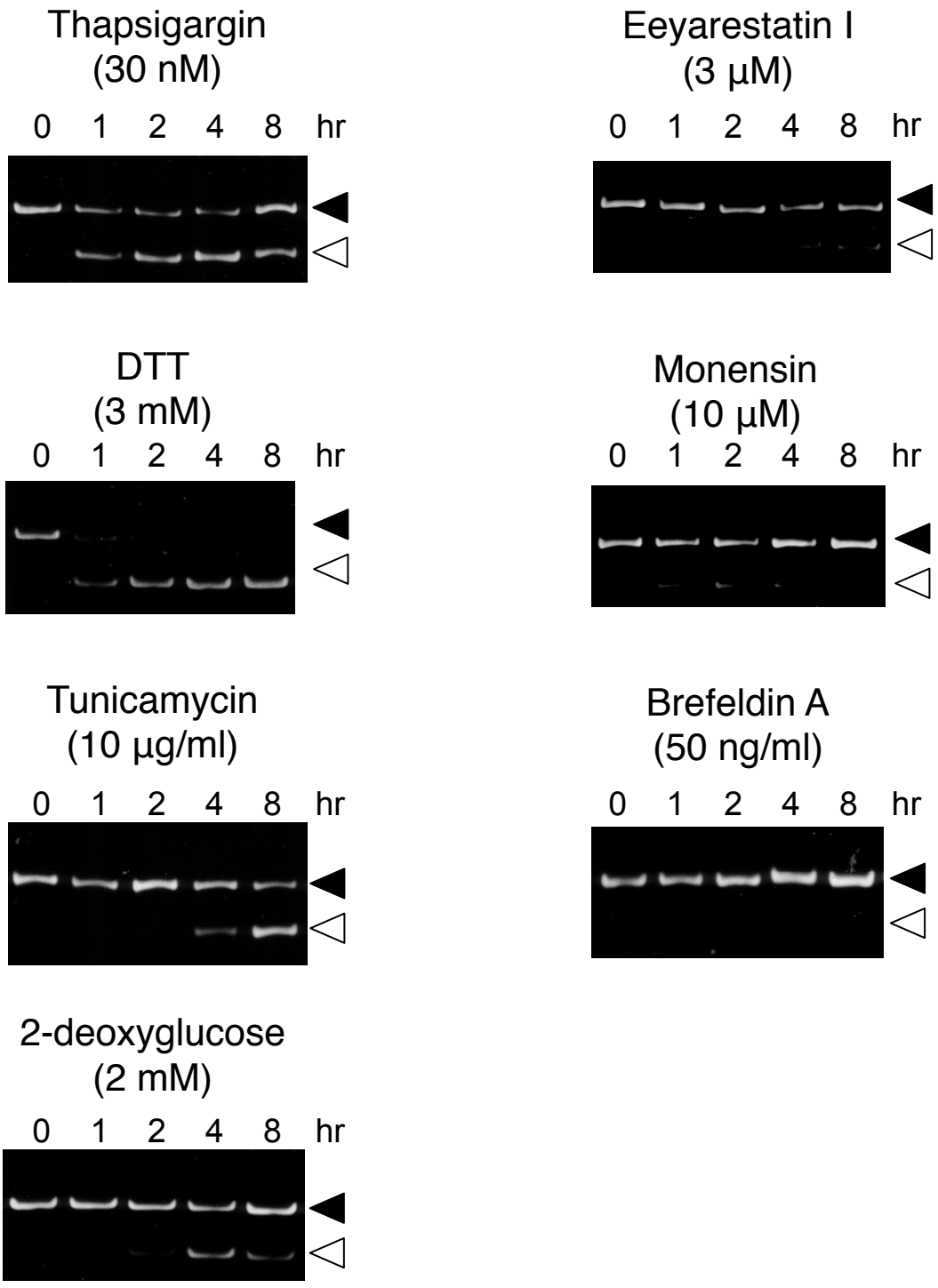

Fig 1-13. Effect of UPR-inducing compounds on the splicing of XBP1 mRNA

HeLa cells were treated with 30 nM thapsigargin, 3 mM DTT, 10 μg/ml tunicamycin, 2 mM 2-deoxyglucose, 3 μM eeyarestatin I, 10 μM monensin, or 50 ng/ml brefeldin A for indicated periods. Spliced- or unspliced-XBP1 mRNA was detected with RT-PCR as described in Materials and methods. Black arrowheads show unspliced inactive form of XBP1 cDNA amplicon (125 bp) and white arrowheads show spliced active form of XBP1 cDNA amplicon (99 bp).

2-3. Discussion

In this study, as a result of hierarchical clustering analysis using Pearson's correlation coefficient, the expression patterns of UPR target genes induced by seven compounds were classified into two clusters. When cells were treated with thapsigargin, tunicamycin, 2-deoxyglucose or brefeldin A at different concentrations, the expression patterns of UPR-target genes were grouped into the same cluster (Fig. 1-8). This suggests that this classification is due to the difference in the mode of action of each compound, rather than its concentrations. On the other hand, upon the treatment of brefeldin A, whereas the protein expression of GRP78 was maximum increase at 50 ng/ml and constant to 5000 ng/ml, the protein expression of GRP94 was maximized at 50 ng/ml and then declined to 5000 ng/ml (Fig. 1-1B). These results suggested that it might have different effect on UPR between 50 ng/ml and 5000 ng/ml of brefeldin A. However, according to the result of hierarchical clustering analysis, the expression pattern of UPR target genes of 5000 ng/ml brefeldin A was most similar to that of 50 ng/ml brefeldin A (Fig. 1-8). Therefore, the difference in the protein expression level of GRP94 between 50 and 5000 ng/ml of brefeldin A might be caused by the degradation rather than the transcriptional regulation of GRP94.

It remains unclear the reason why the compounds in cluster A and B induced different expression patterns of UPR target genes (Fig. 1-8). Since the expression of each UPR target gene is transcriptionally regulated by the activation of the three ER

stress sensors (ATF6, IRE1α, and PERK), it is possible that each of the three ER stress sensors has distinct sensitivity to the compounds belonging to Cluster A and B, resulting in the comparatively higher expression of the genes in Cluster I and II respectively. Therefore, to speculate which of the ER stress sensors were activated by which of the compounds, the author performed another clustering analysis, using Euclidean distance as a similarity. As shown in Fig. 1-10, the compounds in cluster A' and B' up-regulated nine UPR target genes; on the other hands, the compounds in cluster C' hardly up-regulated four of the nine UPR target genes, GRP94, EDEM1, GRP78, and ERdj4, which were classified as cluster III'. Since expression of these genes were reported to be regulated by ATF6 and IRE1α, suggested that the compounds in cluster C' might not or hardly activate ATF6 and IRE1α. The results shown in Figs. 1-11, 1-12 and 1-13, suggested that the compounds in cluster A' might activate all of three ER stress sensors and the compounds in cluster C' might activate only PERK, as expected. However, the compounds in cluster B' was suggested to activate PERK and ATF6, but not IRE1α, which was different from the author's expectation.

The compounds comprising cluster A'—thapsigargin, tunicamycin, 2-deoxyglucose and DTT—showed a distinct mode of action, but they were commonly reported to inhibit the conformational maturation of proteins in the ER (Di Jeso et al., 2003; Fiebiger et al., 2004; Kurtoglu et al., 2007; Parham et al., 1979; Schwarz et al., 1979; Takatsuki et al., 1975), as described in the introduction, leading to the accumulation of

incorrectly folded proteins in the ER. On the other hand, among the compounds classified in cluster C', brefeldin A was reported to accumulate correctly folded conformation of vesicular stomatitis virus G (VSVG) protein, as judged from the detection by I14 antibody, which recognizes only the native or correctly folded conformation of VSVG protein (Lefrancois and Lyles, 1982; Preston et al., 2009). Therefore, it is likely that the compounds in cluster C' induced the expression of UPR target genes by the accumulation of an excess amount of quite correctly folded proteins than incorrectly folded proteins in the ER. If this were the case, the difference in the expression patterns of UPR target genes between cluster A' and C' would be related to the folding status of the accumulated proteins in the ER caused by the compounds in cluster A' and C'. Interestingly, monensin were classified into cluster C', with the expectation that monensin could accumulate an excess amount of correctly folded proteins in the ER. Monensin has been reported to neutralize acidic intracellular compartments such as the trans-Golgi apparatus *via* its ionophore activity, and to inhibit medial- to trans-Golgi protein transport (Dinter and Berger, 1998; Griffiths et al., 1983; Mollenhauer et al., 1990). Therefore, the author cannot exclude the possibility that inhibition of medial- to trans-Golgi protein transport by monensin may affect and abrogate the entire protein transport system, including from the ER to the Golgi apparatus transport, resulting in the accumulation of correctly folded protein in the ER. This possibility was supported by the observation that another polyether K^+/H^+

ionophore, nigericin, which disrupts Golgi function similar to monensin (Craig and Goodchild, 1984; Dinter and Berger, 1998), also up-regulated GRP78 protein expression (Fig. 1-6). Taken together with the suggestions described in the previous paragraph, it is possible that the accumulation of incorrectly folded proteins could activate all of three ER stress sensors, but the accumulation of correctly folded proteins could activate only PERK.

The compound in cluster B', eeyarestatin I, was reported to inhibit ERAD (Fiebiger et al., 2004), indicating that proteins which were failed to form correct conformation were accumulated by eeyarestatin I. On the other hand, since eeyarestatin I was also reported to inhibit protein transport from ER to Golgi apparatus (Aletrari et al., 2011), it is suggested that eeyarestatin I might accumulate both correctly and incorrectly folded proteins in the ER. This might be the reason why eeyarestatin I classified between the compounds in cluster A', which were suggested to accumulate incorrectly folded proteins, and the compounds in cluster C', which were suggested to accumulate correctly folded proteins.

Although UPR was thought to be caused by the accumulation of incorrectly folded proteins from 1980s, in this study, the accumulation of correctly folded proteins was suggested to activate UPR with the different expression pattern of UPR target genes from those induced by the accumulation of incorrectly folded proteins through the activation of PERK. Since the accumulation of correctly folded proteins were not

required to be refolded, it is reasonable that the accumulation of the correctly folded proteins was not thought to activate ATF6 and IRE1α, which regulate the expression of the genes involving protein folding. On the other hand, to recover from the accumulation of correctly folded proteins, the translation attenuation should be induced through the activation of PERK, which is also thought to be reasonable.

To the author's knowledge, although there have been many reports to investigate the regulatory mechanism of each UPR target gene expression by using UPR-inducing compounds, they missed addressing the question whether the difference in mode of action of the UPR-inducing compounds would influence the expression patterns of UPR target genes. This study is the first approach to address this question. Further study is needed to elucidate whether the folding status of the accumulated proteins affects the activation of ER stress sensors, the expression of UPR target genes and consequent responses, such as protein refolding, protein degradation or apoptosis. This would provide a new insight into the regulatory mechanisms of UPR.

2-4. Materials and Methods

2-4-1. Materials

Tunicamycin, 2-deoxyglucose, monensin, and mouse monoclonal anti-β-actin (AC-74) were purchased from Sigma Aldrich (St. Louis, MO, USA). Brefeldin A and DTT were obtained from Calbiochem (San Diego, CA, USA) and Wako Pure Chemical Industries, Ltd. (Osaka, Japan), respectively. Thapsigargin and eeyarestatin I were acquired from Santa Cruz Biotechnology (Santa Cruz, CA, USA). Mouse monoclonal anti-KDEL antibody (10C3) was from ENZO Life Sciences (Farmingdale, NY, USA). Rabbit polyclonal anti-eIF2α and anti-phospho eIF2α antibodies (Ser51) were from Cell Signaling (Beverly, MA, USA). Rabbit polyclonal anti-PERK antibody was obtained from Rockland (Gilbertsville, PA, USA). Horseradish peroxidase-conjugated anti-mouse and anti- rabbit IgG used as a secondary antibody were purchased from GE Healthcare (Little Chalfont, UK).

2-4-2. Cell culture

A human epithelial adenocarcinoma cell line HeLa was cultured in Dulbecco's modified Eagle's medium (DMEM; Nissui, Tokyo, Japan) supplemented with 8% fetal bovine serum at 37 °C in a 5% CO_2–95% air atmosphere.

2-4-3. Western blotting

Cell pellets were lysed using an extraction buffer containing 150 mM NaCl, 2.5 mM EGTA, 1 mM EDTA, 1 mM DTT, 0.1% Tween-20, 10 mM β-glycerophosphate, 1 mM NaF, 0.1 mM Na_3VO_4, 10% glycerol, and 50 mM HEPES (pH 7.5). Lysates were separated by SDS-PAGE and transferred to a PVDF membrane (Millipore, Bedford, MA, USA) by electroblotting. After the membranes had been incubated with primary and secondary antibodies, the immune complexes were detected with an Immobilon Western kit (Millipore), and the luminescence was detected with a LAS-1000 mini CCD camera (Fujifilm, Tokyo, Japan). The visualized bands were quantitated using ImageJ software (http://rsb. info.nih.gov/ij/).

2-4-4. Real-time RT-PCR

Total RNA was extracted from HeLa cells using TRIzol reagent (Life Technologies, Carlsbad, CA, USA). Aliquots of 2 μg of total RNA were treated with M-MLV reverse transcriptase (Promega, Madison, WI, USA) to produce first-strand complementary DNA (cDNA). The synthesized cDNA was subjected to quantitative real-time RT-PCR using SYBR premix Ex Taq (TaKaRa, Shiga, Japan) and detected using the Thermal Cycler Dice Real Time System II (TaKaRa). The data were analyzed using the Smart Cycler software program (Multiplate RQ version 1.00; TaKaRa) with the relative quantification method.

Real-time cycle conditions for ERdj4 were 2 min at 50°C, followed by 10 min at 90°C, and then 45 cycles, with each cycle being 95°C for 30 s, and 63°C for 1 min; the conditions for GAPDH were 10 sec at 95°C and then 35 cycles at each of 95°C for 3 sec, 60°C for 10 sec, and 72°C for 10 sec. RT-PCR conditions for all other genes were 10 sec at 95°C and then 40 cycles, with each cycle being 95°C for 3 sec, 60°C for 10 sec, and 72°C for 15 sec. The sequences of primer sets are shown in Table 1-2.
The amount of total RNA present in each reaction was normalized using GAPDH as an internal control. The data are the average of at least three separate experiments and one outlier was omitted by Dixon's Q-test with 99% confidence level (Dean and Dixon, 1951).

2-4-5. RNA interference

siRNA double-stranded oligonucleotides designed to interfere with the expression of PERK (HSS190343; Life Technologies) and siRNA for a negative control (12935-300; Life Technologies) were used. For transfection for HeLa cells seeded on ϕ60 mm dish, 1.5 μL of siRNA (20 μM) and 3 μL of Lipofectamine (Life Technologies) were diluted in 600 μL of Opti-MEM (Life Technologies) and mixed. After 30 minutes, growth medium was removed from cells and replaced it with 1800 μL of Opti-MEM. Then, the mixture was added to the culture medium. After 4 hours incubation at 37 °C, 600 μL of growth medium containing 40% serum was added to

each well. Twenty-four hours after transfection, cells were trypsinized and seeded to 6-well plates. After another 24 hours, cells were treated with compound and subjected to Western blotting.

2-4-6. Data processing and hierarchical clustering

The acquired data were normalized among genes and named "UPR fingerprints of genes" or then reordered by compound and named "UPR fingerprints of compounds". Pearson's correlation coefficients or Euclidean distance between the UPR fingerprints were calculated and used to determine the degree of similarity. Hierarchical clustering using a complete linkage method was performed using R version 2.13.1. (http://www.R-project.org).

2-4-7. Trypan blue dye exclusion assay

Cells treated with various chemicals were collected and stained with trypan blue solution (NaCl 9g/L, trypan blue (Sigma Aldrich) 4g/L). The ratio of viable cells was determined using a hemocytometer. Cell viability (%) means the ratio of the number of trypan blue-impermeable cells in total cell counts.

2-4-8. RT-PCR for detecting XBP1 mRNA splicing

The first-strand cDNA was subjected to PCR with KOD plus polymerase (Toyobo, Osaka, Japan) using a pair of primers corresponding to nucleotides 505–525 (5'-AATGAAGTGAGGCCAGTGGCC-3') and 609–629 (5'-AATACCGCCAGAATCCATGGG-3') of XBP1 cDNA. The amplified products were separated by electrophoresis on an 8% polyacrylamide gel and visualized by ethidium bromide staining.

Table 1-2: Sequences of primer sets for UPR target genes

Gene Name Accession No.	primer	Product size (bp)
GRP78 NM_005347	Forward: 5'-GCTCGACTCGAATTCCAAAG-3' Reverse: 5'-GATCACCAGAGAGCACACCA-3'	134
ERdj4 NM_012328	Forward: 5'-AAAATAAGAGCCCGGATGCT-3' Reverse: 5'-CGCTTCTTGGATCCAGTGTT-3'	237
EDEM1 NM_014674	Forward: 5'-TGGACTGCAGGTGCTGATAG-3' Reverse: 5'-GGATTCTTGGTTGCCTGGTA-3'	194
$p58^{IPK}$ NM_006260	Forward: 5'-CTCAGTTTCATGCTGCCGTA-3' Reverse: 5'-TTGCTGCAGTGAAGTCCATC-3'	149
GRP94 NM_003299	Forward: 5'-CTGGGTCCAGCAGAAAAGAG-3' Reverse: 5'-CTGGAACCTCTTCCCATCAA-3'	142
GADD34 NM_014330	Forward: 5'-AAACCAGCAGTTCCCTTCCT-3' Reverse: 5'-CTCTTCCTCGGCTTTCTCCT-3'	202
CHOP NM_004083.5	Forward: 5'-GCGCATGAAGGAGAAAGAAC-3' Reverse: 5'-TCACCATTCGGTCAATCAGA-3'	139
PDI NM_000918	Forward: 5'-TCACATCCTGCTGTTCTTGC-3' Reverse: 5'-GTCGCTGTCGATGAAGATGA-3'	117
ATF4 NM_001675	Forward: 5'-TCAAACCTCATGGGTTCTCC-3' Reverse: 5'-GTGTCATCCAACGTGGTCAG-3'	225
GAPDH NM_002046	Forward: 5'-AGGTCGGAGTCAACGGATTT-3' Reverse: 5'-TAGTTGAGGTCAATGAAGGG-3'	111

Chapter 3

Establishment of a New Detection System for the Dimerization of IRE1α by BiFC Assay

3-1. Introduction

As described in Chapter 1, in mammalian cells, UPR is triggered by the activation of three ER stress sensors: ATF6, IRE1α, and PERK. These three ER stress sensors have been reported to display distinct activation behaviors toward different forms of ER stress that are induced by pharmacological agents, DTT, thapsigargin, and tunicamycin (DuRose et al., 2006). Moreover, the previous study described in Chapter 2, in which the author performed the comparative analysis of the expression pattern of UPR target genes induced by several compounds, also suggested that the sensitivity of ER stress sensors might be different among the several UPR-inducing compounds. Therefore, monitoring the activation behavior of ER stress sensors may provide a better understanding of UPR functions in physiological and pharmacological conditions.

Among the three sensors, IRE1 is the most evolutionarily conserved from yeast to mammalian cells (Wang et al., 1998). As illustrated in Fig. 2-1, upon activation the luminal domain of IRE1α undergoes dimerization triggered by dissociation of GRP78 (Bertolotti et al., 2000; Pincus et al., 2010). The dimerization brings the cytosolic Ser/Thr kinase domains into juxtaposition allowing their transautophosphorylation and cofactor binding (Korennykh et al., 2009; Shamu and Walter, 1996), which activates its RNase domain and initiates a non conventional mRNA splicing of XBP1 (Calfon et al., 2002; Yoshida et al., 2001). Translation of spliced form of XBP1 mRNA produces a potent transcription factor, which can up-regulate several UPR target genes (Lee et al.,

2003). Since the dimerization of IRE1α has been reported to be the sufficient and efficient step for the activation (Li et al., 2010; Liu et al., 2000; Liu et al., 2002; Wang et al., 1998; Zhou et al., 2006), the aim of this study is to develop a new detection system for dimerization of IRE1α.

In order to evaluate protein interaction in cultured cells, several methods, biochemical or imaging analyses, are performed. Classical biochemical analysis such as immunoprecipitation is still powerful tool to detect protein interaction, but it lacks subcellular resolution. Moreover, one of the imaging analysis fluorescence resonance energy transfer (FRET) is relatively complex analysis, because both donor and acceptor emission must be monitored to extract the relatively small energy transfer signal from bleedthrough between the detection channels (Rose et al., 2010). On the other hand, BiFC assay has some advantages over these methods. BiFC assay is based on the formation of a fluorescent complex when two proteins fused to non-fluorescent fragments of a fluorescent protein interact with each other. Therefore, BiFC assay enables visualization of protein interactions in living cells with subcellular resolution using the single excitation/emission characteristics of the parent protein (Hu et al., 2002; Hu and Kerppola, 2003). Therefore, the author utilized BiFC assay in order to establish a new detection system for IRE1α dimerization.

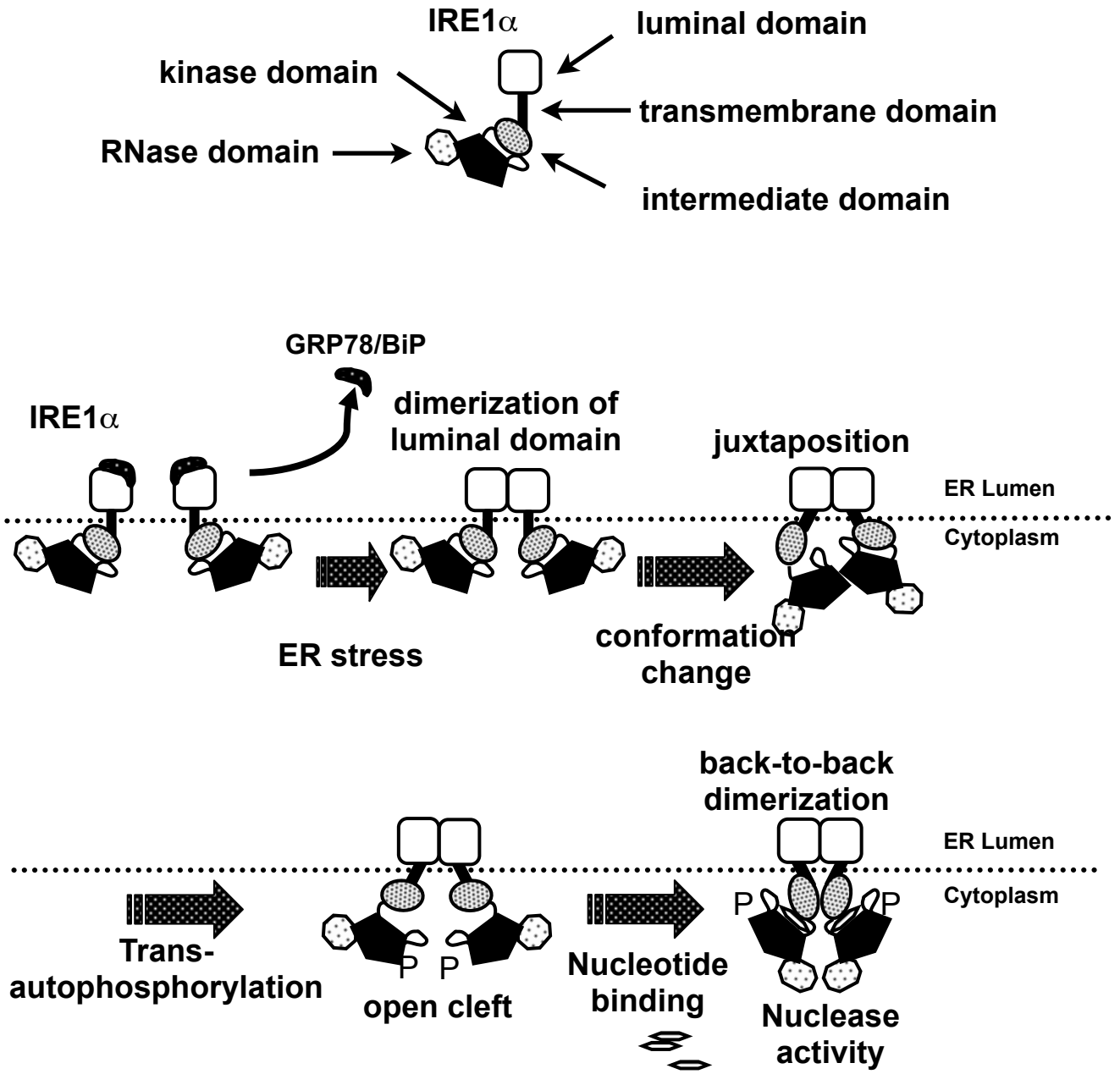

Fig 2-1. Model of IRE1α dimerization induced signaling across the ER membrane

3-2. Results and Discussion

3-2-1. Construction of expressing plasmid of fusion proteins for detecting IRE1α dimerization

To detect dimerization of IRE1α with BiFC method, the author constructed twelve pairs of IRE1α-fused-cerulean-fragment (named IRE1α-BiFC constructs) expressing plasmid (illustrated in Fig. 2-2). Since IRE1α dimerizes at its luminal domain, which locates in N-terminal domain (Liu et al., 2000), the author also constructed the plasmid coding N-terminal domain of IRE1α fused to either N-terminal or C-terminal domain of blue fluorescent protein cerulean. Furthermore, since Li et al. inserted GFP between the transmembrane domain and the kinase domain of IRE1α (Li et al., 2010), the author inserted cerulean fragment to the same position. These pairs of constructs were transfected to HEK293T cells and the expression of constructs was validated with Western blotting (Fig. 2-3). To examine whether the cells were fluorescent or not, the ratio of the cells which exhibited fluorescence (hereafter designated as BiFC-positive cells) were calculated as described in section 3-3-9. As a result, the ratio of BiFC-positive cells was significantly increased in the cells that were transfected with pairs of the constructs possessing kinase and RNase domain deletion mutant of IRE1α (no. 7-9) (Fig 2-4), whereas there was no significant difference between with or without treatment of DTT.

Since in HEK293T cells overexpression of IRE1α has been shown to induce dimerization of IRE1α and subsequent splicing of XBP1 mRNA (Ri et al., 2012) (Fig. 2-5), it is suggested that the overexpression of the fusion proteins would also induce spontaneous dimerization of the fusion proteins due to the high level expression of the proteins. However, in HeLa cells the overexpression of IRE1α did not induce splicing of XBP1 mRNA (Fig. 2-6), it is expected that the spontaneous dimerization of the fusion proteins in HeLa cells would be less than in HEK293T cells. Therefore, HeLa cells were transfected with the plasmids encoding fusion protein pairs no. 7-9 and the expression of each fusion protein was validated with Western blotting (Fig. 2-7). As a result of confocal microscopy, HeLa cells that were transfected with these constructs showed approximately 50% BiFC-positive ratio (Fig. 2-8). Moreover, the ratio of BiFC-positive cells was increased by the treatment of DTT only in the cells transfected with the pair of fusion proteins no.7 (IRE1αΔKR-cerN and –cerC) with statistical significance ($p<0.05$). Since the fluorescence of cerulean was not observed in HeLa cells that expressed each of IRE1αΔKR-cerN and –cerC with or without DTT (Fig. 2-9), it is suggested that the fluorescence of cerulean, which observed in DTT-treated HeLa cells that transiently expressed both IRE1αΔKR-cerN and –cerC, was thought to be a result of hetero-dimerization of IRE1αΔKR-cerN and –cerC. However, the increase of the ratio of BiFC-positive cells in the IRE1αΔKR-cerN and –cerC transfected cells upon treatment of DTT was little, which might be caused by the still high expression

levels of the fusion proteins in individual cell which is enough to dimerize them spontaneously, even in HeLa cells.

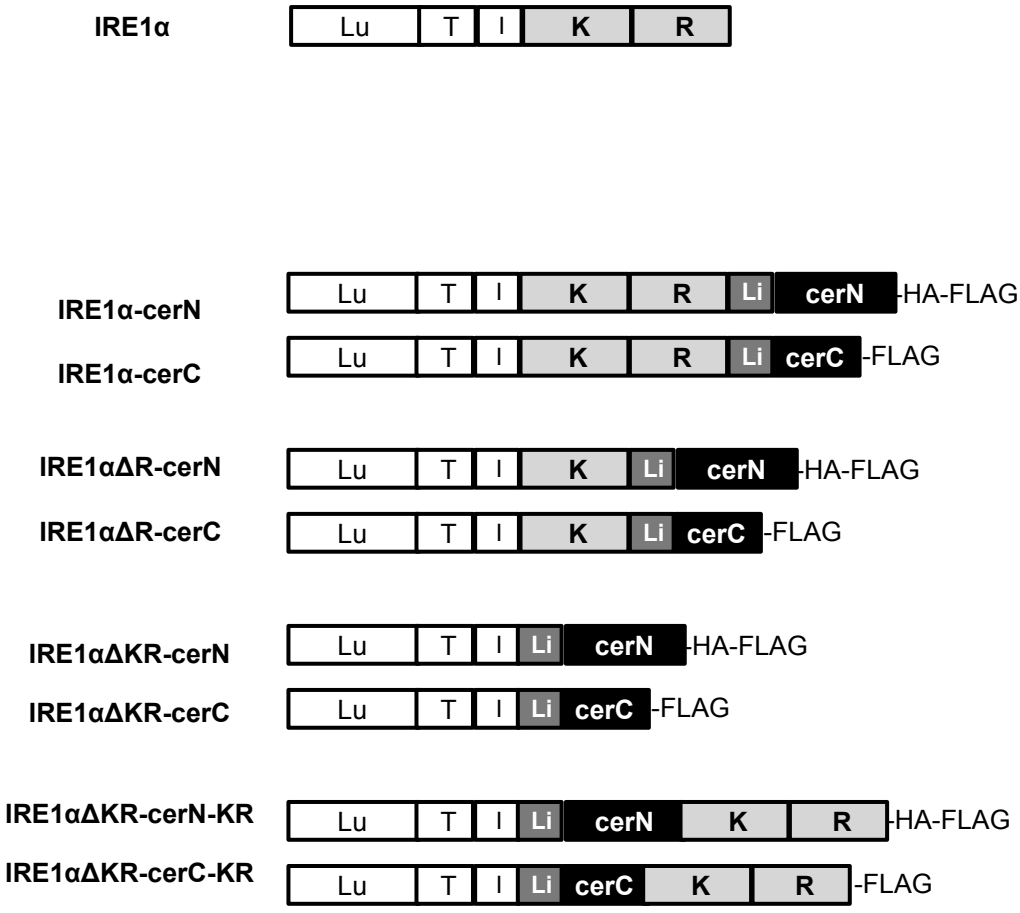

linker		
none	RSIAT	GC linker
no.1	no.2	no.3
no.4	no.5	no.6
no.7	no.8	no.9
no.10	no.11	no.12

Fig 2-2. Design of IRE1α BiFC constructs

Schematic illustration of the fusion proteins designed for detection of IRE1α dimerization with BiFC assay. Lu; luminal domain, T; transmembrane domain, I; intermediate domain, K; kinase domain, R; RNase domain, cerN; N-term fragment of cerulean (1-152 a.a.), cerC; C-term fragment of cerulean (155-239 a.a.), Li; linker sequence. Number shown in the table on the right is the name of the pair of fusion proteins.

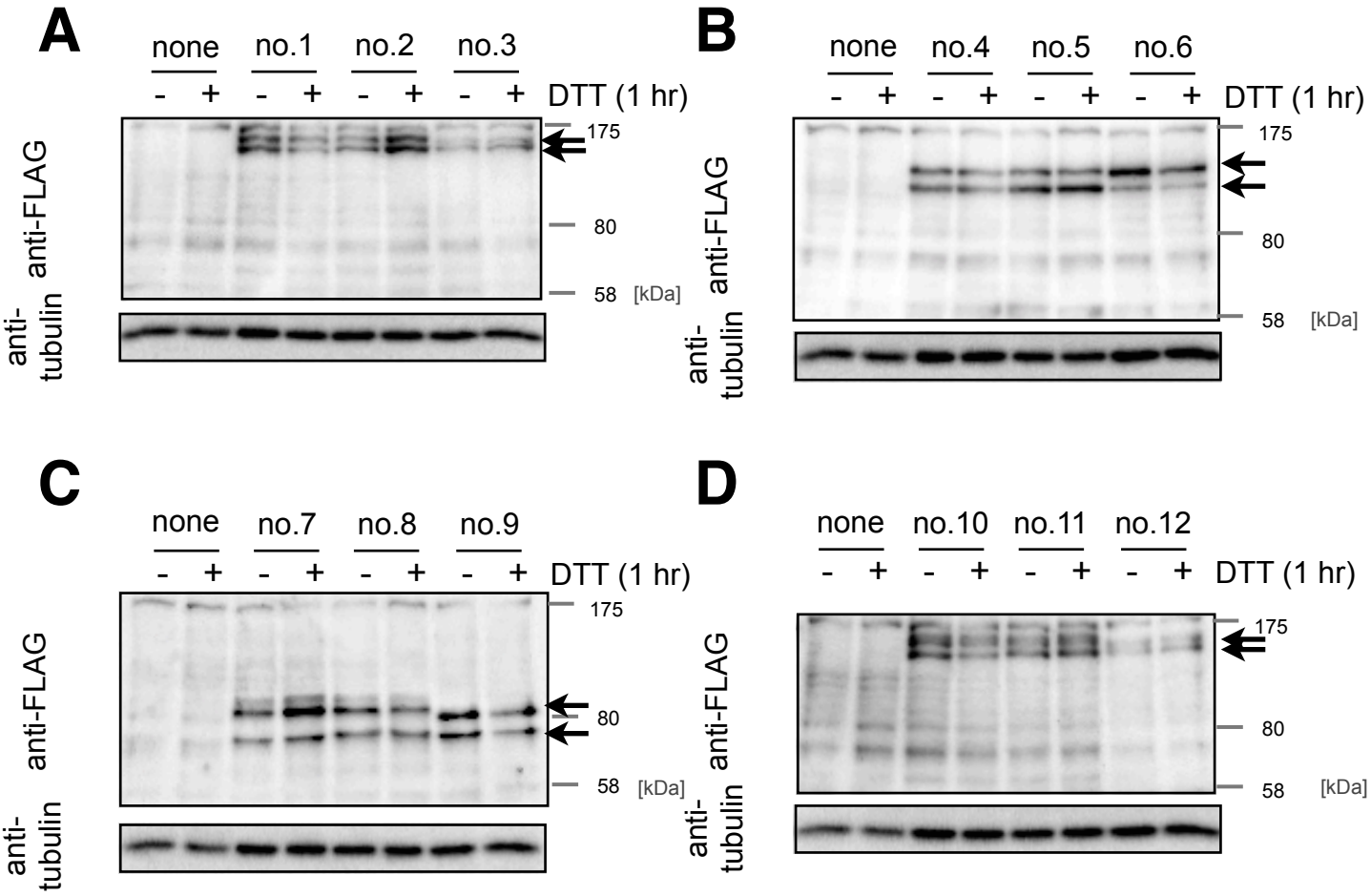

Fig 2-3. Expression of IRE1α BiFC constructs in HEK293T cells

(A-D) HEK293T cells were transiently transfected with indicated constructs. After 24 hours, the cells were treated with 0.3 mM DTT for 1 hour. The cells were lysed and the lysates were subjected to western blotting using the indicated antibodies. The arrow indicates the constructs. Tubulin was immunoblotted as a loading control.

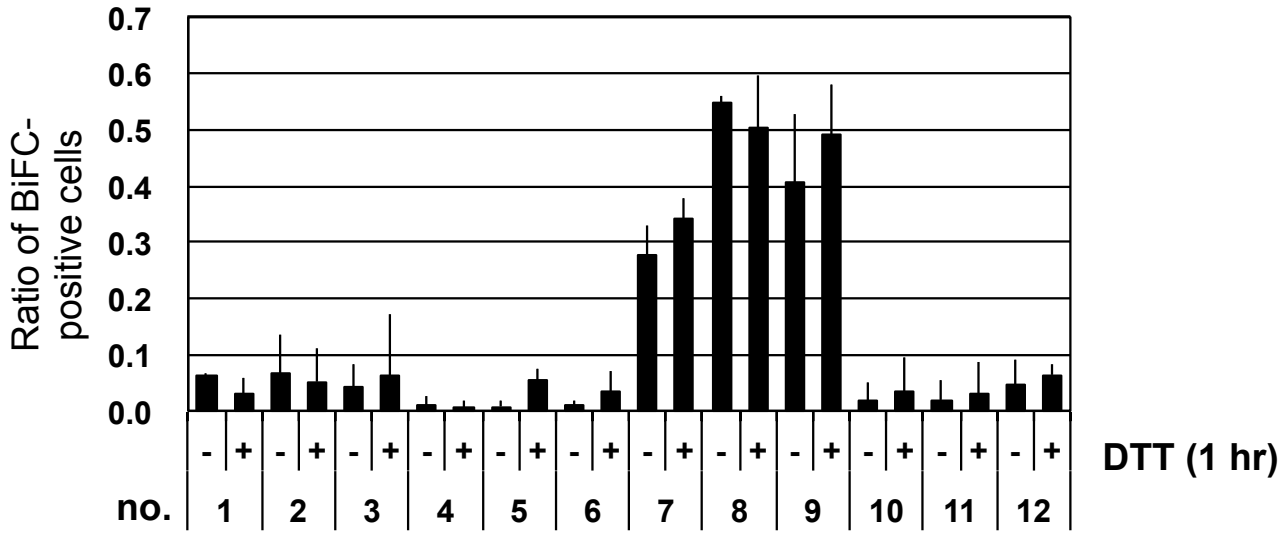

Fig 2-4. Detection of fluorescence derived from cerulean in HEK293T cells expressing IRE1α BiFC constructs

HEK293T cells were transiently transfected with indicated constructs. After 24 hours, the cells were treated with 0.3 mM DTT for 1 hour. The cells were fixed and immunostained using FLAG antibody, and observed under confocal microscope. The ratio of BiFC-positive cells was calculated as described in Materials and methods. Values are the means of three independent determinations. Bars, SD.

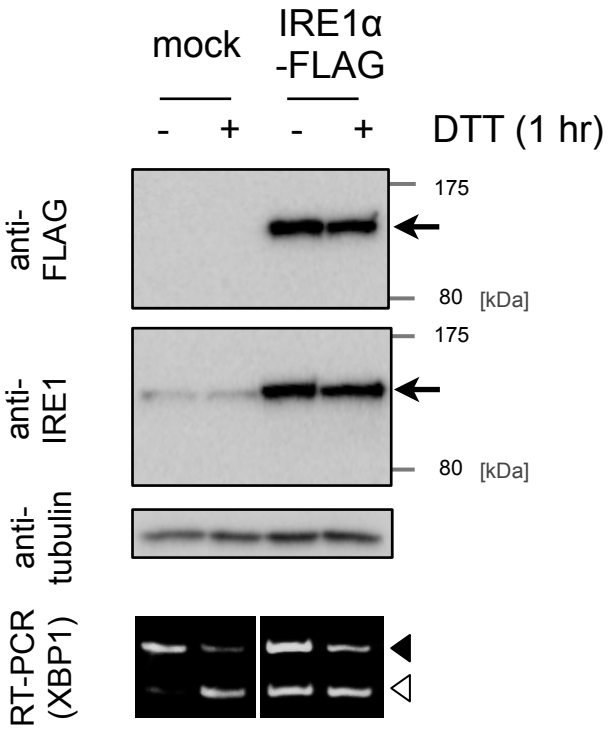

Fig 2-5. Effect of IRE1α-FLAG overexpression on the splicing of XBP1 mRNA in HEK293T cells

HEK293T cells were transiently transfected with indicated constructs. After 24 hours, the cells were treated with 0.3 mM DTT for 1 hour. (upper three panel) The cells were lysed and the lysates were subjected to western blotting using the indicated antibodies. The arrows indicate the IRE1α-FLAG. Tubulin was immunoblotted as a loading control.(lower panel) The cells were collected and RNA extracted. Spliced- or unspliced-XBP1 mRNA was detected with RT-PCR as described in Materials and methods. Black arrowhead shows unspliced inactive form of XBP1 cDNA amplicon (125 bp) and white arrowhead shows spliced active form of XBP1 cDNA amplicon (99 bp).

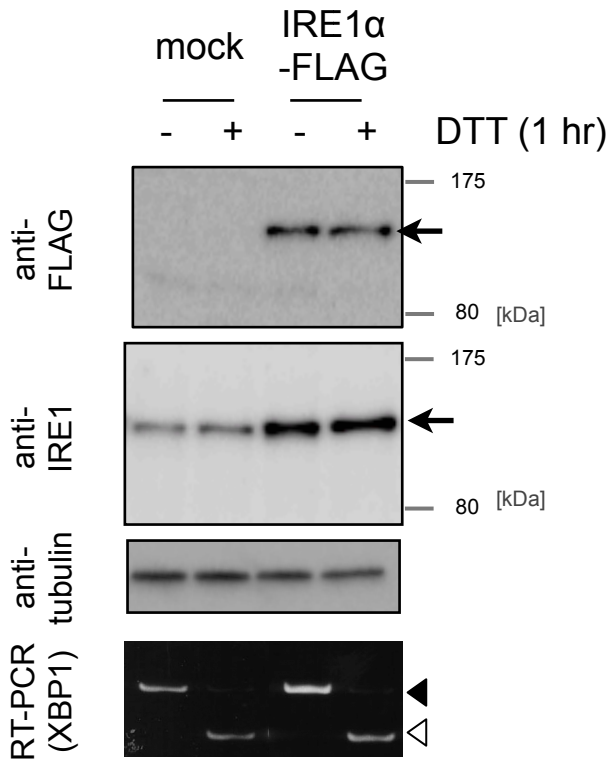

Fig 2-6. Effect of IRE1α-FLAG overexpression on the splicing of XBP1 mRNA in HeLa cells

HeLa cells were transiently transfected with indicated constructs. After 24 hours, the cells were treated with 3 mM DTT for 1 hour. (upper three panel) The cells were lysed and the lysates were subjected to western blotting using the indicated antibodies. The arrows indicate the IRE1α-FLAG. Tubulin was immunoblotted as a loading control.(lower panel) The cells were collected and RNA extracted. Spliced- or unspliced-XBP1 mRNA was detected with RT-PCR as described in Materials and methods. Black arrowhead shows unspliced inactive form of XBP1 cDNA amplicon (125 bp) and white arrowhead shows spliced active form of XBP1 cDNA amplicon (99 bp).

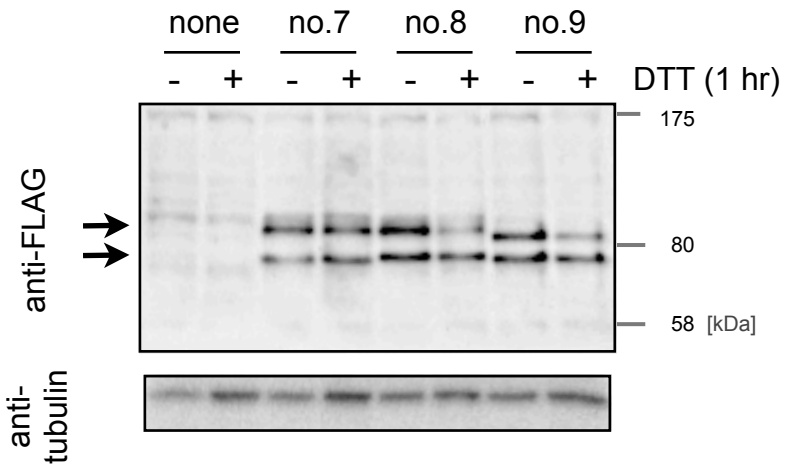

Fig 2-7. Expression of IRE1α BiFC constructs in HeLa cells

HeLa cells were transiently transfected with indicated constructs. After 24 hours, the cells were treated with 3 mM DTT for 1 hour. The cells were lysed and the lysates were subjected to western blotting using the indicated antibodies. The arrows indicate the constructs. Tubulin was immunoblotted as a loading control.

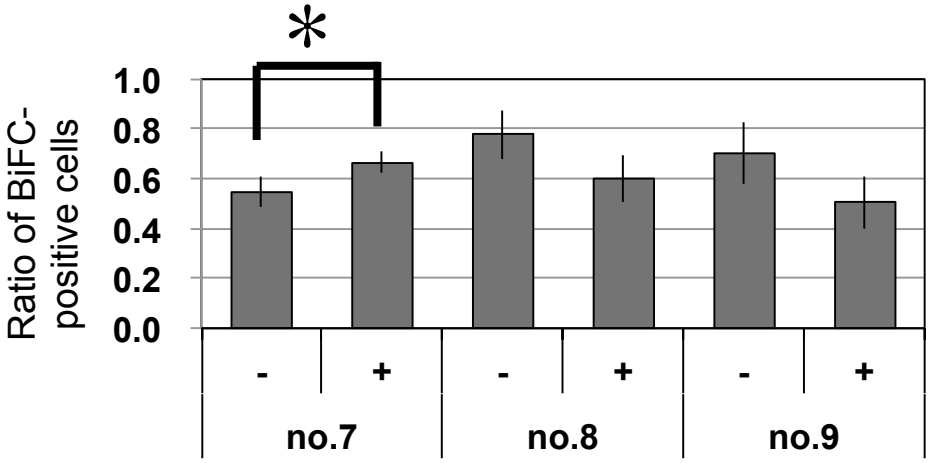

Fig 2-8. Detection of cerulean fluorescent in HeLa cells expressing IRE1α BiFC constructs

HeLa cells were transiently transfected with indicated constructs. After 24 hours, the cells were treated with 3 mM DTT for 1 hour. The cells were fixed and immunostained using FLAG antibody, and observed under confocal microscope. The ratio of CFP fluorescing cells was calculated as described in Materials and methods. Values are the means of three independent determinations. Bars, SD. *, $p < 0.05$.

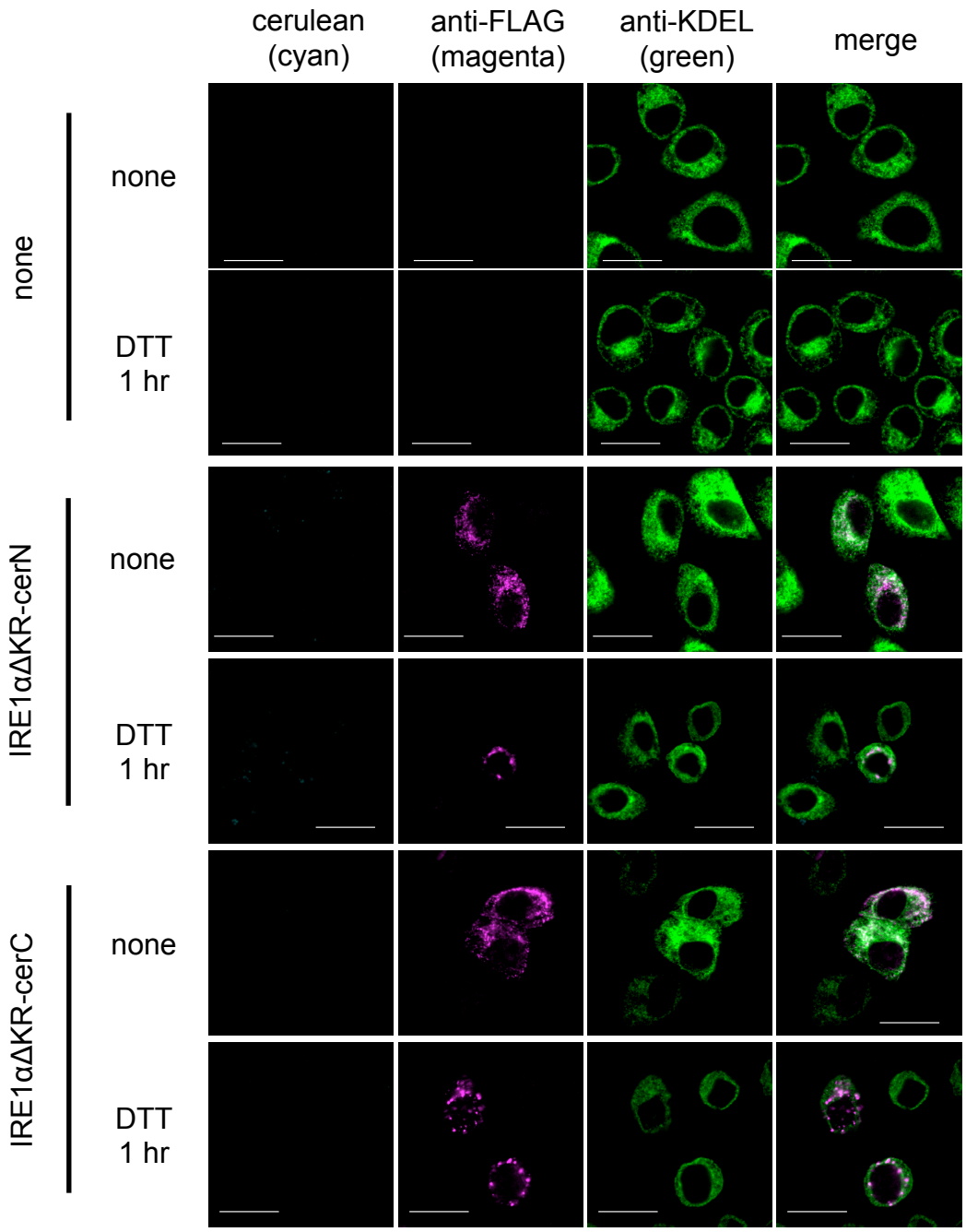

Fig 2-9. Detection of IRE1αΔKR-cerN and IRE1ΔαKR-cerC

HeLa cells were transiently transfected with plasmid expressing indicated fusion proteins. After 24 hours, the cells were treated with 3 mM DTT for 1 hour. The cells were fixed and immunostained using the indicated antibodies, and the photos were taken under confocal microscope. Scale bar, 20 μm. Throughout, the data was representative of at least three independent studies.

3-2-2. Establishment of IRE1αΔKR-cerN and -cerC stably expressing cells

The author next tried to establish IRE1αΔKR-cerN and -cerC expressing stable clone derived from HeLa cells (named HeLa/IRE1α-BiFC cells). In order to express two fusion proteins from one plasmid, the sequence encoding IRE1αΔKR-cerN and -cerC were linked with 2A peptide of TaV (Szymczak et al., 2004), designated as IRE1αΔKR-cerN-2A-IRE1αΔKR-cerC (Fig. 2-10). The author transfected plasmid encoding IRE1αΔKR-cerN-2A-IRE1αΔKR-cerC to HeLa cells, selected neomycin resistant cells. Two independently isolated HeLa transfectants, designated "HeLa/IRE1α-BiFC#5" and "HeLa/IRE1α-BiFC#10", were shown to express both IRE1αΔKR-cerN and -cerC by Western blotting using anti-FLAG antibody (Fig. 2-11). Both IRE1αΔKR-cerN and –cerC were detected as double bands (Fig. 2-11). Since previous studies have reported that a cytoplasmic domain deletion mutant of IRE1α was detected as double bands in Western blot analysis due to the glycosylation at Asn-176 (Liu et al., 2002; Tirasophon et al., 1998), it is likely that the faster and slower migrating form of both IRE1αΔKR-cerN and –cerC are non-glycosylated and glycosylated proteins, respectively. Since it has been reported that IRE1α is localized in the ER (Wang et al., 1998) (Fig. 2-12), the author examined whether IRE1αΔKR-cerN and -cerC localized in the ER by immunofluorescence. As a result, IRE1αΔKR-cerN and –cerC showed perinuclear staining for anti-FLAG, which overlapped with the staining with anti-KDEL antibody that recognized some of the ER chaperones such as

GRP78 and 94. This result indicated that the fusion proteins were expressed in the ER of HeLa/IRE1α-BiFC#5 and #10 cells (Fig. 2-13).

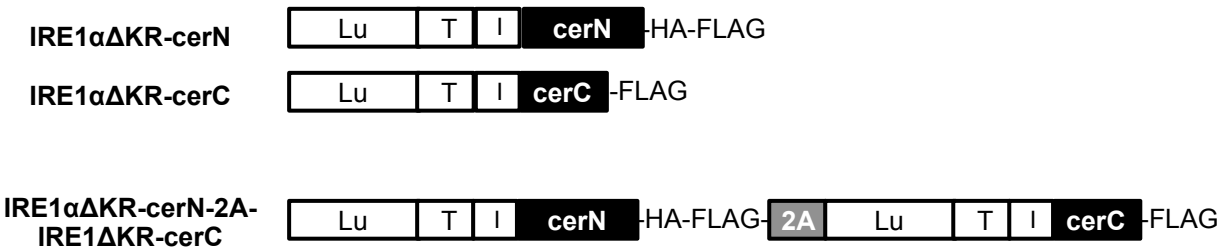

Fig 2-10. Construction of IRE1αΔKR-cerC-2A-IRE1αΔKR-cerN encoding plasmids

Schematic illustration of the fusion proteins designed for detection of IRE1α dimerization with BiFC assay. Lu; luminal domain, T; transmembrane domain, I; intermediate domain, K; kinase domain, R; RNase domain, cerN; N-term fragment of cerulean (1-154 a.a.), cerC; C-term fragment of cerulean (155-239 a.a.), 2A; 2A peptide sequence of TaV.

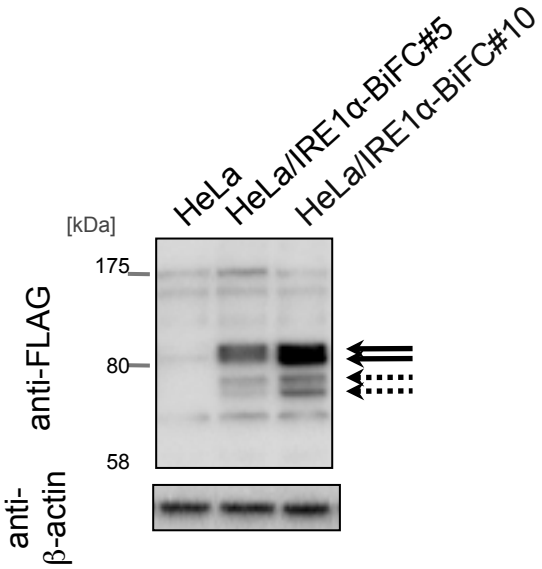

Fig 2-11. Expression of IRE1αΔKR-cerC and IRE1αΔKR-cerN in HeLa/IRE1α-BiFC cells

HeLa, HeLa/IRE1α-BiFC#5 or HeLa/IRE1α-BiFC#10 cells were lysed and the expression of each construct was detected by western blotting using anti-FLAG antibody. The arrows with solid line and dotted lines indicate IRE1αΔKR-cerN and IRE1αΔKR-cerC, respectively. β-actin was immunoblotted as a loading control.

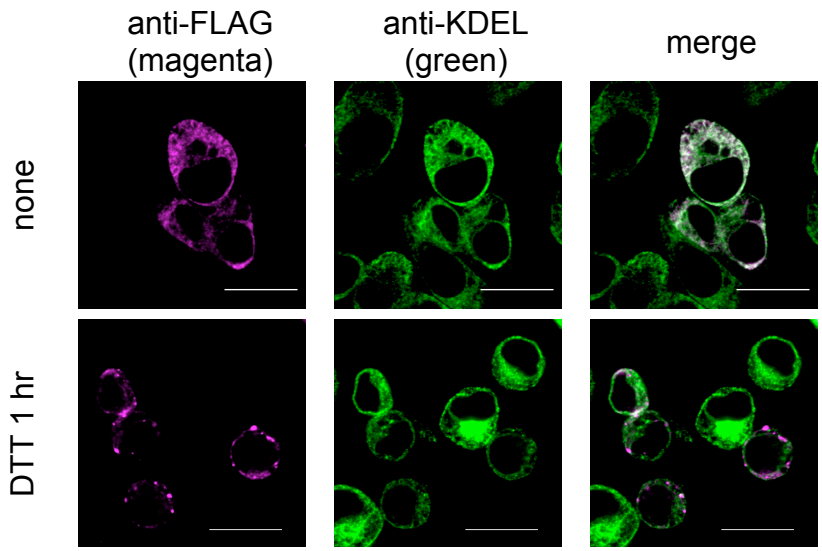

Fig 2-12. Localization of exogenous IRE1α transfected in HeLa cells

HeLa cells were transiently transfected with IRE1α-FLAG. After 24 hours, the cells were treated with 3 mM DTT for 1 hour. The cells were fixed and immunostained using the indicated antibodies, and the photos were taken under confocal microscope. Scale bar, 20 μm.

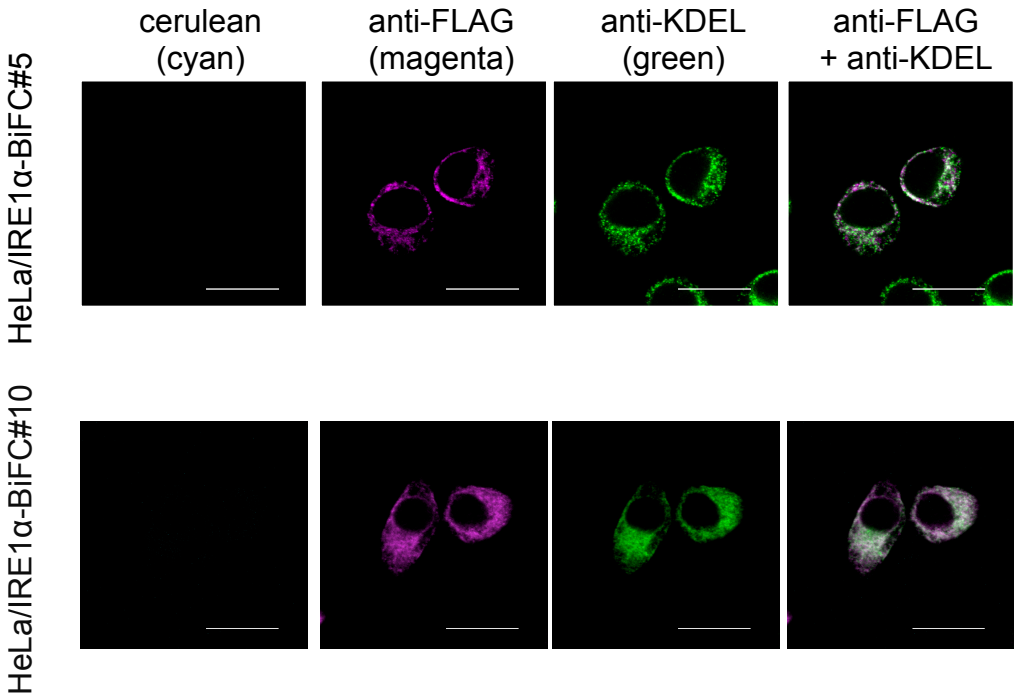

Fig 2-13. Localization of IRE1αΔKR-cerC and IRE1αΔKR-cerN in HeLa/IRE1α-BiFC cells

HeLa/IRE1α-BiFC#5 or #10 cells were fixed and immunostained using the indicated antibodies, and the photos were taken under confocal microscope. Scale bar, 20 μm. The data was representative of at least three independent studies.

3-2-3. Detection of reconstitution of cerulean induced by DTT in HeLa/IRE1α-BiFC cells

Next, the author examined whether the fluorescence derived from cerulean was observed in HeLa/IRE1α-BiFC#5 and #10 cells in response to treatment with DTT. The dimerization of IRE1α was observed after a 1-hour treatment with 3 mM DTT, evaluated by immunoprecipitation in HeLa cells transfected with IRE1α-HA and IRE1α-FLAG expressing plasmids (Fig. 2-14). Therefore, HeLa/IRE1α-BiFC cells were treated with 3 mM DTT for 1 hour, stained with anti-FLAG antibody and observed under a confocal microscope. Whereas the fluorescence derived from cerulean was hardly detected in HeLa/IRE1α-BiFC#5 and #10 cells under normal culture condition, it could be observed in DTT-treated HeLa/IRE1α-BiFC#5 and #10 cells, which showed a dot-like distribution, referred to as "foci" (Fig. 2-15). Furthermore, IRE1αΔKR-cerN and –cerC, which were stained by anti-FLAG, also formed foci and the staining was overlapped with the fluorescence derived from cerulean (Fig. 2-15). Foci formation of IRE1α has been reported to be detected after treatment with tunicamycin or DTT, which is caused by the oligomerization subsequent to the dimerization of IRE1α, because the foci formation is impaired by the dimerization-disrupted mutant of IRE1α (Li et al., 2010). Therefore, the cerulean fluorescence observed in HeLa/IRE1α-BiFC#5 and #10 cells is considered to be the consequence of IRE1α dimerization, as judged from its overlapping with foci.

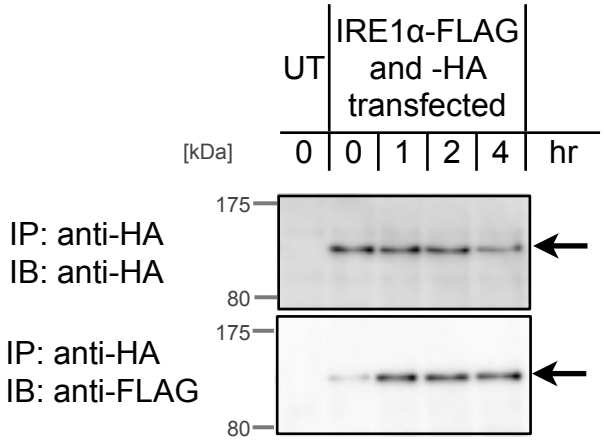

Fig 2-14. Exogenous IRE1α dimerizes by treatment of DTT

HeLa cells were transiently transfected with IRE1α-HA and –FLAG. After 24 hours, the cells were treated with 3 mM DTT for 1-4 hours. The cells were lysed, and the protein complexes were precipitated with anti-HA antibody. The immunoprecipitants were subjected to Western blotting using the indicated antibodies. Throughout, the data were representative of three independent studies.

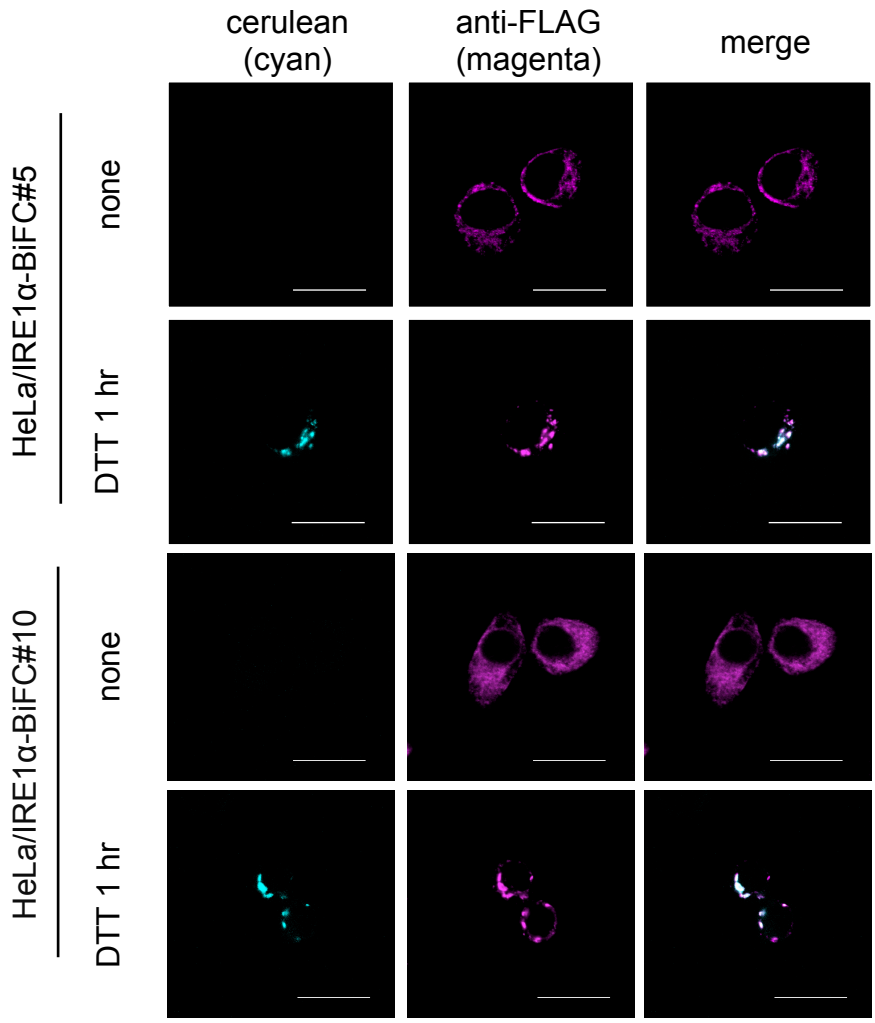

Fig 2-15. Localization of IRE1αΔKR-cerC and IRE1αΔKR-cerN in HeLa/IRE1α-BiFC cells

HeLa/IRE1α-BiFC#5 or #10 cells were treated with 3 mM DTT for 1 hour. Then the cells were fixed and immunostained using the indicated antibodies, and the photos were taken under confocal microscope. Scale bar, 20 μm. The data was representative of at least three independent studies.

3-2-4. Effect of small molecules on reconstitution of cerulean in HeLa/IRE1α-BiFC cells

Furthermore, the author examined whether the fluorescence derived from the reconstituted cerulean was observed in HeLa/IRE1α-BiFC#5 cells which treated with other ER stress inducers, i.e. thapsigargin, tunicamycin, or 2-deoxyglucose. Similar to DTT, the fluorescence induced by thapsigargin, tunicamycin, or 2-deoxyglucose also resulted in the formation of foci, which overlapped with the staining by anti-FLAG (Fig. 2-16). On the other hand, non-ER stress inducers (Gotoh et al., 2002; Nakagawa et al., 2000), i.e. camptothecin, an inhibitor of topoisomerase I, and staurosporine, a kinase inhibitor, induced neither foci formation nor the reconstitution of cerulean (Fig. 2-16) even at the concentrations that inhibited the growth of HeLa cells (Aparicio-Fernandez et al., 2006; Muroi et al., 2010). These results indicated that IRE1α dimerization could be easily detected by the fluorescence derived from the reconstituted cerulean in HeLa/IRE1α-BiFC#5 cells.

In order to quantify the reconstitution of cerulean, the author next calculated the ratio of the cells that exhibited fluorescence (hereafter designated as BiFC-positive cells). As a result, the ratio of BiFC-positive cells was significantly increased approximately two-folds by the treatment of DTT and the ratio was quite constant for 1-8 hours (Fig. 2-17A). These results were consistent with the result of immunoprecipitation, which showed that IRE1α formed dimerization by 1-4 hours DTT

treatment constantly (Fig. 2-14). Moreover, thapsigargin also increased the ratio of BiFC-positive cells, which was constant when measured at time points from 1 to 8 hours treatment, with statistical significance, while tunicamycin and 2-deoxyglucose time-dependently and significantly increased the ratio of BiFC-positive cells after treatment for 4 hours (Figs. 2-18, 19, 20A). To examine when endogenous IRE1α was activated upon treatment with these compounds, the author performed RT-PCR to detect splicing of XBP1 mRNA, a downstream event of IRE1α dimerization. As a result, the ratio of BiFC-positive cells was increased at the same time as or prior to the splicing of XBP1 mRNA (Figs. 2-18, 19, 20B). Therefore, the ratio of BiFC-positive cells is suggested to reflect the activation of endogenous IRE1α. Moreover, these observations were consistent with the previous report by DuRose et al., which indicated that the activation of IRE1α induced by tunicamycin was slower than that induced by DTT and thapsigargin (DuRose et al., 2006). On the other hand, camptothecin and staurosporine, non-ER stress inducers, increased neither the ratio of BiFC-positive cells nor the splicing of XBP1 mRNA at any time point measured between 1 and 8 hours (Figs. 2-21, 22). These results further confirmed that the fluorescence derived from the reconstituted cerulean in HeLa/IRE1α-BiFC cells would reflect endogenous IRE1α dimerization.

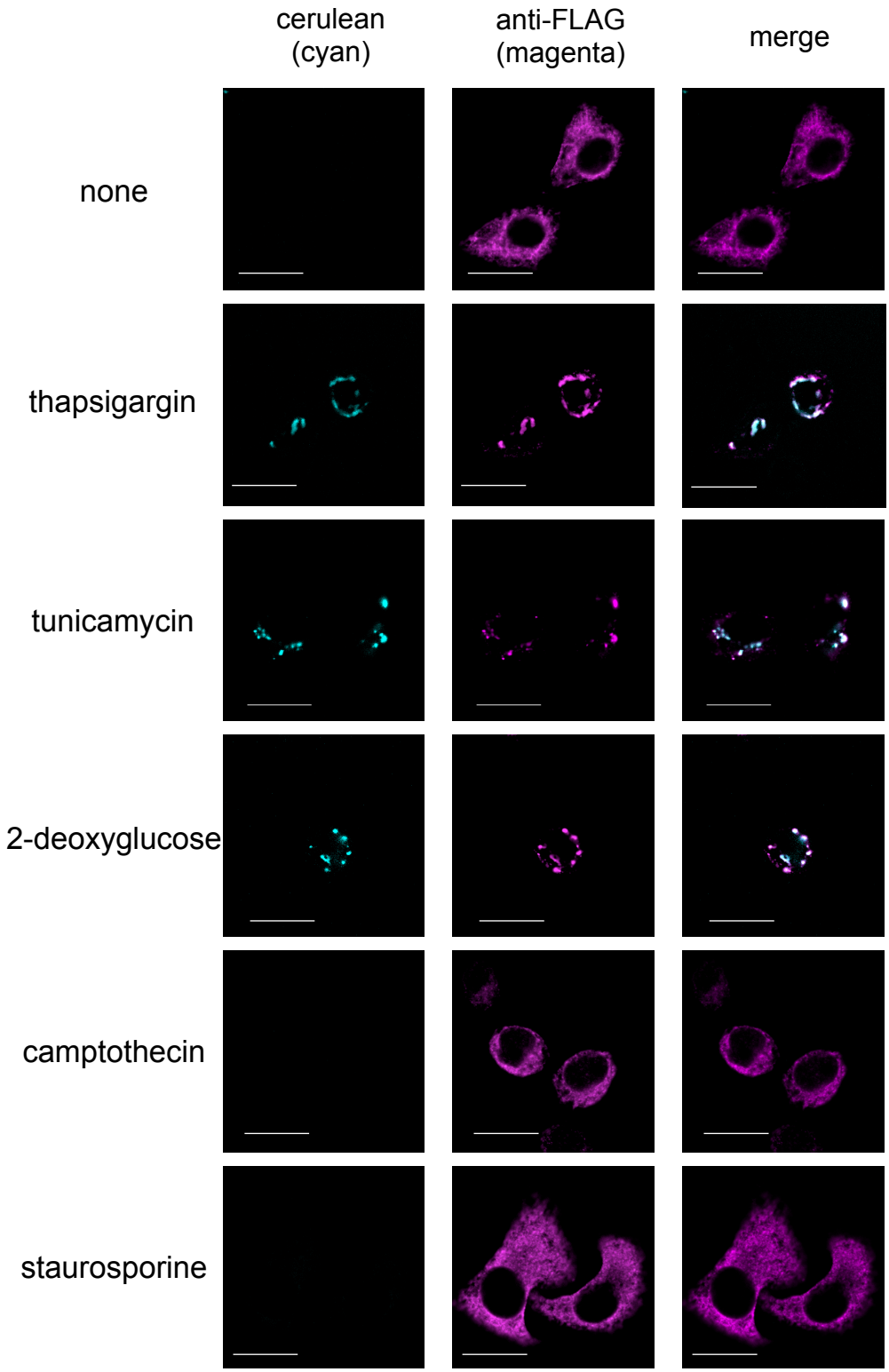

Fig 2-16. Localization of IRE1αΔKR-cerC and IRE1αΔKR-cerN in HeLa/IRE1α-BiFC#5 cells

HeLa/IRE1α-BiFC#5 cells were treated with 30 nM thapsigargin, 10 μg/ml tunicamycin, 2 mM 2-deoxyglucose, 10 μg/ml camptothecin or 0.1 μM staurosporine for 4 hours. The cells were then fixed and immunostained using anti-FLAG antibody, and observed under a confocal microscope. Scale bar, 20 μm. The data was representative of at least three independent studies.

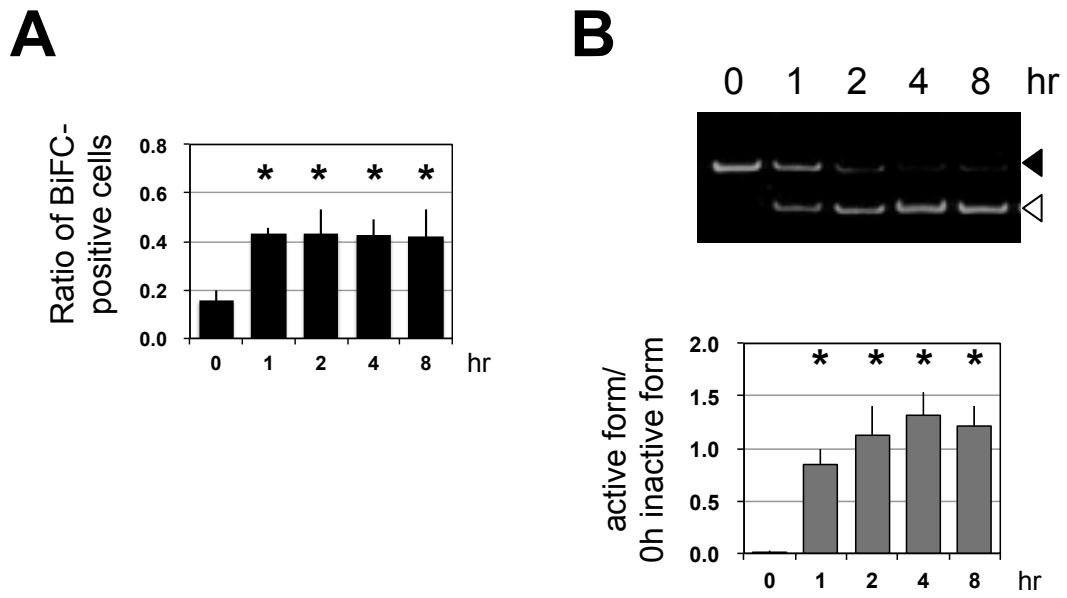

Fig 2-17. DTT increased the ratio of BiFC-positive cells in HeLa/IRE1α-BiFC#5 cells

HeLa/IRE1α-BiFC#5 cells were treated with 3 mM DTT for 1-8 hours. (A) Then the cells were fixed and immunostained using anti-FLAG antibody, and observed under confocal microscope. The ratio of BiFC-positive cells was calculated as described in Materials and methods. Values are the means of three independent experiments. Bars, SD. *, $p < 0.05$. (B) (B, *upper panel*) Spliced- or unspliced-XBP1 mRNA was detected with RT-PCR as described in Materials and Methods. Black arrowhead shows unspliced inactive form of XBP1 cDNA amplicon (125 bp) and white arrowhead shows spliced active form of XBP1 cDNA amplicon (99 bp). (B, *lower panel*) The splicing of XBP1 mRNA was quantified as follows; the intensity of band of active form at each time point divided by the intensity of band of inactive form of 0 hour. Values are the means of three independent experiments. Bars, SD. *, $p < 0.05$.

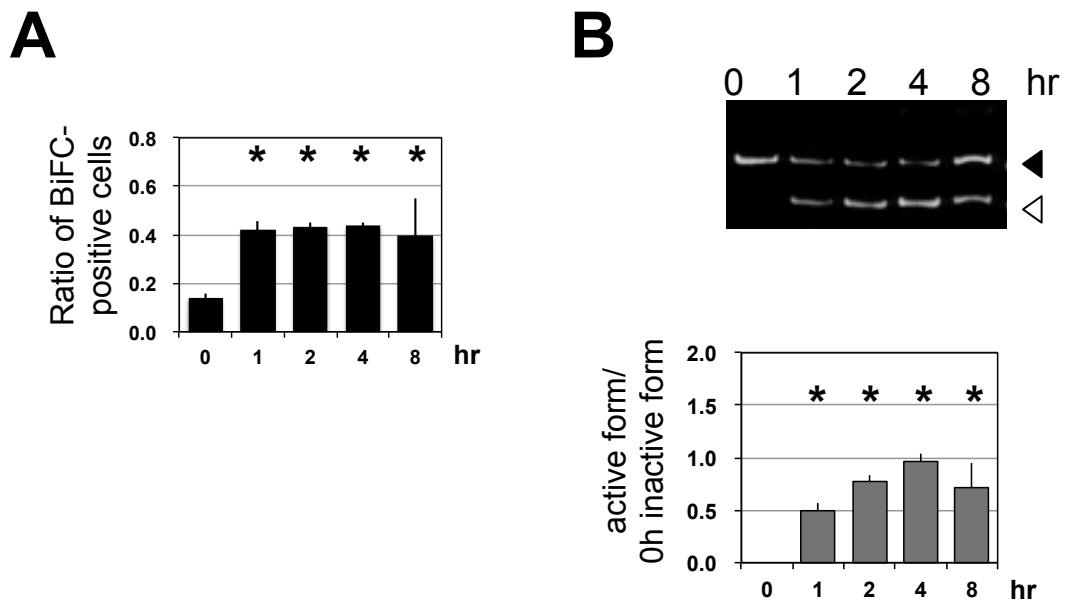

Fig 2-18. Thapsigargin increased the ratio of BiFC-positive cells in HeLa/IRE1α-BiFC#5 cells

HeLa/IRE1α-BiFC#5 cells were treated with 30 nM thapsigargin for 1-8 hours. (A) Then the cells were fixed and immunostained using anti-FLAG antibody, and observed under confocal microscope. The ratio of BiFC-positive cells was calculated as described in Materials and methods. Values are the means of three independent experiments. Bars, SD. *, $p < 0.05$. (B, *upper panel*) Spliced- or unspliced-XBP1 mRNA was detected with RT-PCR as described in Materials and Methods. Black arrowheads show unspliced inactive form of XBP1 cDNA amplicon (125 bp) and white arrowheads show spliced active form of XBP1 cDNA amplicon (99 bp). (B, *lower panel*) The splicing of XBP1 mRNA was quantified as follows; the intensity of band of active form at each time point divided by the intensity of band of inactive form of 0 hour. Values are the means of three independent experiments. Bars, SD. *, $p < 0.05$.

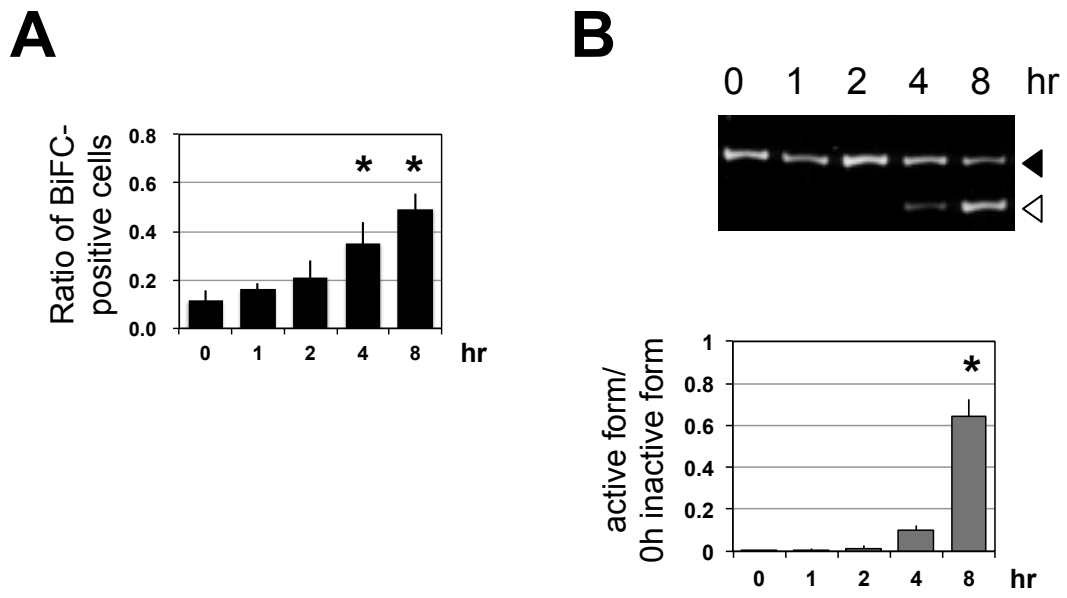

Fig 2-19. Tunicamycin increased the ratio of BiFC-positive cells in HeLa/IRE1α-BiFC#5 cells

HeLa/IRE1α-BiFC#5 cells were treated with 10 μg/ml tunicamycin for 1-8 hours.(A) Then the cells were fixed and immunostained using anti-FLAG antibody, and observed under confocal microscope. The ratio of BiFC-positive cells was calculated as described in Materials and methods. Values are the means of three independent experiments. Bars, SD. *, $p < 0.05$. (B, *upper panel*) Spliced- or unspliced-XBP1 mRNA was detected with RT-PCR as described in Materials and Methods. Black arrowheads show unspliced inactive form of XBP1 cDNA amplicon (125 bp) and white arrowheads show spliced active form of XBP1 cDNA amplicon (99 bp). (B, *lower panel*) The splicing of XBP1 mRNA was quantified as follows; the intensity of band of active form at each time point divided by the intensity of band of inactive form of 0 hour. Values are the means of three independent experiments. Bars, SD. *, $p < 0.05$.

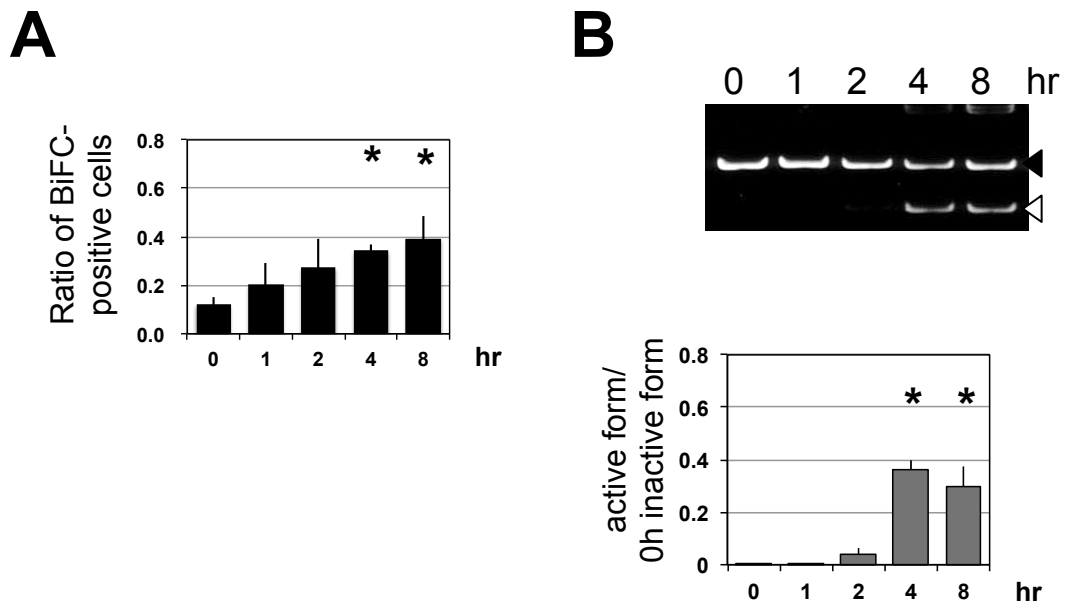

Fig 2-20. 2-deoxyglucose increased the ratio of BiFC-positive cells in HeLa/IRE1α-BiFC#5 cells

HeLa/IRE1α-BiFC#5 cells were treated with 2 mM 2-deoxyglucose for 1-8 hours.(A) Then the cells were fixed and immunostained using anti-FLAG antibody, and observed under confocal microscope. The ratio of BiFC-positive cells was calculated as described in Materials and methods. Values are the means of three independent experiments. Bars, SD. *, $p < 0.05$. (B, *upper panel*) Spliced- or unspliced-XBP1 mRNA was detected with RT-PCR as described in Materials and Methods. Black arrowheads show unspliced inactive form of XBP1 cDNA amplicon (125 bp) and white arrowheads show spliced active form of XBP1 cDNA amplicon (99 bp). (B, *lower panel*) The splicing of XBP1 mRNA was quantified as follows; the intensity of band of active form at each time point divided by the intensity of band of inactive form of 0 hour. Values are the means of three independent experiments. Bars, SD. *, $p < 0.05$.

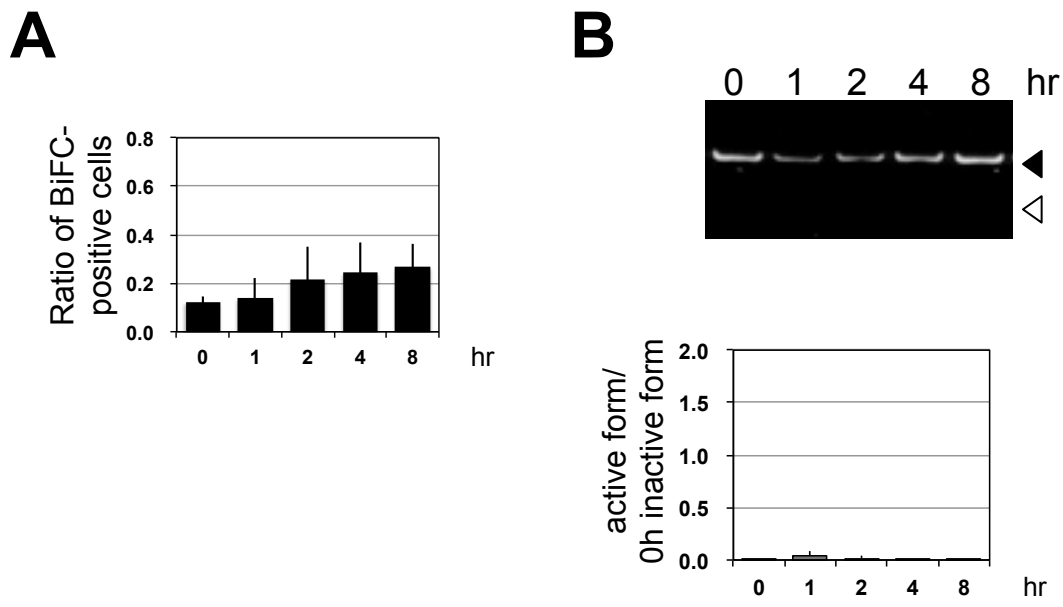

Fig 2-21. Camptothecin did not increase the ratio of BiFC-positive cells in HeLa/IRE1α-BiFC#5 cells

HeLa/IRE1α-BiFC cells were treated with 10 μg/ml camptothecin for 1-8 hours. (A) Then the cells were fixed and immunostained using anti-FLAG antibody, and observed under confocal microscope. The ratio of BiFC-positive cells was calculated as described in Materials and methods. Values are the means of three independent experiments. Bars, SD. *, $p < 0.05$. (B) (upper panel) Spliced- or unspliced-XBP1 mRNA was detected with RT-PCR as described in Materials and Methods. Black arrowhead shows unspliced inactive form of XBP1 cDNA amplicon (125 bp) and white arrowhead shows spliced active form of XBP1 cDNA amplicon (99 bp). (lower panel) The splicing of XBP1 mRNA was quantified as follows; the intensity of band of active form at each time point divided by the intensity of band of inactive form of 0 hour. Values are the means of three independent experiments. Bars, SD. *, $p < 0.05$.

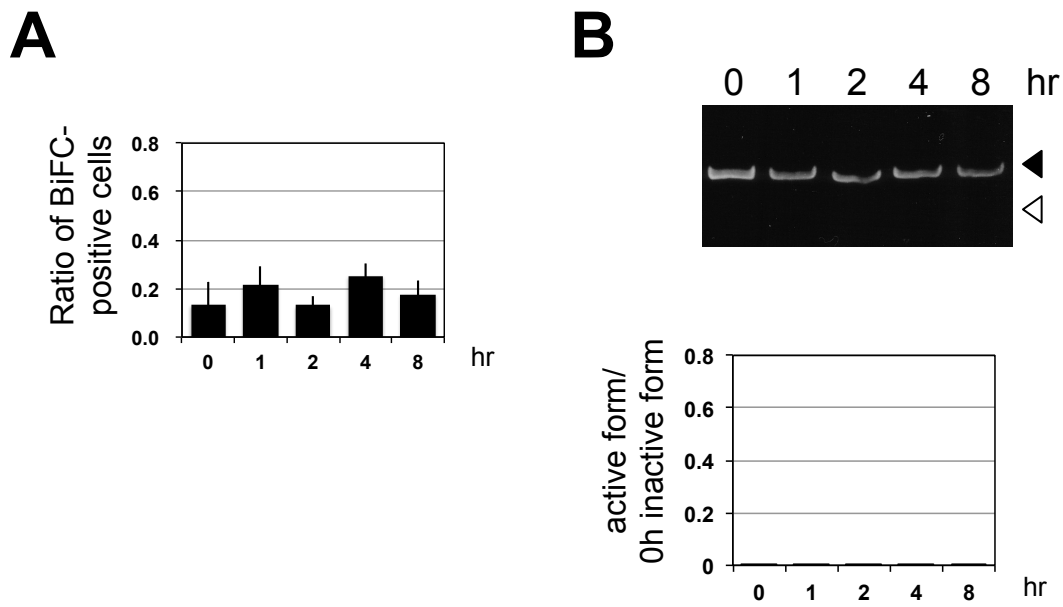

Fig 2-22. Staurosporine did not increase the ratio of BiFC-positive cells in HeLa/IRE1α-BiFC#5 cells

HeLa/IRE1α-BiFC#5 cells were treated with 0.1 μM staurosporine for 1-8 hours. (A) Then the cells were fixed and immunostained using anti-FLAG antibody, and observed under confocal microscope. The ratio of BiFC-positive cells was calculated as described in Materials and methods. Values are the means of three independent experiments. Bars, SD. *, $p < 0.05$. (B) (upper panel) Spliced- or unspliced-XBP1 mRNA was detected with RT-PCR as described in Materials and Methods. Black arrowhead shows unspliced inactive form of XBP1 cDNA amplicon (125 bp) and white arrowhead shows spliced active form of XBP1 cDNA amplicon (99 bp). (lower panel) The splicing of XBP1 mRNA was quantified as follows; the intensity of band of active form at each time point divided by the intensity of band of inactive form of 0 hour. Values are the means of three independent experiments. Bars, SD. *, $p < 0.05$.

3-2-5. Effect of brefeldin A and monensin on reconstitution of cerulean in HeLa/IRE1α-BiFC cells

In Chapter 2 of this thesis, brefeldin A and monensin were suggested to fail to activate IRE1α, although these compounds were supposed to induce UPR, which was verified with GRP78 induction (cf. Figs. 1-1B, 1-4, and 1-13). Therefore, the author examined whether brefeldin A and monensin would not induce reconstitution of cerulean in HeLa/IRE1α-BiFC cells. As results shown in Figs. 2-23 and 2-24, brefeldin A and monensin did not increased neither the ratio of BiFC-positive cells nor the splicing of XBP1 mRNA at any time point measured between 1 and 8 hours. These results indicated that this BiFC assay could distinguish the UPR inducers, which activate and do not activate IRE1α.

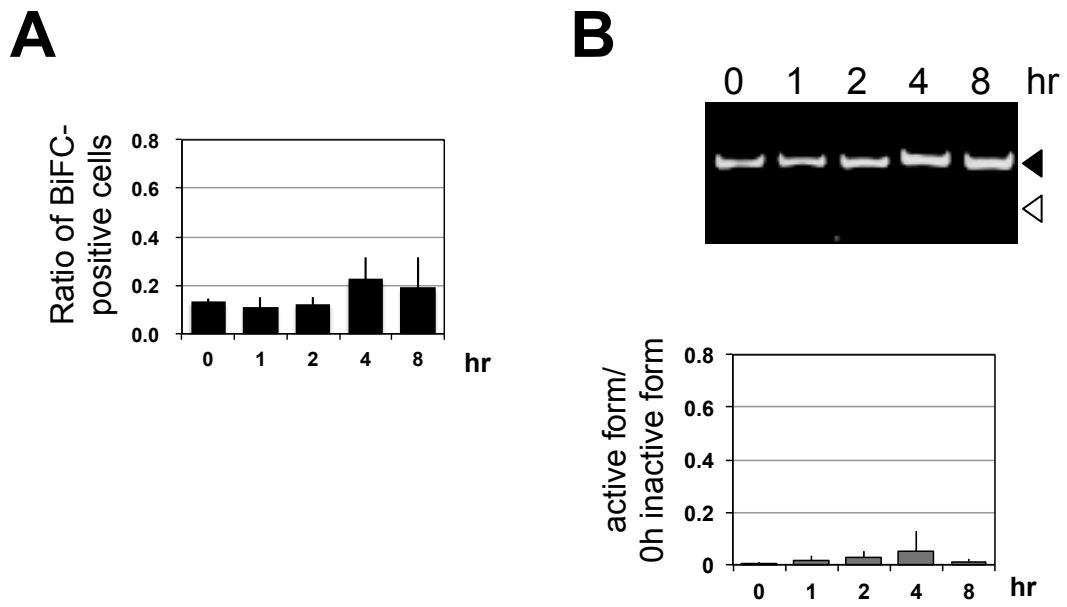

Fig 2-23. Effect of brefeldin A on the ratio of HeLa/IRE1α-BiFC#5 cells of fluorescence

HeLa/IRE1α-BiFC#5 cells were treated with 50 ng/ml brefeldin A for 1-8 hours. (A) Then the cells were fixed and immunostained using anti-FLAG antibody, and observed under confocal microscope. The ratio of BiFC-positive cells was calculated as described in Materials and Methods. Values are the means of three independent experiments. Bars, SD. *, $p < 0.05$. (B, *upper panel*) Spliced- or unspliced-XBP1 mRNA was detected with RT-PCR as described in Materials and Methods. Black arrowheads show unspliced inactive form of XBP1 cDNA amplicon (125 bp) and white arrowheads show spliced active form of XBP1 cDNA amplicon (99 bp). (B, *lower panel*) The splicing of XBP1 mRNA was quantified as follows; the intensity of band of active form at each time point divided by the intensity of band of inactive form of 0 hour. Values are the means of three independent experiments. Bars, SD. *, $p < 0.05$.

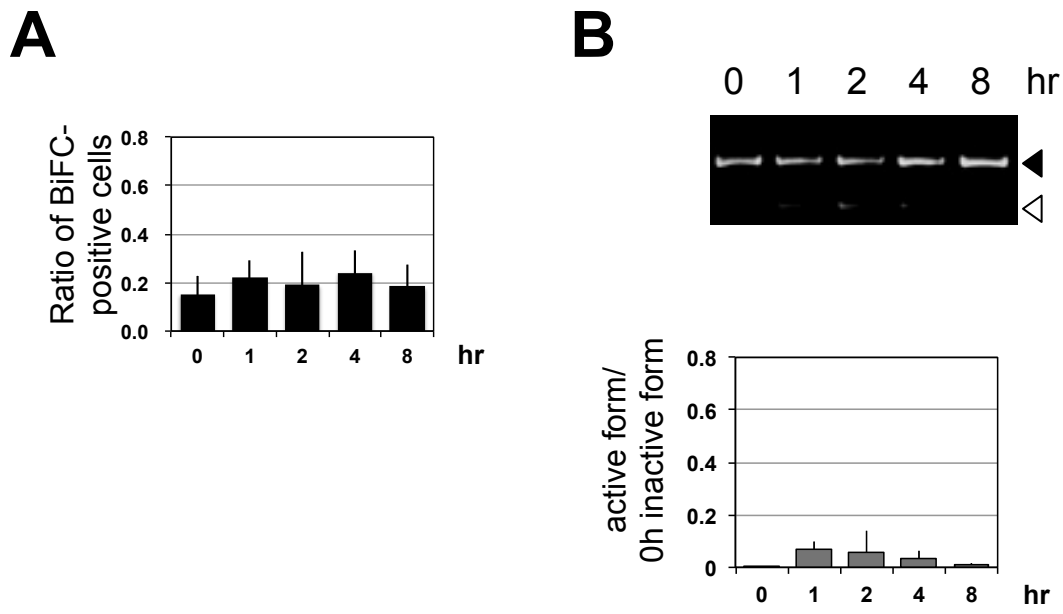

Fig 2-24. Effect of monensin on the ratio of HeLa/IRE1α-BiFC#5 cells of fluorescence

HeLa/IRE1α-BiFC#5 cells were treated with 10 μM monensin for 1-8 hours. (A) Then the cells were fixed and immunostained using anti-FLAG antibody, and observed under confocal microscope. The ratio of BiFC-positive cells was calculated as described in Materials and Methods. Values are the means of three independent experiments. Bars, SD. *, $p < 0.05$. (B, *upper panel*) Spliced- or unspliced-XBP1 mRNA was detected with RT-PCR as described in Materials and Methods. Black arrowheads show unspliced inactive form of XBP1 cDNA amplicon (125 bp) and white arrowheads show spliced active form of XBP1 cDNA amplicon (99 bp). (B, *lower panel*) The splicing of XBP1 mRNA was quantified as follows; the intensity of band of active form at each time point divided by the intensity of band of inactive form of 0 hour. Values are the means of three independent experiments. Bars, SD. *, $p < 0.05$.

3-3. Conclusion

In conclusion, the author established a new assay system for the detection of IRE1α dimerization using a BiFC assay. In this assay system, the fluorescence derived from the reconstituted cerulean was successfully observed in response to treatment with ER stress-inducing compounds. Moreover, this assay system enables us to distinguish between the activation behaviors of IRE1α induced by tunicamycin from those induced by DTT and thapsigargin, which was consistent with a previous report (DuRose et al., 2006). Therefore, while IRE1α dimerization could be evaluated by detecting foci formation of IRE1α-GFP (Li et al., 2010), this method might be also useful for the quantitative detection of the dimerization of IRE1α.

3-4. Materials and Methods

3-4-1. Materials

Tunicamycin, monensin, anti-tubulin antibody, rabbit polyclonal anti-FLAG antibody, and mouse monoclonal anti-FLAG (M2) antibody were purchased from Sigma Aldrich (St. Louis, MO, USA). Brefeldin A and thapsigargin were purchased from Calbiochem (San Diego, CA, USA) and from Santa Cruz Biotechnology (Santa Cruz, CA, USA), respectively. DTT was purchased from Wako Pure Chemical Industries, Ltd. (Osaka, Japan). Mouse monoclonal anti-KDEL antibody (10C3) was purchased from ENZO life sciences (Farmingdale, NY, USA). Horseradish peroxidase-conjugated anti-mouse and anti-rabbit IgG used as secondary antibodies were purchased from GE Healthcare (Little Chalfont, UK). Anti-rabbit IgG tagged with Alexa Fluor 546 and anti-mouse IgG tagged with Alexa Fluor 647 were purchased from Life Technologies (Carlsbad, CA, USA).

3-4-2. Cell culture

A human epithelial adenocarcinoma cell line HeLa and a human embryonic kidney cell line HEK2993T cells were cultured in DMEM (Nissui, Tokyo, Japan) supplemented with 8 % and 10% FBS, respectively at 37 °C in a 5% CO_2–95% air atmosphere.

3-4-3. RT-PCR for detecting XBP1 mRNA splicing

Total RNA was extracted from HeLa cells using TRIzol reagent (Life Technologies). Aliquots of 2 μg of total RNA were treated with M-MLV reverse transcriptase (Promega, Madison, WI, USA) to produce first-strand complementary DNA (cDNA). The first-strand cDNA was subjected to PCR with KOD plus polymerase (Toyobo, Osaka, Japan) using a pair of primers corresponding to nucleotides 505–525 (5'-AATGAAGTGAGGCCAGTGGCC-3') and 609–629 (5'-AATACCGCCAGAATCCATGGG-3') of XBP1 cDNA. The amplified products were separated by electrophoresis on an 8% polyacrylamide gel and visualized by ethidium bromide staining. The intensity of each band was quantified using ImageJ software (http://rsb. info.nih.gov/ij/).

3-4-4. Plasmid construction and transfection

For construction of a C-terminal HA-tagged IRE1α, full length of IRE1α was amplified with PCR from pcDNA3-IRE1α-FLAG (Ri et al., 2012). The amplicon was inserted into pcDNA3.1-zeo(+) (Invitrogen).

As illustrated in Fig. 2-3, the plasmids for expression of fusion proteins illustrated in Fig. 2-2 were constructed as follows: at first, full length or deletion mutants of IRE1α (IRE1α (1-2931 nucleotides), IRE1αΔR (1-2502 nucleotides) or IRE1αΔKR (1-1662 nucleotides)) were amplified from pcDNA3-IRE1α-FLAG and the amplicons were

inserted to pCI-neo (Promega). On the other hand, cerulean N-term (cerN; 1-462 nucleotides) and C-term (cerC; 463-717 nucleotides) were amplified from pmCerulean-C1 (provided by Dr. Miyawaki). The split site of cerulean was referred the previous report (Hu and Kerppola, 2003). These cerulean fragments, cerN and cerC, were inserted to pCI-neo-IRE1α, IRE1αΔR, or IRE1αΔKR at the 3'term of IRE1α.

To construct the plasmid expressing cerulean fragment inserted between the transmembrane domain and the kinase domain of IRE1α, EcoRI site was inserted between 1662nd and 1663rd nucleotide of IRE1α with PCR. The cerulean fragments, cerN or cerC, were inserted to this EcoRI site.

To link IRE1αΔKR-cerN and IRE1αΔKR-cerC with 2A peptide sequence of the Thosea asigna virus (TaV) (5'-ggcagtggagagggcagaggaagtctgctaacatgcggtgacgtcgaggag aatcctggccca-3' and translated to GSGEGRGSLLTCGDVEENPGP) (Szymczak et al., 2004; Trichas et al., 2008), constructs were amplified using pCI-neo-IRE1αΔKR-cerN as a template. The amplicon was inserted to pCI-neo-IRE1αΔKR-cerC at the 3'term of cerC. This construct was named as pCI-neo-IRE1α-BiFC.

All of cerN possessing construct have FLAG-tag at their C-term and all of the cerC possessing construct have FLAG-tag and HA-tag at their C-term.

For transient transfection of HeLa cells seeded on 12-well plates, plasmids and 2 μL of Plus Reagent (Life Technologies) were diluted in 100 μL of Opti-MEM (Life Technologies) and mixed. After 15 minutes, 2 μL of lipofectamine (Life Technologies)

was added to the mixture. After another 30 minutes, growth medium was removed from cells and replaced it with 300 μL of Opti-MEM. Then, the mixture was added to the culture medium. After 4 hours incubation at 37 °C, 100 μL of growth medium containing 40% serum was added to each well. Twenty-four hours after transfection, cells were treated with compound and subjected to immunostaining or RT-PCR. For Western blotting and immunoprecipitation, the cells were seeded on 6-well plates and ϕ100 mm dish, respectively; therefore the amounts of the reagents were scaled up to twofold and tenfold of 12-well plates format, respectively.

For transient transfection of HEK293T cells seeded on 12-well plates, plasmids and 1 μL of Lipofectamine were diluted in 100 μL of Opti-MEM and mixed. After 30 minutes, growth medium was removed from cells and replaced it with 300 μL of Opti-MEM. Then, the mixture was added to the culture medium. After 4 hours incubation at 37 °C, 100 μL of growth medium containing 50% serum was added to each well. Twenty-four hours after transfection, cells were treated with compound and subjected to immunostaining or RT-PCR. For Western blotting, the cells were seeded on 6-well plates; therefore the amounts of reagents were scaled up to twofold of 12-well plates format.

3-4-5. Western Blotting

Cell pellets were lysed using an extraction buffer containing 150 mM NaCl, 2.5 mM EGTA, 1 mM EDTA, 1 mM DTT, 0.1 % Tween-20, 10 mM β-glycerophosphate, 1 mM NaF, 0.1 mM Na_3VO_4, 10% glycerol, and 50 mM HEPES (pH 7.5). Lysates were separated by SDS-PAGE and transferred to a PVDF membrane (Millipore, Bedford, MA, USA) by electroblotting. After the membranes had been incubated with primary and secondary antibodies, the immune complexes were detected with an Immobilon Western kit (Millipore), and the luminescence was detected with a LAS-1000 mini CCD camera (Fujifilm, Tokyo, Japan). The visualized bands were quantitated using ImageJ software (http://rsb. info.nih.gov/ij/).

3-4-6. Immunoprecipitation

HeLa cells were transiently transfected with pcDNA3-IRE1α-FLAG and pcDNA3.1-zeo(+)-IRE1α-HA. Following 24 hours of transfection, the cells were treated with 3 mM DTT. The cells were collected and lysed with freeze and thaw 4 times in extraction buffer. The cell lysates were cleared by centrifugation at 13,000 rpm for 15 min at 4 °C. The lysates were precleared with protein A/G-agarose beads (Santa Cruz Biotechnology) for 1 hour, incubated with anti-HA antibody at 4 °C for 4 hours, followed by incubation with protein A/G-agarose beads overnight. The immunoprecipitants were washed three times with extraction buffer. The bound proteins

were eluted by boiling in SDS sample buffer for 5 min and subjected to Western blotting.

3-4-7. Immunostaining

The cells treated with various compounds were fixed, permeabilized and incubated in blocking buffer (3% bovine serum albumin in PBS) for 30 min. The cells were incubated with anti-FLAG antibody from rabbit (1:1000) with or without anti-KDEL antibody from mouse (1:1000) in blocking buffer at 4 °C for overnight. After rinsing three times with PBS, the cells were incubated with anti-rabbit IgG tagged with Alexa Fluor 546 (1:1000) with or without anti-mouse IgG tagged with Alexa Fluor 647 (1:1000) at room temperature for 1 hour. Fluorescence images were obtained using a confocal laser scanning microscope system FV1000 (Olympus Corp. Tokyo, Japan).

3-4-8. Establishment of HeLa cells stably expressing IRE1αΔKR-cerN and -cerC

HeLa cells were transfected with pCI-neo-IRE1α-BiFC using Lipofectamine and Plus Reagent (Life Technologies). Transfected cells were selected by 600 μg/ml geneticin (Wako). Expression of IRE1αΔKR-cerN and IRE1αΔKR-cerC was evaluated by Western blotting.

3-4-9. Calculation of the ratio of the cells exhibited fluorescence of cerulean

The author defined the BiFC-positive cells as the cells showed the fluorescence above threshold, which was empirically defined. Moreover, the cells expressing fusion proteins were extracted as the cells showed the fluorescence of Alexa-546 above threshold. These analyses were performed with ImageJ software (http://rsbweb.nih.gov/ij/). To calculate the ratio of BiFC-positive cells, the number of the cells expressing fusion proteins divided the number of the BiFC-positive cells.

3-4-10. Statistical analysis

Data were analyzed using one-way ANOVA between subjects, and post hoc comparisons were made using the Tukey HSD test. Statistical analyses were performed using IBM SPSS software version 20 (IBM SPSS, Chicago, IL, USA). In all cases, statistical significance was set at $P < 0.05$.

Chapter 4

Conclusion

In 1977, glucose-regulated protein 78 and 94 (GRP78 and 94) were discovered that their expressions are regulated by glucose concentration (Shiu et al., 1977). After this discovery, the expression of GRP78 and/or GRP94 has been reported to be induced by various stimuli such as the perturbation of calcium concentration (Welch et al., 1983), inhibition of glycosylation (Olden et al., 1979), disruption of disulfide bond formation (Whelan and Hightower, 1985), or some kind of protein mutation (Lee et al., 1986; Pouyssegur et al., 1977). From the report by Kohno et al., the response involving upregulation of GRP78 and 94 has been referred to "unfolded protein response" (Kohno et al., 1993). Moreover, not only ER chaperone like GRP78 and 94, but also the genes related to protein degradation or apoptosis were revealed to be upregulated by the similar stimuli that could upregulate GRP78 and 94. Whereas it had been revealed that various genes, which have several functions for UPR, were involved in the UPR and that various kind of stimuli or various compounds, which have different modes of action, could activate UPR as described above, there are some unsolved questions in the field of UPR research (Walter and Ron, 2011). Therefore, in this thesis, the author sought to approach these questions.

In Chapter 2, since it was unclear whether the modes of action of the compounds could be affect to the expression patterns of UPR target genes; the author compared the expression patterns of nine UPR target genes induced by seven UPR inducing

compounds. As a result of hierarchical clustering using Pearson's correlation coefficient as a similarity, the expression patterns induced by seven compounds were classified into two clusters; cluster A (induced by thapsigargin, tunicamycin, 2-deoxyglucose and DTT) and cluster B (induced by brefeldin A, eeyarestatin I and monensin). To the author's knowledge, this is the first report to suggest that the mode of action of the compounds could affect the expression patterns of UPR target genes.

Furthermore, it is suggested that the compounds in cluster A' and C', which classification was obtained from another clustering analysis using Euclidean distance as a similarity, would accumulate incorrectly and correctly folded proteins in the ER, respectively. Moreover, the compounds in cluster A', which upregulated the nine UPR target genes, is suggested to activate all of three ER stress sensors; conversely, the compounds in cluster C', which upregulated the genes in cluster I' and II' but hardly those in cluster III', is suggested to activate only PERK. These suggestions were confirmed by the results shown in Figs. 1-11, 12, and 13. Taken together with these suggestions, the accumulation of incorrectly folded proteins in the ER might activate all of three ER stress sensors, on the other hand, the accumulation of correctly folded proteins in the ER might activate only PERK.

Although the UPR was thought to be activated by the accumulation of incorrectly folded proteins as described in Introduction section, this thesis suggested that the accumulation of correctly folded proteins was suggested to activate UPR with the

different expression pattern of UPR target genes from those induced by the accumulation of incorrectly folded proteins. However, the mechanism how the accumulation of correctly folded proteins could active PERK was not revealed, therefore it should be examined.

Furthermore, most of the researches investigating the molecular machinery of UPR or the biological roles of UPR in the pathology utilized tunicamycin or thapsigargin, which thought to accumulate the incorrectly folded proteins, as UPR inducer (Katayama et al., 1999; Nishitoh et al., 2002; Yamamoto et al., 2007; Yoshida et al., 2001). Therefore, since the UPR induced by the compounds thought to accumulate the correctly folded proteins in the ER was less analyzed, if these compounds were used in the similar analysis to the previous study described above, the results of these reports could be different and the novel findings would be revealed.

Moreover, it should be examined whether the folding statuses of the accumulated proteins itself indeed affect the activation pattern of ER stress sensors and subsequent expression pattern of UPR target genes. This could be attained by comparing the effects of the mutants mimicking the accumulation of incorrectly and correctly folded proteins, (e.g. the unfolded mutants, which might induce the accumulation of unfolded proteins in the ER, and ER retention mutants, which might induce the accumulation of correctly folded proteins in the ER, of influenza virus hemagglutinin or rhodopsin) on the activation of ER stress sensors or the expression of UPR target genes,

In Chapter 3, since the detection of the activation of ER stress sensors is essential for analysis of UPR, the quantitative detection system for three ER stress sensors would be required. Therefore, at first, IRE1α dimerization, the trigger step for activation of ER stress sensor IRE1α, was sought to be established. As a result, it is suggested that the reconstitution of cerulean in HeLa/IRE1α-BiFC cells was induced by DTT, tunicamycin, thapsigargin and 2-deoxyglucose, the compounds in cluster A, which would reflect the dimerization of IRE1α. On the other hand, brefeldin A and monensin, the compounds in cluster B, induce neither cerulean reconstitution nor XBP1 mRNA splicing, the downstream event. These results indicated that the author succeeded in the establishment of detection system of IRE1α dimerization with BiFC method.

This is the first research to detect human IRE1α dimerization with BiFC assay. Although the several methods were established to detect IRE1 dimerizaion with FRET or detecting change of localization (Li et al., 2010; Pincus et al., 2010), this BiFC method has advantages towards these previous reports; BiFC assay enables the visualization of protein interactions in living cells using the single excitation/emission characteristics of the parent protein and the fluorescent was reflected the dimerization (Hu et al., 2002; Hu and Kerppola, 2003).

In the end, the author hopes that solving the questions arisen from this study and the detection system towards the activation of ER stress sensors would contribute to the development of the research field of UPR.

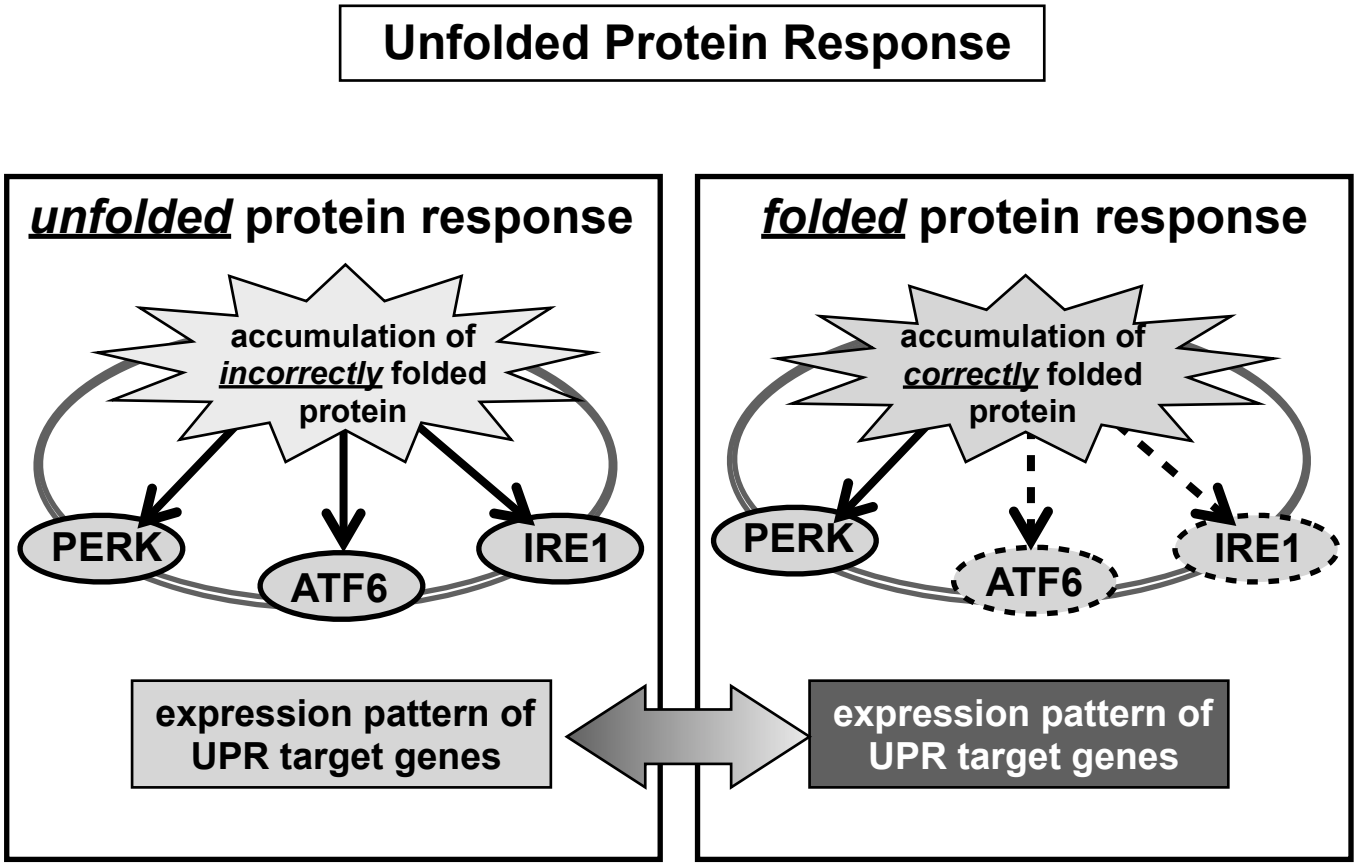

Fig. 3-1. Schematic illustration of the hypothesis of this thesis

References

Aletrari, M.-O., McKibbin, C., Williams, H., Pawar, V., Pietroni, P., Lord, J.M., Flitsch, S.L., Whitehead, R., Swanton, E., High, S., *et al*. (2011). Eeyarestatin 1 interferes with both retrograde and anterograde intracellular trafficking pathways. PLoS ONE *6*, e22713.

Anfinsen, C.B., Haber, E., Sela, M., and White, F.H., Jr. (1961). The kinetics of formation of native ribonuclease during oxidation of the reduced polypeptide chain. Proc Natl Acad Sci U S A *47*, 1309-1314.

Aparicio-Fernandez, X., Garcia-Gasca, T., Yousef, G.G., Lila, M.A., Gonzalez de Mejia, E., and Loarca-Pina, G. (2006). Chemopreventive activity of polyphenolics from black Jamapa bean (Phaseolus vulgaris L.) on HeLa and HaCaT cells. J Agric Food Chem *54*, 2116-2122.

Bertolotti, A., Zhang, Y., Hendershot, L.M., Harding, H.P., and Ron, D. (2000). Dynamic interaction of BiP and ER stress transducers in the unfolded-protein response. Nat Cell Biol *2*, 326-332.

Calfon, M., Zeng, H., Urano, F., Till, J.H., Hubbard, S.R., Harding, H.P., Clark, S.G., and Ron, D. (2002). IRE1 couples endoplasmic reticulum load to secretory capacity by processing the XBP-1 mRNA. Nature *415*, 92-96.

Citterio, C., Vichi, A., Pacheco-Rodriguez, G., Aponte, A.M., Moss, J., and Vaughan, M. (2008). Unfolded protein response and cell death after depletion of

brefeldin A-inhibited guanine nucleotide-exchange protein GBF1. Proc Natl Acad Sci U S A *105*, 2877-2882.

Cleland, W.W. (1964). Dithiothreitol, a New Protective Reagent for SH Groups. Biochemistry *3*, 480-482.

Craig, S., and Goodchild, D.J. (1984). Golgi-Mediated Vicilin Accumulation in Pea Cotyledon Cells Is Re-Directed by Monensin and Nigericin. Protoplasma *122*, 91-97.

Dean, R., and Dixon, W. (1951). Simplified Statistics for Small Numbers of Observations. Analytical Chemistry *23*, 636-638.

Di Jeso, B., Ulianich, L., Pacifico, F., Leonardi, A., Vito, P., Consiglio, E., Formisano, S., and Arvan, P. (2003). Folding of thyroglobulin in the calnexin/calreticulin pathway and its alteration by loss of Ca2+ from the endoplasmic reticulum. Biochem J *370*, 449-458.

Dinter, A., and Berger, E.G. (1998). Golgi-disturbing agents. Histochemistry and cell biology *109*, 571-590.

DuRose, J.B., Tam, A.B., and Niwa, M. (2006). Intrinsic Capacities of Molecular Sensors of the Unfolded Protein Response to Sense Alternate Forms of Endoplasmic Reticulum Stress. Molecular Biology of the Cell *17*, 3095-3107.

Ellgaard, L., Molinari, M., and Helenius, A. (1999). Setting the standards: quality control in the secretory pathway. Science *286*, 1882-1888.

Feinstein, M.B., and Felsenfeld, H. (1971). The detection of ionophorous antibiotic-cation complexes in water with fluorescent probes. Proc Natl Acad Sci U S A *68*, 2037-2041.

Fewell, S.W., Travers, K.J., Weissman, J.S., and Brodsky, J.L. (2001). The action of molecular chaperones in the early secretory pathway. Annu Rev Genet *35*, 149-191.

Fiebiger, E., Hirsch, C., Vyas, J.M., Gordon, E., Ploegh, H.L., and Tortorella, D. (2004). Dissection of the dislocation pathway for type I membrane proteins with a new small molecule inhibitor, eeyarestatin. Molecular Biology of the Cell *15*, 1635-1646.

Gotoh, T., Oyadomari, S., Mori, K., and Mori, M. (2002). Nitric oxide-induced apoptosis in RAW 264.7 macrophages is mediated by endoplasmic reticulum stress pathway involving ATF6 and CHOP. J Biol Chem *277*, 12343-12350.

Griffiths, G., Quinn, P., and Warren, G. (1983). Dissection of the Golgi complex. I. Monensin inhibits the transport of viral membrane proteins from medial to trans Golgi cisternae in baby hamster kidney cells infected with Semliki Forest virus. Journal of cell biology *96*, 835-850.

Halleck, M.M., Holbrook, N.J., Skinner, J., Liu, H., and Stevens, J.L. (1997). The molecular response to reductive stress in LLC-PK1 renal epithelial cells: coordinate transcriptional regulation of gadd153 and grp78 genes by thiols. Cell stress & chaperones *2*, 31-40.

Haney, M.E., Jr., and Hoehn, M.M. (1967). Monensin, a new biologically active compound. I. Discovery and isolation. Antimicrob Agents Chemother (Bethesda) *7*, 349-352.

Harding, H.P., Novoa, I., Zhang, Y., Zeng, H., Wek, R., Schapira, M., and Ron, D. (2000). Regulated translation initiation controls stress-induced gene expression in mammalian cells. Mol Cell *6*, 1099-1108.

Harding, H.P., Zhang, Y., and Ron, D. (1999). Protein translation and folding are coupled by an endoplasmic-reticulum-resident kinase. Nature *397*, 271-274.

Heifetz, A., Keenan, R.W., and Elbein, A.D. (1979). Mechanism of action of tunicamycin on the UDP-GlcNAc:dolichyl-phosphate Glc-NAc-1-phosphate transferase. Biochemistry *18*, 2186-2192.

Hu, C.D., Chinenov, Y., and Kerppola, T.K. (2002). Visualization of interactions among bZIP and Rel family proteins in living cells using bimolecular fluorescence complementation. Mol Cell *9*, 789-798.

Hu, C.D., and Kerppola, T.K. (2003). Simultaneous visualization of multiple protein interactions in living cells using multicolor fluorescence complementation analysis. Nat Biotechnol *21*, 539-545.

Hubbard, S.C., and Ivatt, R.J. (1981). Synthesis and processing of asparagine-linked oligosaccharides. Annu Rev Biochem *50*, 555-583.

Iwawaki, T., Akai, R., Kohno, K., and Miura, M. (2004). A transgenic mouse

model for monitoring endoplasmic reticulum stress. Nat Med *10*, 98-102.

Katayama, T., Imaizumi, K., Sato, N., Miyoshi, K., Kudo, T., Hitomi, J., Morihara, T., Yoneda, T., Gomi, F., Mori, Y., *et al*. (1999). Presenilin-1 mutations downregulate the signalling pathway of the unfolded-protein response. Nat Cell Biol *1*, 479-485.

Kohno, K., Normington, K., Sambrook, J., Gething, M.J., and Mori, K. (1993). The promoter region of the yeast KAR2 (BiP) gene contains a regulatory domain that responds to the presence of unfolded proteins in the endoplasmic reticulum. Mol Cell Biol *13*, 877-890.

Korennykh, A.V., Egea, P.F., Korostelev, A.A., Finer-Moore, J., Zhang, C., Shokat, K.M., Stroud, R.M., and Walter, P. (2009). The unfolded protein response signals through high-order assembly of Ire1. Nature *457*, 687-693.

Kornfeld, R., and Kornfeld, S. (1985). Assembly of asparagine-linked oligosaccharides. Annu Rev Biochem *54*, 631-664.

Kurtoglu, M., Gao, N., Shang, J., Maher, J.C., Lehrman, M.A., Wangpaichitr, M., Savaraj, N., Lane, A.N., and Lampidis, T.J. (2007). Under normoxia, 2-deoxy-D-glucose elicits cell death in select tumor types not by inhibition of glycolysis but by interfering with N-linked glycosylation. Mol Cancer Ther *6*, 3049-3058.

Lee, A.H., Iwakoshi, N.N., and Glimcher, L.H. (2003). XBP-1 regulates a subset of endoplasmic reticulum resident chaperone genes in the unfolded protein response.

Mol Cell Biol *23*, 7448-7459.

Lee, A.S., Wells, S., Kim, K.S., and Scheffler, I.E. (1986). Enhanced synthesis of the glucose/calcium-regulated proteins in a hamster cell mutant deficient in transfer of oligosaccharide core to polypeptides. Journal of cellular physiology *129*, 277-282.

Lee, K., Tirasophon, W., Shen, X., Michalak, M., Prywes, R., Okada, T., Yoshida, H., Mori, K., and Kaufman, R.J. (2002). IRE1-mediated unconventional mRNA splicing and S2P-mediated ATF6 cleavage merge to regulate XBP1 in signaling the unfolded protein response. Genes Dev *16*, 452-466.

Lefrancois, L., and Lyles, D.S. (1982). The interaction of antibody with the major surface glycoprotein of vesicular stomatitis virus. I. Analysis of neutralizing epitopes with monoclonal antibodies. Virology *121*, 157-167.

Li, H., Korennykh, A.V., Behrman, S.L., and Walter, P. (2010). Mammalian endoplasmic reticulum stress sensor IRE1 signals by dynamic clustering. Proc Natl Acad Sci U S A *107*, 16113-16118.

Liu, C.Y., Schroder, M., and Kaufman, R.J. (2000). Ligand-independent dimerization activates the stress response kinases IRE1 and PERK in the lumen of the endoplasmic reticulum. J Biol Chem *275*, 24881-24885.

Liu, C.Y., Wong, H.N., Schauerte, J.A., and Kaufman, R.J. (2002). The protein kinase/endoribonuclease IRE1alpha that signals the unfolded protein response has a luminal N-terminal ligand-independent dimerization domain. J Biol Chem *277*,

18346-18356.

Liu, E., and Ou, J. (1992). Brefeldin A as a regulator of grp78 gene expression in mammalian cells. J Biol Chem *267*, 7128-7133.

Mollenhauer, H.H., Morre, D.J., and Rowe, L.D. (1990). Alteration of intracellular traffic by monensin; mechanism, specificity and relationship to toxicity. Biochimica et biophysica acta *1031*, 225-246.

Muroi, M., Kazami, S., Noda, K., Kondo, H., Takayama, H., Kawatani, M., Usui, T., and Osada, H. (2010). Application of proteomic profiling based on 2D-DIGE for classification of compounds according to the mechanism of action. Chem Biol *17*, 460-470.

Nakagawa, T., Zhu, H., Morishima, N., Li, E., Xu, J., Yankner, B.A., and Yuan, J. (2000). Caspase-12 mediates endoplasmic-reticulum-specific apoptosis and cytotoxicity by amyloid-beta. Nature *403*, 98-103.

Nishitoh, H., Matsuzawa, A., Tobiume, K., Saegusa, K., Takeda, K., Inoue, K., Hori, S., Kakizuka, A., and Ichijo, H. (2002). ASK1 is essential for endoplasmic reticulum stress-induced neuronal cell death triggered by expanded polyglutamine repeats. Genes Dev *16*, 1345-1355.

Novoa, I., Zeng, H., Harding, H.P., and Ron, D. (2001). Feedback inhibition of the unfolded protein response by GADD34-mediated dephosphorylation of eIF2alpha. Journal of Cell Biology *153*, 1011-1022.

Okada, T., Yoshida, H., Akazawa, R., Negishi, M., and Mori, K. (2002). Distinct roles of activating transcription factor 6 (ATF6) and double-stranded RNA-activated protein kinase-like endoplasmic reticulum kinase (PERK) in transcription during the mammalian unfolded protein response. Biochem J *366*, 585-594.

Olden, K., Pratt, R.M., Jaworski, C., and Yamada, K.M. (1979). Evidence for role of glycoprotein carbohydrates in membrane transport: specific inhibition by tunicamycin. Proc Natl Acad Sci U S A *76*, 791-795.

Parham, P., Barnstable, C.J., and Bodmer, W.F. (1979). Use of a monoclonal antibody (W6/32) in structural studies of HLA-A,B,C, antigens. J Immunol *123*, 342-349.

Park, H.-R., Tomida, A., Sato, S., Tsukumo, Y., Yun, J., Yamori, T., Hayakawa, Y., Tsuruo, T., and Shin-ya, K. (2004). Effect on tumor cells of blocking survival response to glucose deprivation. Journal of the National Cancer Institute *96*, 1300-1310.

Pincus, D., Chevalier, M.W., Aragon, T., van Anken, E., Vidal, S.E., El-Samad, H., and Walter, P. (2010). BiP binding to the ER-stress sensor Ire1 tunes the homeostatic behavior of the unfolded protein response. PLoS Biol *8*, e1000415.

Pouyssegur, J., Shiu, R.P., and Pastan, I. (1977). Induction of two transformation-sensitive membrane polypeptides in normal fibroblasts by a block in glycoprotein synthesis or glucose deprivation. Cell *11*, 941-947.

Preston, A.M., Gurisik, E., Bartley, C., Laybutt, D.R., and Biden, T.J. (2009).

Reduced endoplasmic reticulum (ER)-to-Golgi protein trafficking contributes to ER stress in lipotoxic mouse beta cells by promoting protein overload. Diabetologia *52*, 2369-2373.

Price, B.D., Mannheim-Rodman, L.A., and Calderwood, S.K. (1992). Brefeldin A, thapsigargin, and AIF4- stimulate the accumulation of GRP78 mRNA in a cycloheximide dependent manner, whilst induction by hypoxia is independent of protein synthesis. Journal of Cellular Physiology *152*, 545-552.

Ri, M., Tashiro, E., Oikawa, D., Shinjo, S., Tokuda, M., Yokouchi, Y., Narita, T., Masaki, A., Ito, A., Ding, J.*, et al*. (2012). Identification of Toyocamycin, an agent cytotoxic for multiple myeloma cells, as a potent inhibitor of ER stress-induced XBP1 mRNA splicing. Blood Cancer J *2*, e79.

Ron, D., and Walter, P. (2007). Signal integration in the endoplasmic reticulum unfolded protein response. Nature Reviews Molecular Cell Biology *8*, 519-529.

Rose, R.H., Briddon, S.J., and Holliday, N.D. (2010). Bimolecular fluorescence complementation: lighting up seven transmembrane domain receptor signalling networks. Br J Pharmacol *159*, 738-750.

Rutkowski, D.T., and Hegde, R.S. (2010). Regulation of basal cellular physiology by the homeostatic unfolded protein response. J Cell Biol *189*, 783-794.

Samali, A., Fitzgerald, U., Deegan, S., and Gupta, S. (2010). Methods for monitoring endoplasmic reticulum stress and the unfolded protein response. Int J Cell

Biol *2010*, 830307.

Scheuner, D., Song, B., McEwen, E., Liu, C., Laybutt, R., Gillespie, P., Saunders, T., Bonner-Weir, S., and Kaufman, R.J. (2001). Translational control is required for the unfolded protein response and in vivo glucose homeostasis. Mol Cell *7*, 1165-1176.

Schroder, M., and Kaufman, R.J. (2005). ER stress and the unfolded protein response. Mutat Res *569*, 29-63.

Schwarz, R.T., Schmidt, M.F., and Datema, R. (1979). Inhibition of glycosylation of viral glycoproteins. Biochem Soc Trans *7*, 322-326.

Shamu, C.E., and Walter, P. (1996). Oligomerization and phosphorylation of the Ire1p kinase during intracellular signaling from the endoplasmic reticulum to the nucleus. Embo J *15*, 3028-3039.

Shiu, R.P., Pouyssegur, J., and Pastan, I. (1977). Glucose depletion accounts for the induction of two transformation-sensitive membrane proteinsin Rous sarcoma virus-transformed chick embryo fibroblasts. Proc Natl Acad Sci U S A *74*, 3840-3844.

Szymczak, A.L., Workman, C.J., Wang, Y., Vignali, K.M., Dilioglou, S., Vanin, E.F., and Vignali, D.A. (2004). Correction of multi-gene deficiency in vivo using a single 'self-cleaving' 2A peptide-based retroviral vector. Nat Biotechnol *22*, 589-594.

Takatsuki, A., Kohno, K., and Tamura, G. (1975). Inhibition of biosynthesis of polyisoprenol sugars in chick embryo microsomes by tunicamycin. Agricultural and

Biological Chemistry *39*, 2089-2091.

Thastrup, O., Cullen, P.J., Drøbak, B.K., Hanley, M.R., and Dawson, A.P. (1990). Thapsigargin, a tumor promoter, discharges intracellular Ca2+ stores by specific inhibition of the endoplasmic reticulum Ca2(+)-ATPase. Proc Natl Acad Sci U S A *87*, 2466-2470.

Tirasophon, W., Welihinda, A.A., and Kaufman, R.J. (1998). A stress response pathway from the endoplasmic reticulum to the nucleus requires a novel bifunctional protein kinase/endoribonuclease (Ire1p) in mammalian cells. Genes Dev *12*, 1812-1824.

Trichas, G., Begbie, J., and Srinivas, S. (2008). Use of the viral 2A peptide for bicistronic expression in transgenic mice. BMC Biol *6*, 40.

Walter, P., and Ron, D. (2011). The unfolded protein response: from stress pathway to homeostatic regulation. Science *334*, 1081-1086.

Wang, Q., Mora-Jensen, H., Weniger, M.A., Perez-Galan, P., Wolford, C., Hai, T., Ron, D., Chen, W., Trenkle, W., Wiestner, A.*, et al*. (2009). ERAD inhibitors integrate ER stress with an epigenetic mechanism to activate BH3-only protein NOXA in cancer cells. Proc Natl Acad Sci U S A *106*, 2200-2205.

Wang, X.Z., Harding, H.P., Zhang, Y., Jolicoeur, E.M., Kuroda, M., and Ron, D. (1998). Cloning of mammalian Ire1 reveals diversity in the ER stress responses. Embo J *17*, 5708-5717.

Wek, R.C., and Cavener, D.R. (2007). Translational control and the unfolded

protein response. Antioxid Redox Signal *9*, 2357-2371.

Welch, W.J., Garrels, J.I., Thomas, G.P., Lin, J.J., and Feramisco, J.R. (1983). Biochemical characterization of the mammalian stress proteins and identification of two stress proteins as glucose- and Ca2+-ionophore-regulated proteins. J Biol Chem *258*, 7102-7111.

Whelan, S.A., and Hightower, L.E. (1985). Differential induction of glucose-regulated and heat shock proteins: effects of pH and sulfhydryl-reducing agents on chicken embryo cells. Journal of cellular physiology *125*, 251-258.

Wu, J., Rutkowski, D.T., Dubois, M., Swathirajan, J., Saunders, T., Wang, J., Song, B., Yau, G.D., and Kaufman, R.J. (2007). ATF6alpha optimizes long-term endoplasmic reticulum function to protect cells from chronic stress. Developmental cell *13*, 351-364.

Yamamoto, K., Sato, T., Matsui, T., Sato, M., Okada, T., Yoshida, H., Harada, A., and Mori, K. (2007). Transcriptional induction of mammalian ER quality control proteins is mediated by single or combined action of ATF6alpha and XBP1. Developmental cell *13*, 365-376.

Yan, W., Frank, C.L., Korth, M.J., Sopher, B.L., Novoa, I., Ron, D., and Katze, M.G. (2002). Control of PERK eIF2alpha kinase activity by the endoplasmic reticulum stress-induced molecular chaperone P58IPK. Proc Natl Acad Sci U S A *99*, 15920-15925.

Yoshida, H. (2007). Unconventional splicing of XBP-1 mRNA in the unfolded protein response. Antioxid Redox Signal *9*, 2323-2333.

Yoshida, H., Haze, K., Yanagi, H., Yura, T., and Mori, K. (1998). Identification of the cis-acting endoplasmic reticulum stress response element responsible for transcriptional induction of mammalian glucose-regulated proteins. Involvement of basic leucine zipper transcription factors. J Biol Chem *273*, 33741-33749.

Yoshida, H., Matsui, T., Yamamoto, A., Okada, T., and Mori, K. (2001). XBP1 mRNA is induced by ATF6 and spliced by IRE1 in response to ER stress to produce a highly active transcription factor. Cell *107*, 881-891.

Zhao, L., and Ackerman, S.L. (2006). Endoplasmic reticulum stress in health and disease. Curr Opin Cell Biol *18*, 444-452.

Zhao, X., Claude, A., Chun, J., Shields, D.J., Presley, J.F., and Melancon, P. (2006). GBF1, a cis-Golgi and VTCs-localized ARF-GEF, is implicated in ER-to-Golgi protein traffic. Journal of cell science *119*, 3743-3753.

Zhou, J., Liu, C.Y., Back, S.H., Clark, R.L., Peisach, D., Xu, Z., and Kaufman, R.J. (2006). The crystal structure of human IRE1 luminal domain reveals a conserved dimerization interface required for activation of the unfolded protein response. Proceedings of the National Academy of Sciences of the United States of America *103*, 14343-14348.

謝辞

本研究は、著者が慶應義塾大学大学院理工学研究科後期博士課程在学中に、同大学理工学部教授 井本正哉 博士の指導のもとに行いました。終始親身にご指導ご高配賜りましたことに謹んで感謝の意を表します。

また、本研究を遂行するにあたり、常々ご教授ご鞭撻賜りました慶應義塾大学理工学部専任講師 田代悦 博士に謹んで感謝の意を表します。

本論文の執筆にあたり、ご指導、ご助言をいただきました慶應義塾大学理工学部教授 岡浩太郎 博士、慶應義塾大学理工学部教授 榊原康文 博士、慶應義塾大学理工学部准教授 清水史郎 博士に熱く御礼申し上げます。

UPR 関連遺伝子の発現比較解析に際し、慶應義塾大学理工学部ケミカルバイオロジー研究室 修士１年 溝谷優治くんに大変なご助力をいただきました。厚く感謝いたします。

Cerulean 発現プラスミド pmCerulean-C1 を御供与くださいました理化学研究所 宮脇敦史 博士に御礼申し上げます。

また、早稲田大学理工学術院教授 合田亘人 博士、早稲田大学理工学術院客員准教授 松田七美 博士、先端科学・健康医療融合研究機構 招聘研究員 金井麻衣 博士に感謝いたします。研究生活の最初の６年間、互いに切磋琢磨し合った同期の笹澤有紀子 博士、山本浩太 博士に心より感謝します。研究生活を様々な面でサポートしていただきましたケミカルバイオロジー研究室秘書 梅崎秀香 さんに厚く御礼申し上げます。また、日々の研究生活の中で多くのことを学ばせていただいた、ケミカルバイオロジー研究室の諸先輩方ならびに鈴木麻友さん、冨山隼輔くんをはじめとする卒業生、後輩の皆様に感謝致します。

最後に、研究生活を常にサポートしてくれた家族に心より感謝致します。